Electronic Supplementary Material (ESI) for Polymer Chemistry.

Supporting Information

For

Impact of Backbone Composition on Homopolymer Dynamics and Brush Block Copolymer Self-Assembly

Bret M. Boyle, Joseph L. Collins, Tara E. Mensch, Matthew D. Ryan, Brian S. Newell, and Garret M. Miyake[a*]

[a]Department of Chemistry,
Colorado State University, Fort Collins, Colorado
*Corresponding Authors: Garret.Miyake@colostate.edu

TABLE OF CONTENTS

Materials and Methods:

$(H_2IMes)(PPh_3)(Cl)_2RuCHPh$ was purchased from Umicore and was converted to $(H_2IMes)(py)_2(Cl)_2RuCHPh$ via literature procedure.[1] All other chemicals were purchased from Sigma-Aldrich or VWR. All polymerizations were performed in a nitrogen-filled glovebox unless stated otherwise. Columns were run using a Combiflash Rf+ autocolumn from Teledyne ISCO. NMR spectra were recorded on a Bruker Ultrashield 400 MHz spectrometer. Chemical shifts were referenced using internal solvent resonance, ^1H: 7.26 ppm and ^{13}C: 77.16 ppm for $CDCl_3$. The chemical shifts are reported as parts per million relative to tetramethylsilane. Deuterated chloroform was purchased from Cambridge Isotope Laboratories.

Analysis of isolated and vacuum-dried polymer molecular weight and dispersity was performed using gel permeation chromatography (GPC) coupled with multi-angle light scattering (MALS), using an Agilent HPLC fitted with one guard column and three Plgel 5 uM MIXED-C gel permeation columns in series. The detectors used were a Wyatt Technology TrEX differential refractometer and a Wyatt Technology miniDAWN TREOS light scattering detector, which allows the direct measurement of absolute molecular weight. Absolute molecular weights were determined using dn/dc values calculated by assuming 100% mass recovery of the polymer sample injection into the GPC. The solvent used was tetrahydrofuran (THF) with a flow rate of 1.0 mL per minute. The R_z value of each polymer was calculated using the multi angle light scattering detector in the miniDAWN TREOS.

Thermal Gravimetric Analysis (TGA) was conducted using a TA Instruments TGA Q50 or TGA Q500. The thermal decomposition data was obtained under a nitrogen gas flow of 40 mL/min by ramping the temperature from 25 °C up to 850 °C at a ramp rate of about 10 °C/minute.

Differential Scanning Calorimetry (DSC) was conducted using a TA Instruments DSC 2500. To erase thermal history, an initial sweep ramped from 0 °C to 200 °C at a ramp rate of 10 °C/min. The temperature was held constant at 200 °C for 3 minutes before it was cooled to 0 °C at a ramp rate of -10 °C/min where the temperature was held constant at 0°C for 3 minutes. Thermal data was collected from the second sweep which consists of ramping the temperature from 0 °C up to 200 °C at a rate of 5 °C/min., isotherming at 200 °C again for 3 minutes before ramping back to 0 °C at a rate of -5 °C/minute. However, for the NB-Hep polymer, the range of the test was -90 °C to 150 °C, but the rates of heating and cooling were the same as the rates used to test the rest of the polymers. This was done to accommodate the low glass transition temperature of that particular polymer.

The rheological experiments were performed using a DHR-2 rheometer (TA Instruments) with 8 mm parallel plate geometry under nitrogen purge. The sample was loaded onto the 8 mm plate at experimental conditions until melting and then slowly pressed until the gap was approximately 1 mm using axial stress. Before testing, the samples were kept for 30 minutes – 2 hours until the axial stress was 0.0 ± 0.2 N. First, strain sweep experiments were performed to determine the linear viscoelastic region of the materials. Oscillatory frequency sweep was carried out from 0.01 to 100 rad/s with a strain in the linear strain regime. The temperature regime for the reference temperature of the time-temperature superposition (TTS) was determined based on the T_g of the polymer

series. The TTS was completed with a vertical and lateral shift within the TA Trios Software. Van Gurp-Palmen plots were used to establish the validity of the time-temperature superposition of the polymer series.

Reflection measurements were performed on a Cary 5000 UV/vis/NIR spectrophotometer, equipped with an integrating sphere diffuse reflectance accessory (DRA) (Internal DRA-2500) using the standard wide-open aperture. The samples were scanned at a rate of 600 nm/min from 800 to 280 nm.

Scanning electron microscopy images were taken on a JEOL JSM-6500F field emission scanning electron microscope after freeze fracturing the films and then staining the fractured films with RuO_4. The samples were coated with a 10 nm thick layer of gold before imaging.

Small-Angle X-ray Scattering (SAXS) characterization was carried out at the beamline 12-ID-B of the Advanced Photon Source (APS) at Argonne National Laboratory. X-rays of wavelength 0.9322 Å (13.3 keV) were used, and the sample to detector distance was calibrated using silver behenate as a standard. Samples were mounted on an XY stage with thermal capabilities. Each sample was exposed to the X-ray beam for 1s. The scattered X-rays were collected with a Pilatus2M detector located about 2 m downstream from the sample position. The 1D scattering spectra were obtained by radially averaging the images into scattering intensities versus the scattering vector, q.

Procedures:

Monomer Synthesis:

Exo-5-Norbornene-2-methanol

Preparation of exo-5-norbornene-2-methanol was prepared *via* slight modification to a previously reported procedure.[2] 12.4 g (3.0 eq, 326 mmol) of lithium aluminum hydride (LAH) was suspended in anhydrous THF (300 mL) under nitrogen atmosphere at 0C. 15.0 g of exo-5-norbornene-2-carboxylic acid was added to the suspension as a solution in dry THF (15.0 g/20 mL). The 1000 mL flask was placed in an oil bath, and the reaction mixture refluxed for 16 h. Next, the reaction mixture was cooled in an ice bath, and Feiser workup procedure followed: dilute with ether at 0 °C, slowly add 0.5 mL water, add 0.5 mL 15% aqueous sodium hydroxide, add 1.3 mL water, warm to room temperature and stir for 20 minutes, add magnesium sulfate, stir for 20 minutes, filter to remove salts. Next, the solution was concentrated under reduced pressure to yield a slightly yellow oil. The product was purified *via* distillation, yielding a colorless oil. Yield = 12.9 g, 95.5 %. ^{1}H NMR (400 MHz, $CDCl_3$) δ 6.05 (m, 2H), 3.67 (m, 1H), 3.50 (m, 1H), 2.99 (s, 0.15H), 2.91 (s, 0.15H), 2.79 (s, 1H), 2.73 (s, 1H), 2.10 (s, 1H), 1.83 (m, 0.1H), 1.59 (m, 1H), 1.27 (m, 3H), 1.08 (m, 1H).

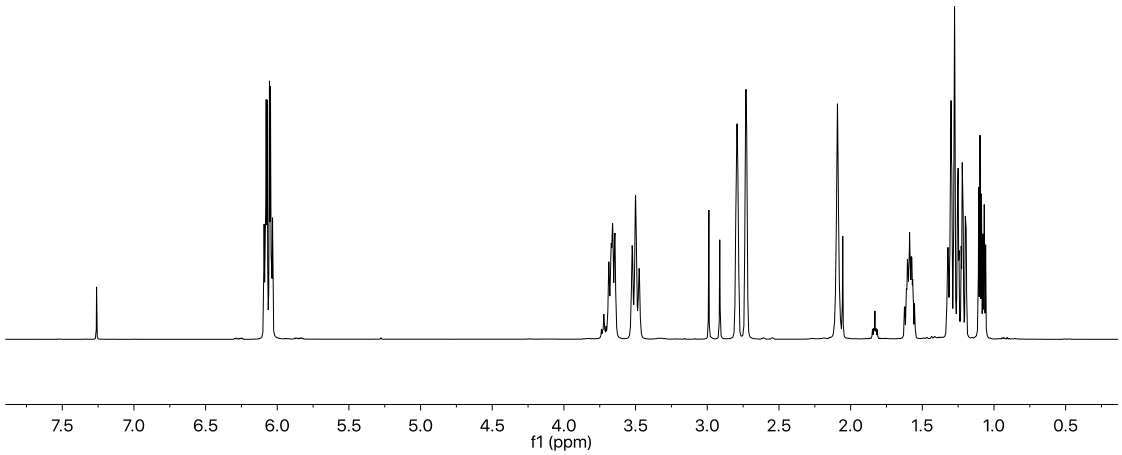

Figure S1. ^{1}H NMR spectra of exo-5-norbornene-2-methanol in CDCl3.

***Exo*-5-Norbornene-2-methyl heptanoate Monomer (NB-Hep)**

A 100 mL Schlenk flask was charged with a stir bar and flame-dried. Once the flask was backfilled with nitrogen, 1.0 g (1.1 eq, 8.1 mmol) of *exo*-5-norbornene-2-methanol, 0.95 g (1.0 eq, 7.3 mmol) of *n*-heptanoic acid, and 0.089 g (0.1 eq, 0.73 mmol) of 4-Dimethylaminopyridine was added to the Schlenk flask under positive nitrogen. These solids were then dissolved in 50 mL of anhydrous dichloromethane. The solution was then cooled to 0 °C while stirring before 1.5 g (1.5 eq., 9.5 mmol) of 1-Ethyl-3-(3-dimethylaminopropyl)carbodiimide was added slowly under positive nitrogen. The reaction solution was then allowed to stir and warm to room temperature for 16 hours. Next, the solution was washed with 0.1 M HCl twice and the organic layer was then dried over $MgSO_4$. The $MgSO_4$ was then filtered out before the solution was concentrated to an oily substance. Then, the crude product was dissolved in hexanes and run through a silica plug with 100 % Hexanes. The 1st peak was collected and concentrated in vacuo to yield the product as a clear oil. Yield = 0.77 g, 81 %. ^{1}H NMR (400 MHz, $CDCl_3$) δ 6.06 (m, 2H), 4.10 (m, 1H), 3.92 (m, 1H), 2.79 (s, 1H), 2.65 (s, 1H), 2.27 (t, 2H), 1.67 (m, 1H) 1.60 (m, 2H), 1.27 (m, 10H), 1.10 (m, 1H), 0.85 (m, 3H); ^{13}C NMR (101 MHz, $CDCl_3$) δ 173.79, 136.89, 136.26, 68.25, 44.95, 43.64, 41.59, 37.97, 34.47, 31.46, 29.64, 28.80, 24.94, 22.52, 14.07.

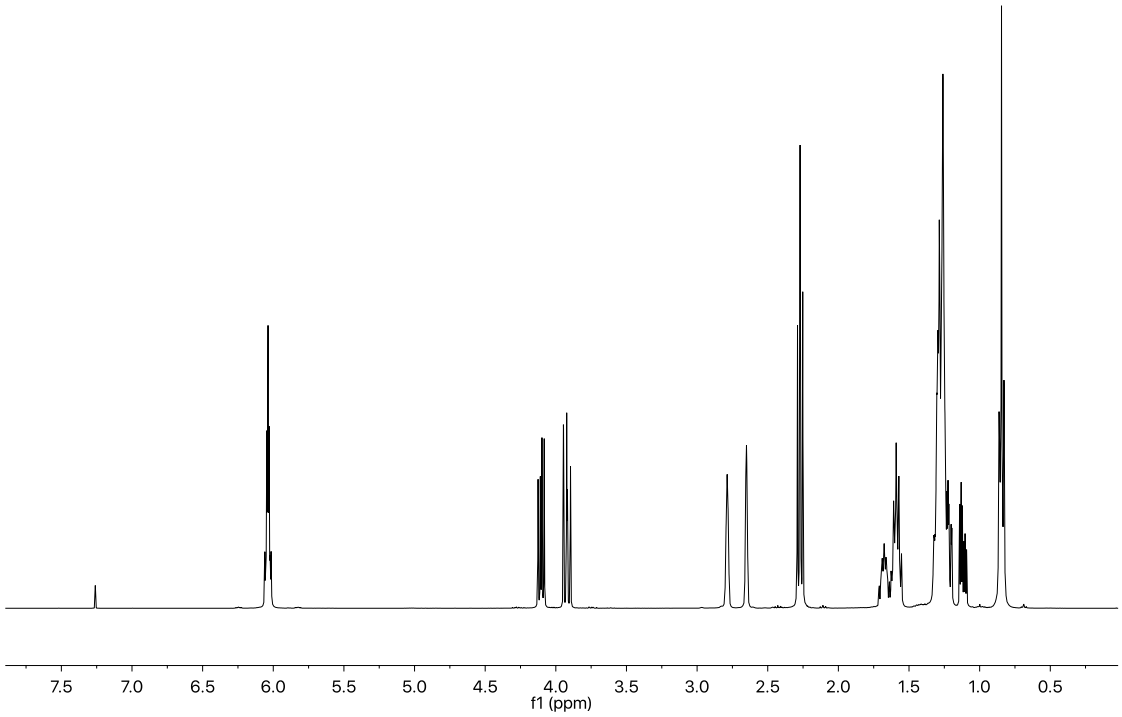

Figure S2. ^{1}H NMR spectra of NB-Hep monomer in CDCl3.

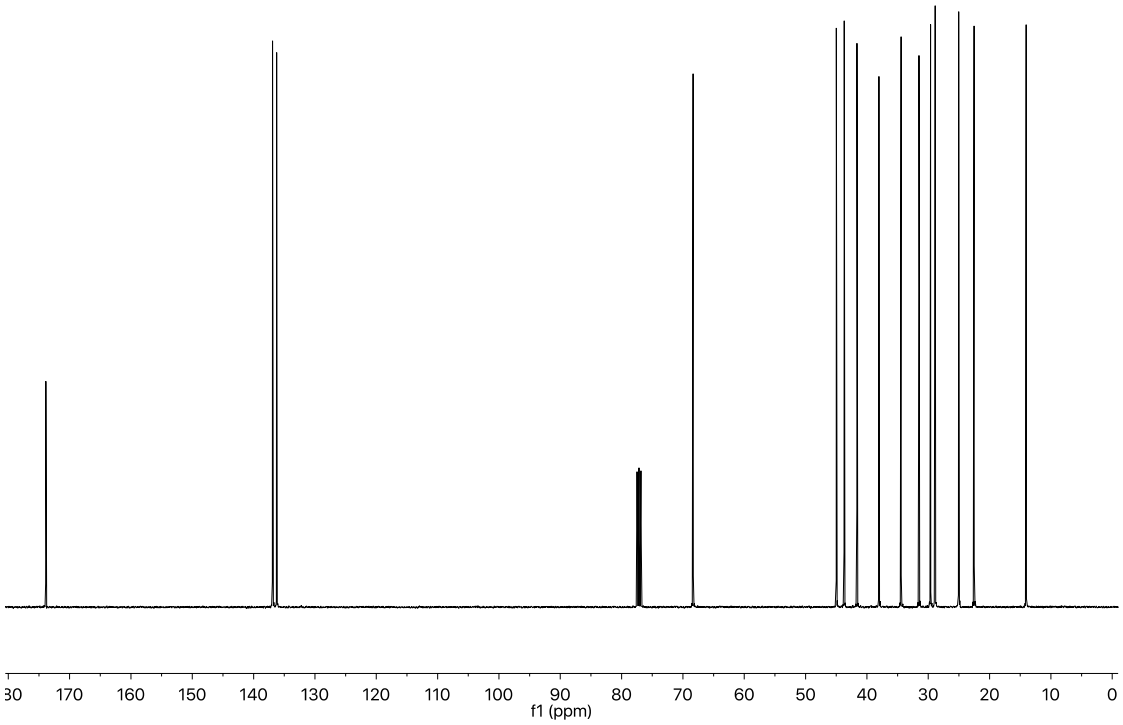

Figure S3. ^{13}C NMR spectra of NB-Hep monomer in CDCl3.

N-Methyl heptanoate -*exo*-Norbornene-5,6-dicarboximide Monomer (NBI-Hep)

N-(hydroxylethyl)-cis-5-norbornene-exo-2,3-dicarboximide was prepared according to literature procedure.[3] A 100 mL Schlenk flask was charged with a stir bar and flame-dried. Once the flask was backfilled with nitrogen, 2.0 g (1.1 eq, 9.7 mmol) of N-(hydroxylethyl)-cis-5-norbornene-exo-2,3-dicarboximide, 1.1 g (1.0 eq, 8.8 mmol) of *n*-heptanoic acid, and 0.32 g (0.1 eq, 2.6 mmol) of 4-Dimethylaminopyridine was added to the Schlenk flask under positive nitrogen. These solids were then dissolved in 30 mL of anhydrous dichloromethane. The solution was then cooled to 0 °C while stirring before 2.3 g (1.5 eq., 13 mmol) of 1-Ethyl-3-(3-dimethylaminopropyl)carbodiimide was added slowly under positive nitrogen. The reaction solution was then allowed to stir and warm to room temperature for 16 hours. Next, the solution was washed with 0.1 M HCl twice and the organic layer was then dried over $MgSO_4$. The $MgSO_4$ was then filtered out before the solution was concentrated to an oily substance. Then, the crude product was dissolved in a 2 hexanes : 1 ethyl acetate mixture and run through a silica column. The product peak was collected and concentrated in vacuo to yield the product as a clear oil. Yield = 1.6 g, 80 %. ^{1}H NMR (400 MHz, $CDCl_3$) δ 6.28 (s, 2H), 4.23 (t, 2H), 3.74 (t, 2H), 3.27 (t, 2H), 2.69 (s, 2H), 2.25 (t, 2H), 1.55 (m, 3H), 1.28 (m, 7H), 0.85 (m, 3H); ^{13}C NMR (101 MHz, $CDCl_3$) δ 178.20, 173.06, 138.01, 60.55, 47.95, 45.37, 42.81, 37.72, 34.24, 31.57, 28.90, 24.78, 22.60, 14.14.

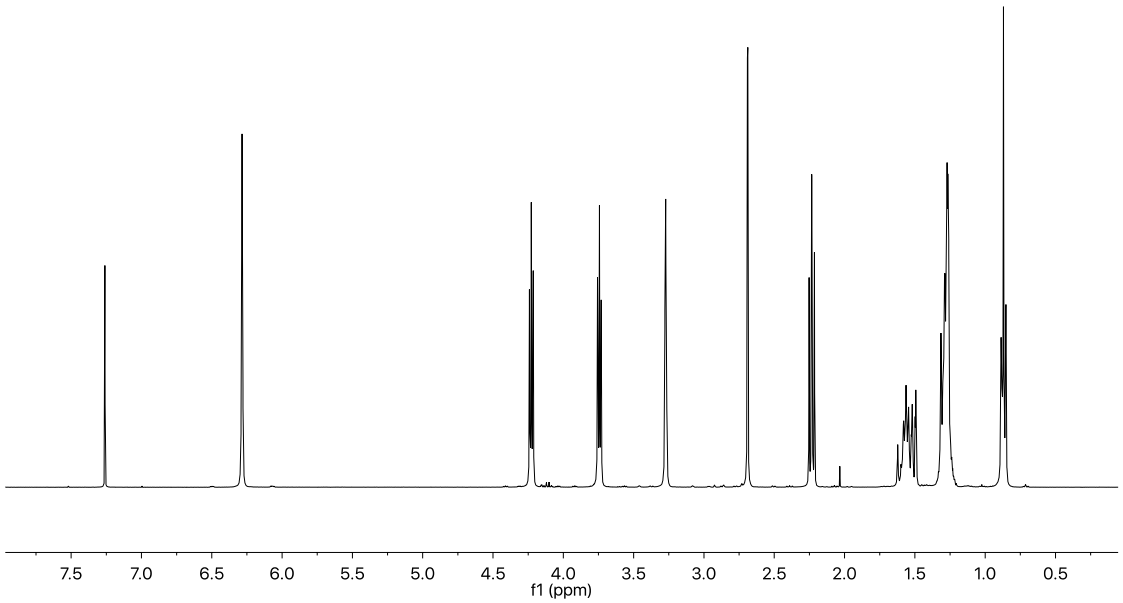

Figure S4. ^{1}H NMR spectra of NBI-Hep monomer in CDCl3.

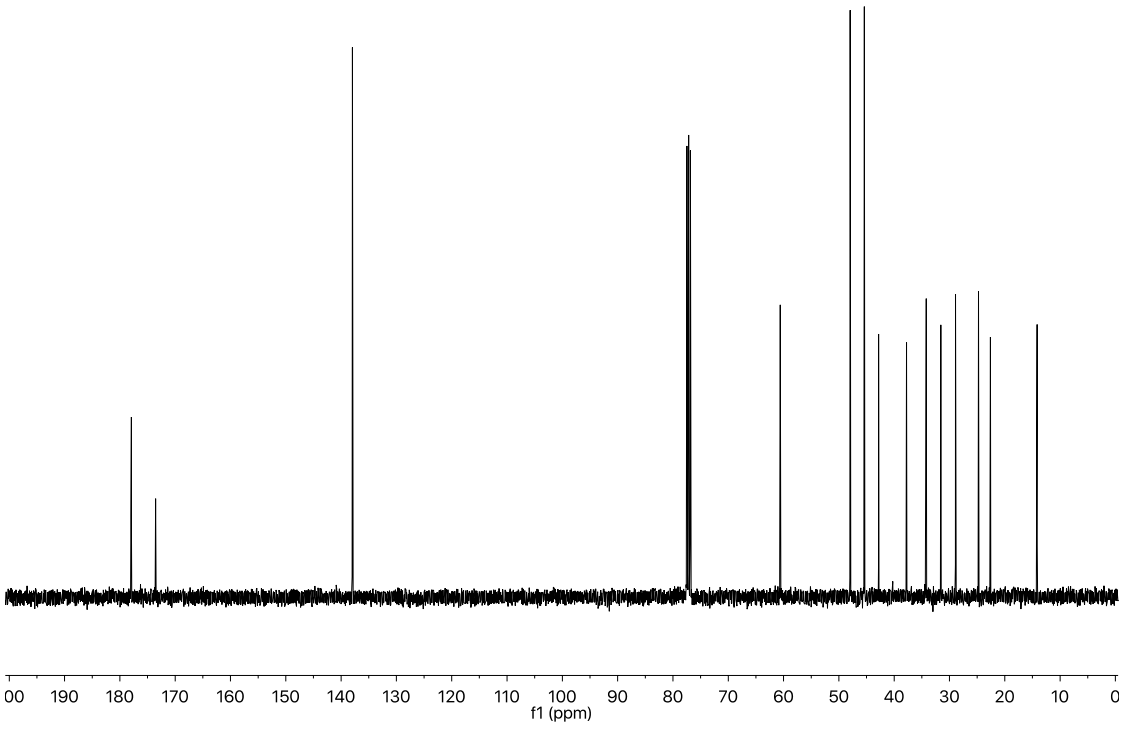

Figure S5. ^{13}C NMR spectra of NBI-Hep monomer in CDCl3.

N-Decyl-*exo*-Norbornene-5,6-dicarboximide Monomer (DecNBI)

N-Decyl-exo-Norbornene-5,6-dicarboximide was prepared according to literature procedure.[4] There was one adjustment made to the reported synthetic procedure, which was to use *n*-decylamine instead of *n*-hexylamine. ^{1}H NMR (400 MHz, $CDCl_3$) δ 6.25 (s, 2H), 3.41 (t, 2H), 3.25 (s, 2H), 2.64 (s, 2H), 1.50 (m, 3H), 1.25 (m, 16H), 0.85 (t, 3H).

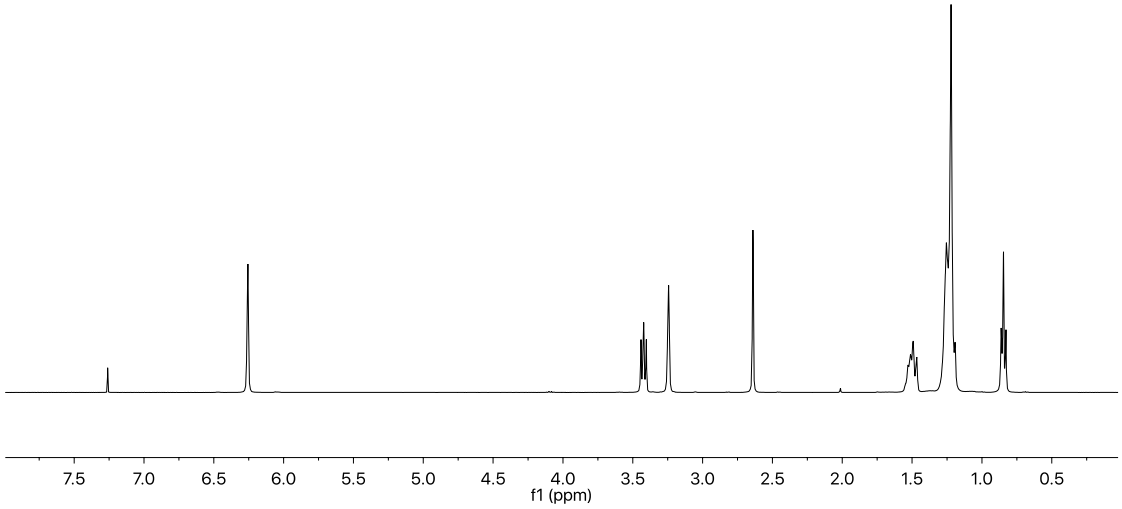

Figure S6. ^{1}H NMR spectra of NBI-Decyl monomer in CDCl3.

Macromonomer Synthesis:

Norbornene capped Poly(lactide) Macromonomer (NB-PLA MM)

To a degassed, backfilled with nitrogen, and three times flame dried 500mL Schlenk flask equipped with a stir bar was added freshly sublimed and stored under nitrogen racemic lactide monomer (20.0 g, 0.14 mol, 22 eq.), $Sn(Oct_2)$ [purity 92.5-100% purchased from Sigma and used as is] (4.2 uL, 0.4% wt. relative to alcohol initiator), and exo-5-norbornene-2-methanol (1.3 g, 11 mmol, 1.0 eq.). Once combined, the reaction mixture was placed in an oil bath preheated to 130 °C. During the reaction, the lactide sublimes on the sidewalls of the flask: to mitigate this issue, a Bunsen burner was used to heat the sidewalls every 15 minutes to melt lactide monomer back into solution. This heating of the sidewalls was done to ensure consumption of monomer. The reaction was complete in 4 hours, which was qualitatively tracked by the rate of sublimation of lactide onto the sidewalls. After monomer consumption was determined to be complete, the NB-PLA was allowed to cool and dissolved in anhydrous DCM and diluted to a concentration of 1g NB-PLA / 15 mL. The DCM solution was filtered through ~100 g of celite to remove tin catalyst. Once the solution was completely filtered an additional 200 mL of

DCM was washed through the celite pad to recover any remaining polymer. Solvent was removed under reduced pressure. The NB-PLA was then dried in a vacuum overnight at 60 - 70 °C to remove remaining solvent, giving a near quantitative yield (<95%). For the BBCP MM, the GPC results show a MM with M_n = 3,251 g/mol PDI = 1.07. For the homobrush MM, the GPC results show a MM with M_n = 3,065 g/mol PDI = 1.21.

Norbornene-imide capped Poly(lactide) Macromonomer (NBI-PLA MM)

The procedure for the synthesis of NB-PLA was used to make NBI-PLA, however, N-(hydroxylethyl)-cis-5-norbornene-exo-2,3-dicarboximide was used in place of exo-5-norbornene-2-methanol as the initiator. For the BBCP MM, the GPC results show a MM with M_n = 3,428 g/mol PDI = 1.06. For the homobrush MM, the GPC results show a MM with M_n = 3,150 g/mol PDI = 1.13.

Norbornene capped Poly(styrene) Macromonomer (NB-PS MM)

This macromonomer was made following the universal thermally-driven ATRP conditions for styrene with slight modifications.[5] The ATRP initiator, N - ((2 – Bromo – 2 - methylpropanoyl) ethyl) – cis – 5 – norbornene – *exo* -2 – methanol, was prepared as previously reported.[6]

To a degassed, backfilled with nitrogen, and three times flame dried 200 mL Schlenk flask equipped with a stir bar was added freshly distilled styrene monomer (23 g, 0.23 mol, 58 eq.), N - ((2 – Bromo – 2 - methylpropanoyl) ethyl) – cis – 5 – norbornene – *exo* -2 - methanol (1.1 g, 3.9 mmol, 1.0 eq.), pre-activated copper wire (5 cm), copper bromide (0.043 g, 0.19 mmol, 0.05 eq), and 2-propanol (26 mL). To pre-activate the copper wire, it was soaked in concentrated hydrochloric acid for 15 minutes, and rinsed in DI water and dried. This mixture was then sparged with nitrogen for 15 minutes. Once the solution had been sparged, N-pentamethyldiethylenetriamine (0.24 g, 1.4 mmol, 0.36 eq) was added to the mixture and heated to 60 °C while stirring. The reaction was monitored via NMR and was cooled down to room temperature at 50 % conversion of monomer to polymer.

Once cooled, the reaction mixture was dissolved in DCM and filtered through a large, neutral alumina column to remove the copper salts. The resulting solution was then concentrated in vacuo before using column chromatography to purify the product. Three 80 gram silica columns were loaded with the crude polymer product and a gradient column was run starting with 35 % DCM and 65 % Hexanes ramping up to 100 % DCM. The purified product peak was then isolated and concentrated in vacuo. This product was then dissolved in DCM and precipitated into room temperature methanol. The precipitate was then filtered and dried in a vacuum oven overnight at 70 °C. Yield = 16 %, M_n = 3,649 g/mol, PDI = 1.05

Norbornene-imide capped Poly(styrene) Macromonomer (NBI-PS MM)

The same procedure for the synthesis of NB-PS was used to make NBI-PS, however, the ATRP initiator, N - ((2 – Bromo – 2 - methylpropanoyl) ethyl) – cis – 5 – norbornene – *exo* -2,3-dicarboximide (3.5 g, 9.9 mmol, 1.0 eq.), was used in place of the previous initiator, N - ((2 – Bromo – 2 - methylpropanoyl) ethyl) – cis – 5 – norbornene – *exo* -2 - methanol. This procedure was completed as previously reported.[7] Yield = 10 %, M_n = 4,422 g/mol, PDI = 1.01.

General Homopolymer Synthesis:

In a nitrogen-filled glovebox, a 20 mL vial was charged with a stir bar, 0.1 g of monomer or macromonomer and diluted to 0.05 M with anhydrous THF. With rapid stirring, the appropriate amount of G3 catalyst completely dissolved in THF was quickly added via syringe. At full conversion determined by GPC, the polymerization was quenched by the addition of 0.5 mL of ethyl vinyl ether. The polymer was precipitated out into 20 mL of methanol at room temperature (except for the PLA homobrushes and NB-Hep polymers which were precipitated into methanol at -78 °C), after which the polymer was isolated, washed with excess methanol, and dried under reduced pressure at 50 °C to a constant weight. Yield was near quantitative by mass.

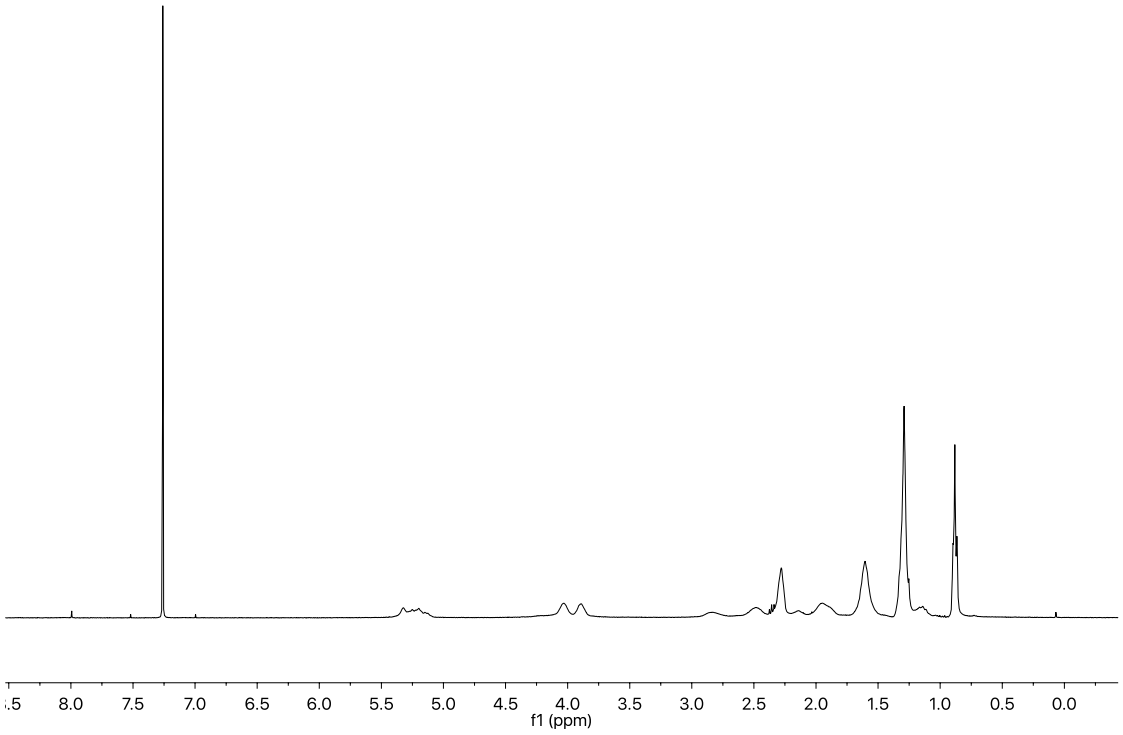

Figure S7. Isolated and representative poly(NB-Hep) (polymer shown M_n = 2.55x10^2 kg/mol) ^{1}H NMR (400 MHz, CDCl3): δ 5.27 (m), 3.97 (d), 2.86 (bs), 2.5 (bs), 2.29 (m), 2.15 (bs), 1.97 (bs), 1.61 (bs), 1.24 (m), 0.90 (s) [Water singlet from CDCl3 at 1.55 ppm].

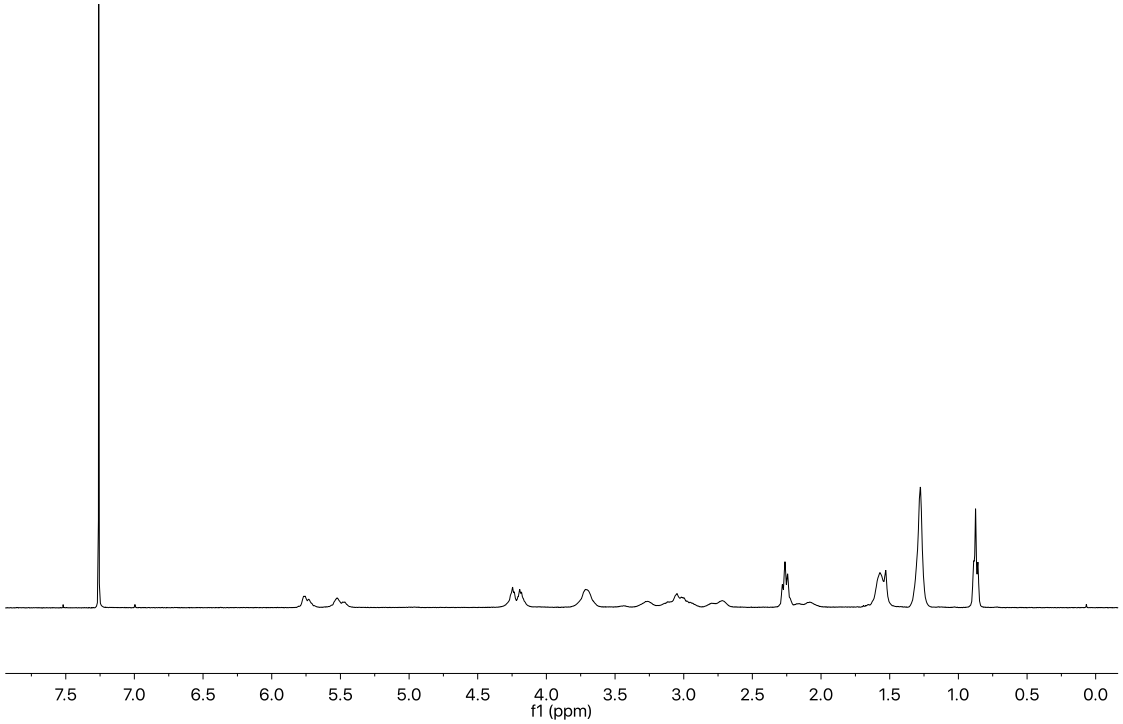

Figure S8. Isolated and representative poly(NBI-Hep) (polymer shown M_n = 3.74x10^2 kg/mol) ^{1}H NMR (400 MHz, CDCl3): δ 5.75 (d), 5.50 (d), 4.23 (d), 3.71 (bs), 3.02 (m), 2.25 (m), 1.57 (bs), 1.28 (bs), 0.88 (m) [Water singlet from CDCl3 at 1.55 ppm].

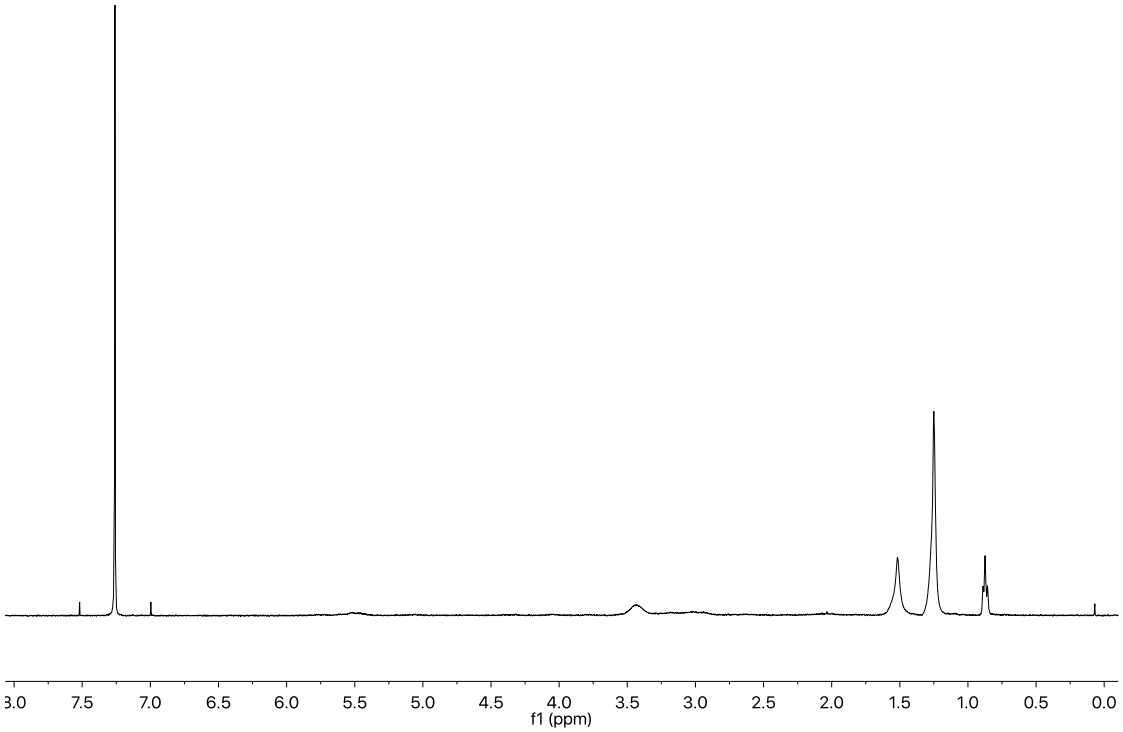

Figure S9. Isolated and representative poly(NBI-Dec) (polymer shown M_n = 7.80x10^2 kg/mol) ^{1}H NMR (400 MHz, CDCl3): δ 5.50 (bs), 3.43 (bs), 1.51 (bs), 1.24 (s), 0.88 (t) [Water singlet from CDCl3 at 1.55 ppm].

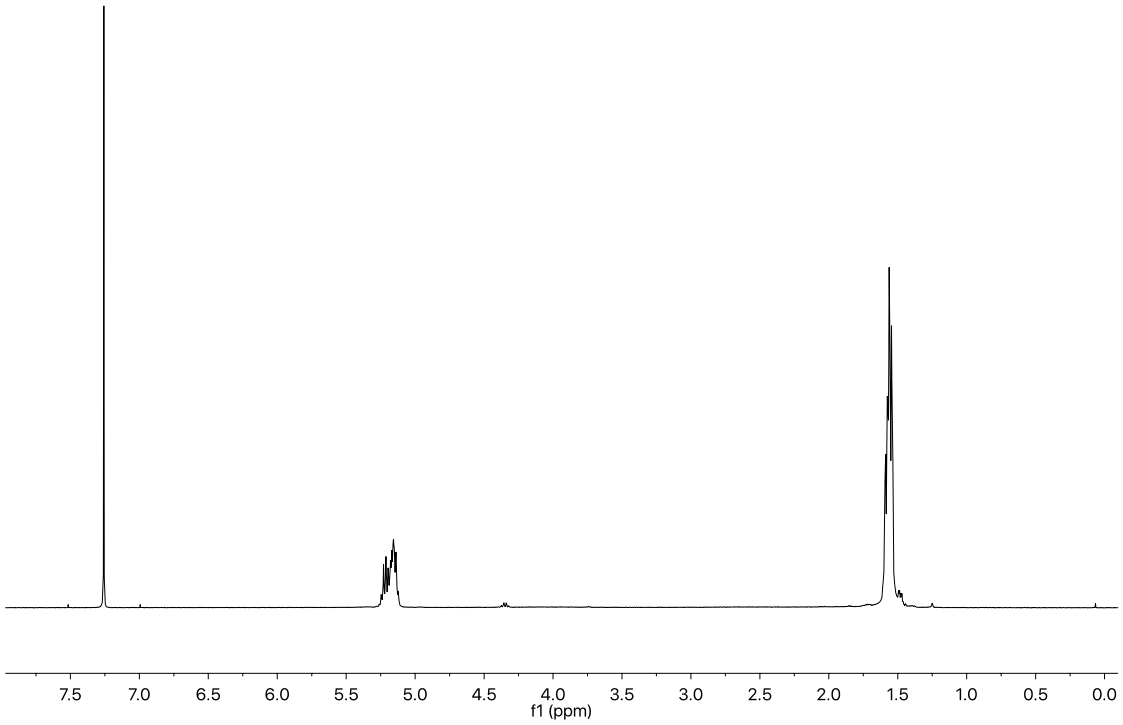

Figure S10. Isolated and representative poly(NB-PLA) (polymer shown M_n = 1.56x10^3 kg/mol) ^{1}H NMR (400 MHz, CDCl3): δ 5.18 (m), 4.35 (q), 1.56 (m), 1.26 (s) [Water singlet from CDCl3 at 1.55 ppm].

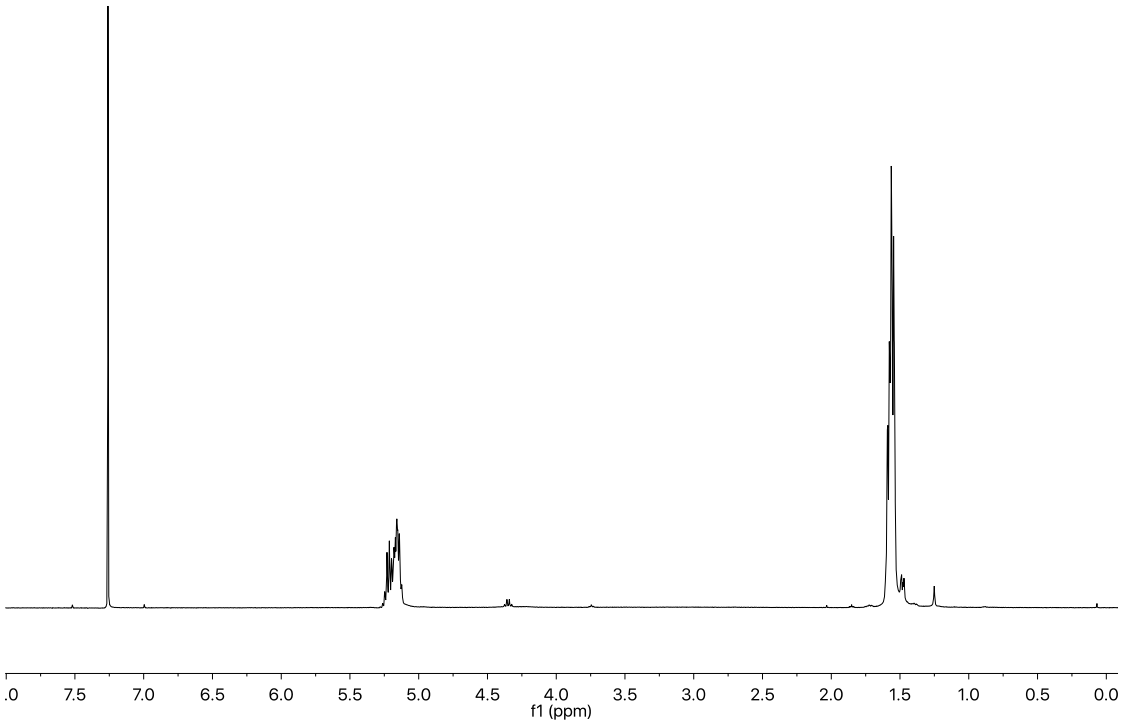

Figure S11. Isolated and representative poly(NBI-PLA) (polymer shown M_n = 3.58x10^3 kg/mol) ^{1}H NMR (400 MHz, CDCl3): δ 5.18 (m), 4.35 (q), 3.75 (m), 1.56 (m), 1.26 (s) [Water singlet from CDCl3 at 1.55 ppm].

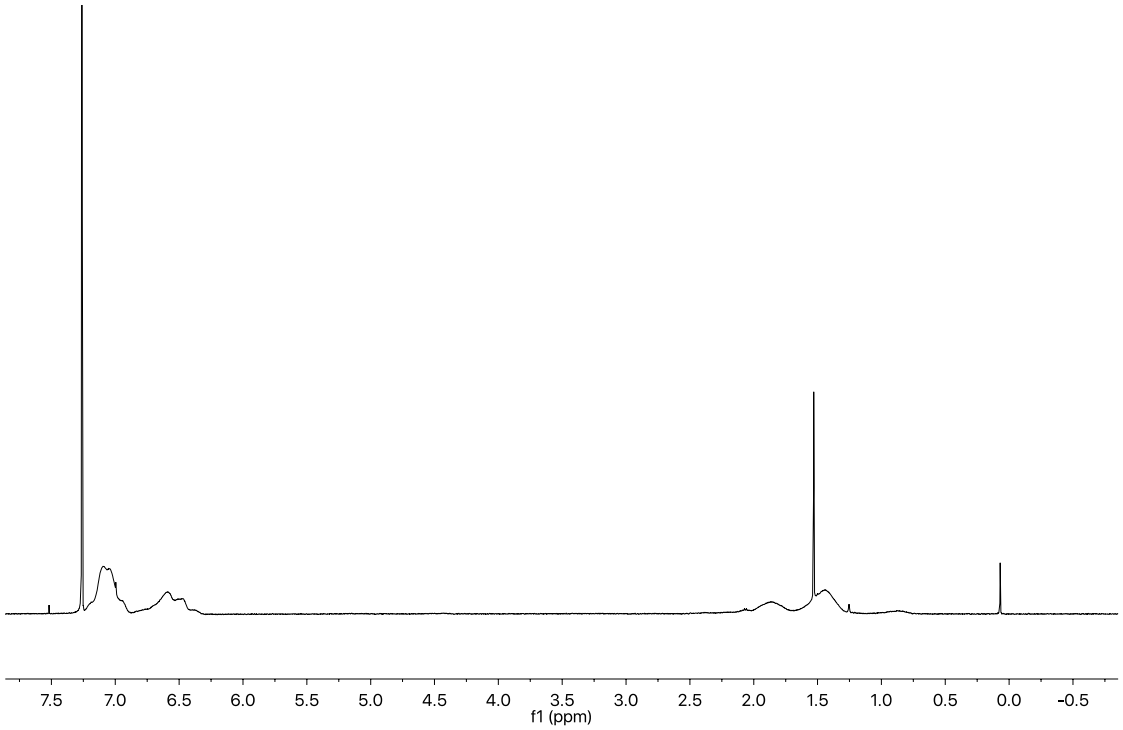

Figure S12. Isolated and representative poly(NB-PS) (polymer shown M_n = 1.24x10^3 kg/mol) ^{1}H NMR (400 MHz, CDCl3): δ 7.08 (m), 6.62 (m), 1.86 (bs), 1.46 (bs), 0.87 (bs), [Water singlet from CDCl3 at 1.55 ppm].

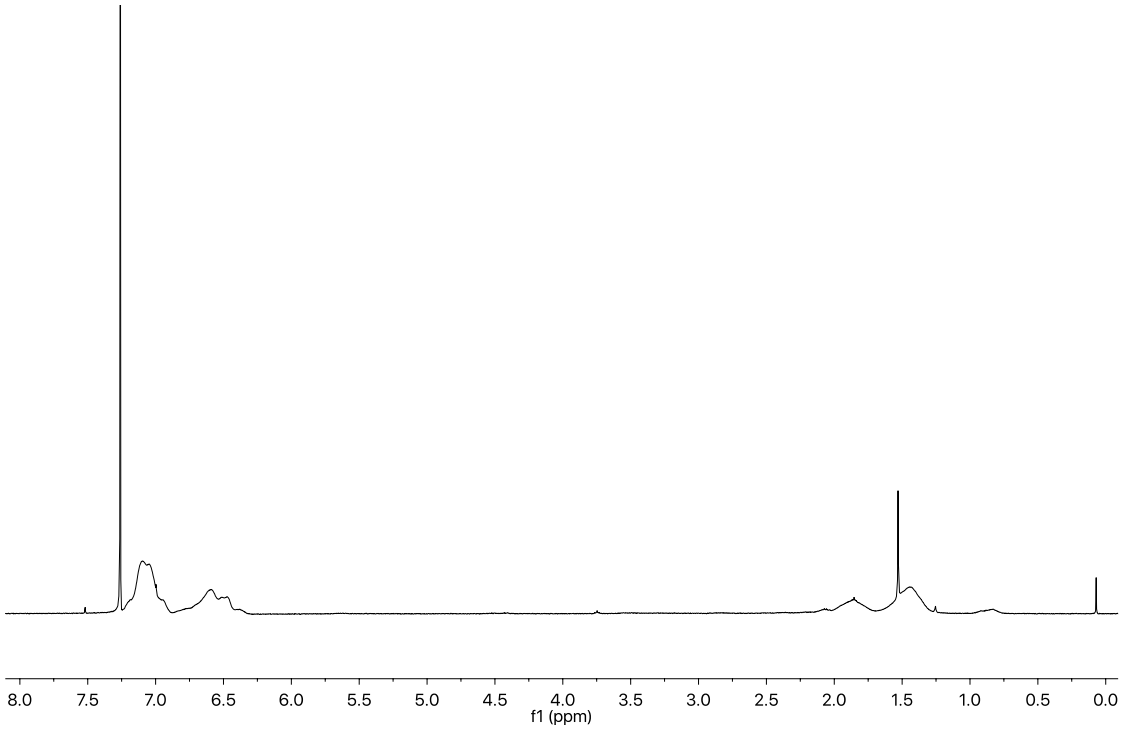

Figure S13. Isolated and representative poly(NBI-PS) (polymer shown M_n = 1.12x10^3 kg/mol) ^{1}H NMR (400 MHz, CDCl3): δ 7.08 (m), 6.62 (m), 1.86 (bs), 1.46 (bs), 0.86 (bs), [Water singlet from CDCl3 at 1.55 ppm].

Homopolymer Characterization via Gel Permeation – Multi Angle Light Scattering Traces (GPC-MALS):

Table S1. GPC-MALS analysis data of poly(NB-Hep) MW series.

Polymer Sample	GPC M_n (kg/mol)	GPC M_w (kg/mol)	Dispersity (M_w/M_n)	Degree of Polymerization from M_n
p(NB-Hep)-DP107	25.3	25.5	1.01	107
p(NB-Hep)-DP325	76.9	80.6	1.05	325
p(NB-Hep)-DP376	89.0	96.1	1.08	376
p(NB-Hep)-DP437	$1.03x10^2$	$1.18x10^2$	1.14	437
p(NB-Hep)-DP465	$1.10x10^2$	$1.45x10^2$	1.32	465
p(NB-Hep)-DP721	$1.70x10^2$	$1.94x10^2$	1.14	721
p(NB-Hep)-DP996	$2.36x10^2$	$2.58x10^2$	1.10	996
p(NB-Hep)-DP1028	$2.43x10^2$	$3.50x10^2$	1.44	1,028
p(NB-Hep)-DP1077	$2.55\ x10^2$	$3.09x10^2$	1.21	1,077

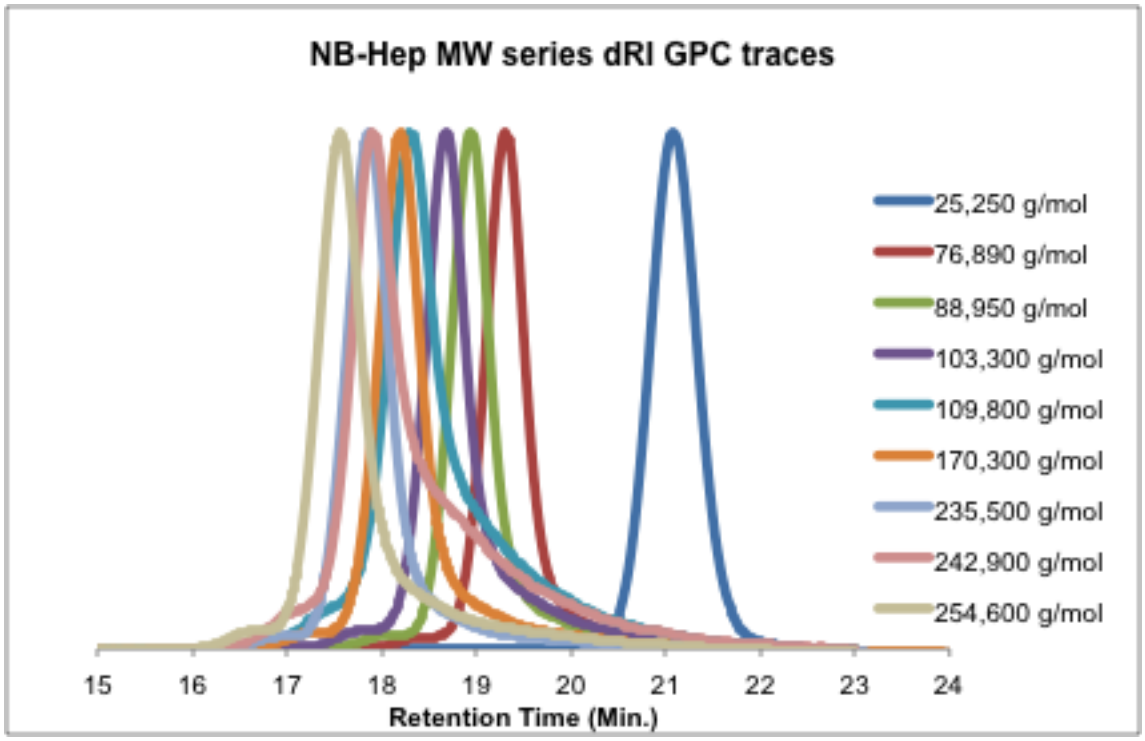

Figure S14. Relative Scaling of GPC RI detector traces for p(NB-Hep) MW series.

Table S2. GPC-MALS analysis data of poly(NBI-Hep) MW series.

Polymer Sample	GPC M_n (kg/mol)	GPC M_w (kg/mol)	Dispersity (M_w/M_n)	Degree of Polymerization from M_n
p(NBI-Hep)-DP29	9.20	9.49	1.03	29
p(NBI-Hep)-DP75	23.9	24.5	1.02	75
p(NBI-Hep)-DP110	35.4	36.0	1.02	110
p(NBI-Hep)-DP148	47.3	47.8	1.01	148
p(NBI-Hep)-DP260	83.0	84.1	1.01	260
p(NBI-Hep)-DP360	$1.15x10^2$	$1.17x10^2$	1.02	360
p(NBI-Hep)-DP454	$1.45x10^2$	$1.48x10^2$	1.02	454
p(NBI-Hep)-DP495	$1.58x10^2$	$1.61x10^2$	1.02	495
p(NBI-Hep)-DP618	$1.98x10^2$	$2.08x10^2$	1.05	618
p(NBI-Hep)-DP621	$1.98x10^2$	$2.04x10^2$	1.03	621
p(NBI-Hep)-DP1051	$3.36x10^2$	$3.46x10^2$	1.03	1,051
p(NBI-Hep)-DP1135	$3.63x10^2$	$3.73x10^2$	1.03	1,135
p(NBI-Hep)-DP1172	$3.74x10^2$	$3.83x10^2$	1.02	1,172

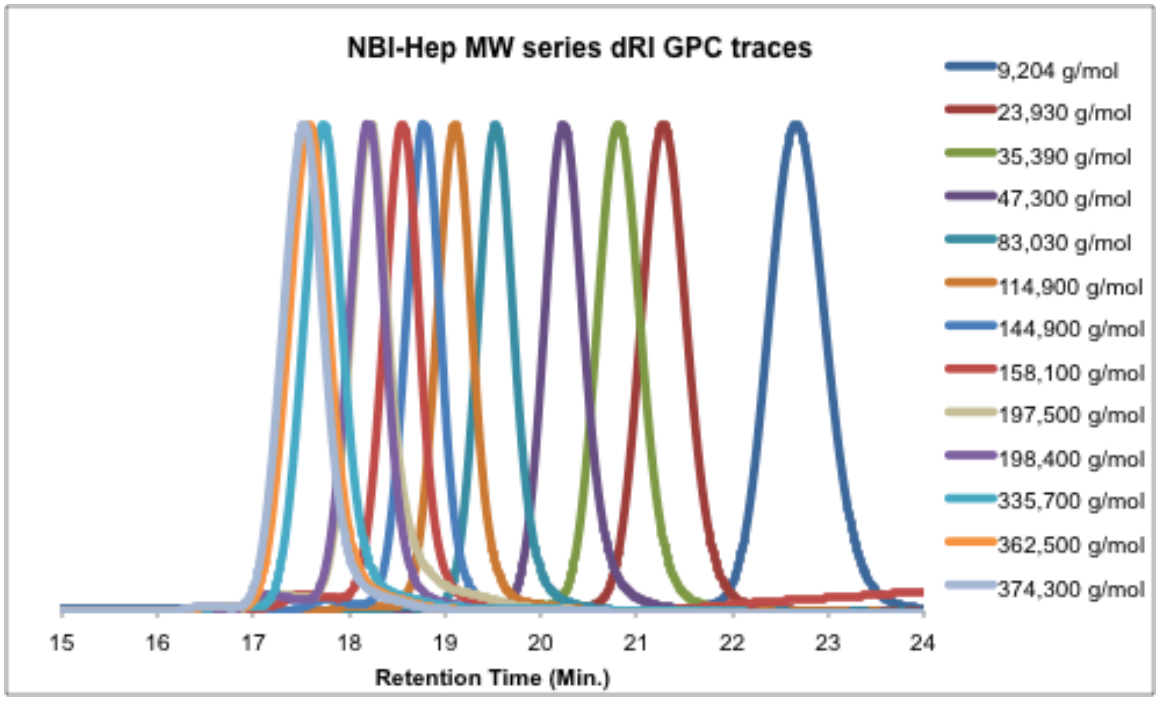

Figure S15. Relative Scaling of GPC RI detector traces for p(NBI-Hep) MW series.

Table S3. GPC-MALS analysis data of poly(NBI-Dec) MW series.

Polymer Sample	GPC M_n (kg/mol)	GPC M_w (kg/mol)	Dispersity (M_w/M_n)	Degree of Polymerization from M_n
p(NBI-Dec)-DP227	68.8	69.9	1.02	227
p(NBI-Dec)-DP376	$1.14x10^2$	$1.16x10^2$	1.02	376
p(NBI-Dec)-DP512	$1.56x10^2$	$1.58x10^2$	1.02	512
p(NBI-Dec)-DP863	$2.62x10^2$	$2.69x10^2$	1.03	863
p(NBI-Dec)-DP972	$2.95x10^2$	$3.07x10^2$	1.04	972
p(NBI-Dec)-DP1575	$4.78x10^2$	$5.48x10^2$	1.15	1,575
p(NBI-Dec)-DP2261	$6.86x10^2$	$7.92x10^2$	1.15	2,261
p(NBI-Dec)-DP2570	$7.80x10^2$	$9.50x10^2$	1.22	2,570

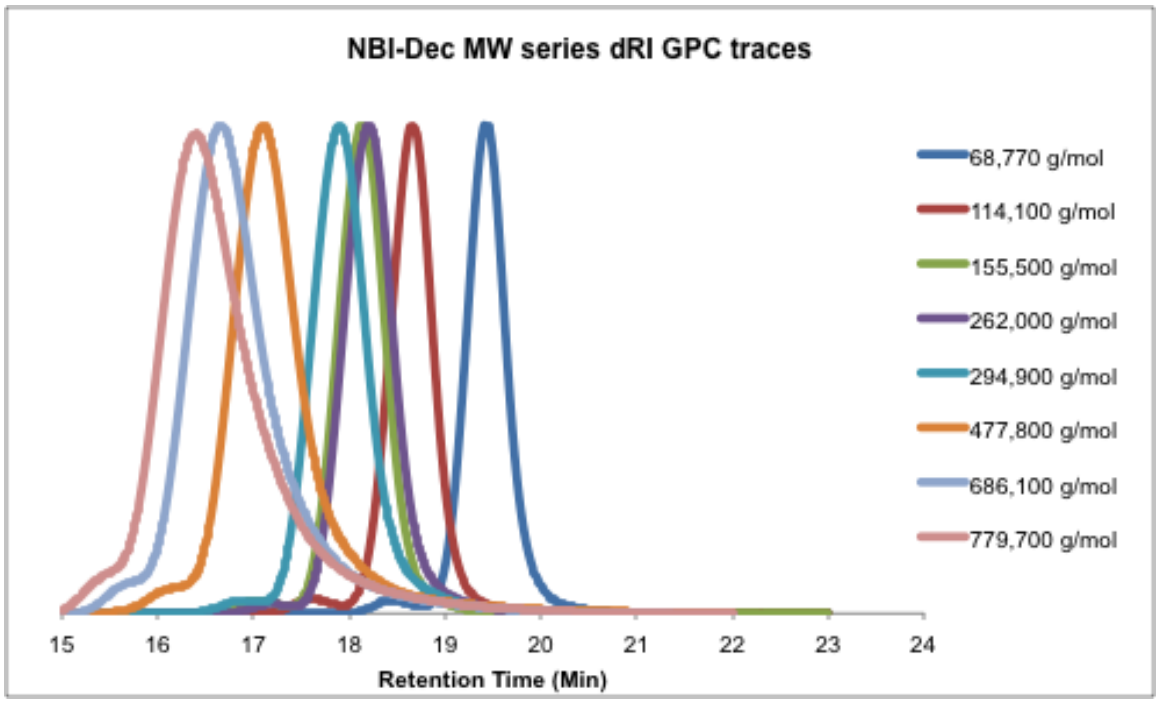

Figure S16. Relative Scaling of GPC RI detector traces for p(NBI-Dec) MW series.

Table S4. GPC-MALS analysis data of poly(NB-PLA) MW series.

Polymer Sample	GPC M_n (kg/mol)	GPC M_w (kg/mol)	Dispersity (M_w/M_n)	Degree of Polymerization from M_n
p(NB-PLA)-DP14	42.3	43.0	1.02	14
p(NB-PLA)-DP22	68.2	69.9	1.03	22
p(NB-PLA)-DP24	74.7	75.5	1.01	24
p(NB-PLA)-DP68	2.10×10^2	2.12×10^2	1.01	68
p(NB-PLA)-DP69	2.12×10^2	2.16×10^2	1.02	69
p(NB-PLA)-DP95	2.91×10^2	2.99×10^2	1.03	95
p(NB-PLA)-DP147	4.50×10^2	4.65×10^2	1.03	147
p(NB-PLA)-DP184	5.65×10^2	5.79×10^2	1.02	184
p(NB-PLA)-DP298	9.13×10^2	9.50×10^2	1.04	298
p(NB-PLA)-DP442	1.36×10^3	1.53×10^3	1.13	442
p(NB-PLA)-DP510	1.56×10^3	1.88×10^3	1.20	510

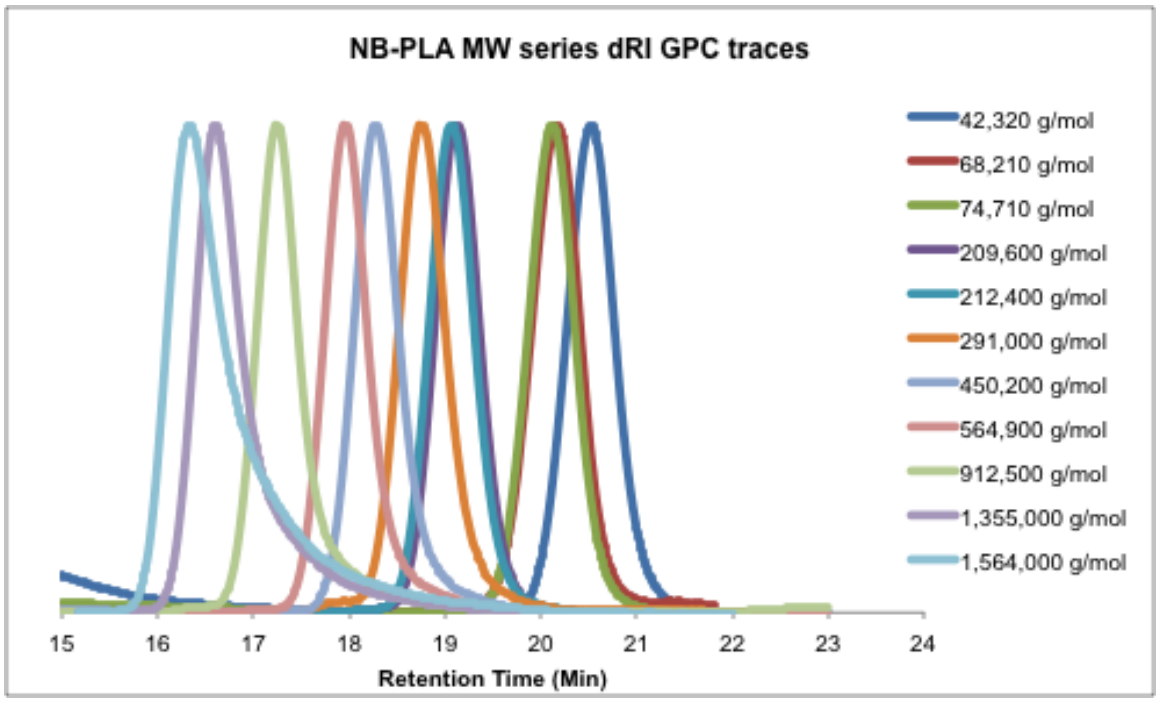

Figure S17. Relative Scaling of GPC RI detector traces for p(NB-PLA) MW series.

Table S5. GPC-MALS analysis data of poly(NBI-PLA) MW series.

Polymer Sample	GPC M_n (kg/mol)	GPC M_w (kg/mol)	Dispersity (M_w/M_n)	Degree of Polymerization from M_n
p(NBI-PLA)-DP22	69.7	71.0	1.02	22
p(NBI-PLA)-DP67	$2.12x10^2$	$2.19x10^2$	1.03	67
p(NBI-PLA)-DP81	$2.55x10^2$	$2.70x10^2$	1.06	81
p(NBI-PLA)-DP185	$5.84x10^2$	$5.91x10^2$	1.01	185
p(NBI-PLA)-DP339	$1.07x10^3$	$1.12\ x10^3$	1.05	339
p(NBI-PLA)-DP526	$1.66x10^3$	$1.73x10^3$	1.05	526
p(NBI-PLA)-DP1135	$3.58x10^3$	$3.77x10^3$	1.05	1,135

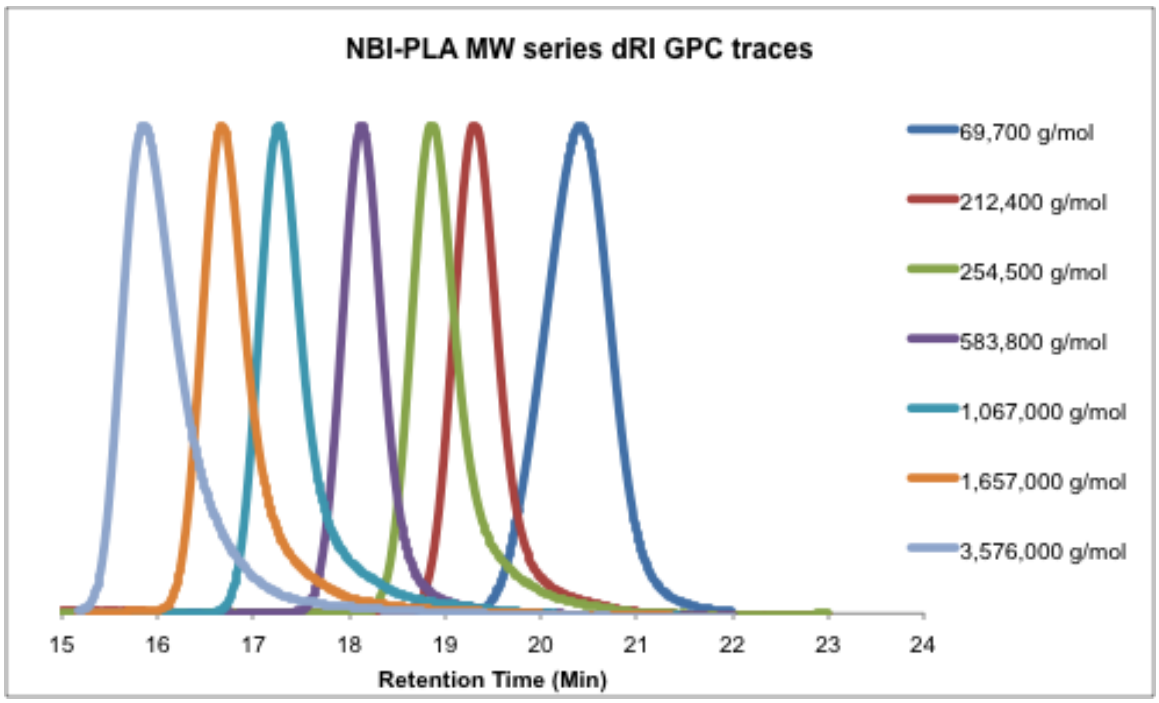

Figure S18. Relative Scaling of GPC RI detector traces for p(NBI-PLA) MW series.

Table S6. GPC-MALS analysis data of poly(NB-PS) MW series

Polymer Sample	GPC M_n (kg/mol)	GPC M_w (kg/mol)	Dispersity (M_w/M_n)	Degree of Polymerization from M_n
p(NB-PS)-DP61	$2.24x10^2$	$2.28x10^2$	1.02	61
p(NB-PS)-DP172	$6.26x10^2$	$6.39x10^2$	1.02	172
p(NB-PS)-DP289	$1.06x10^3$	$1.08x10^3$	1.02	289
p(NB-PS)-DP340	$1.24x10^3$	$1.33x10^3$	1.07	340

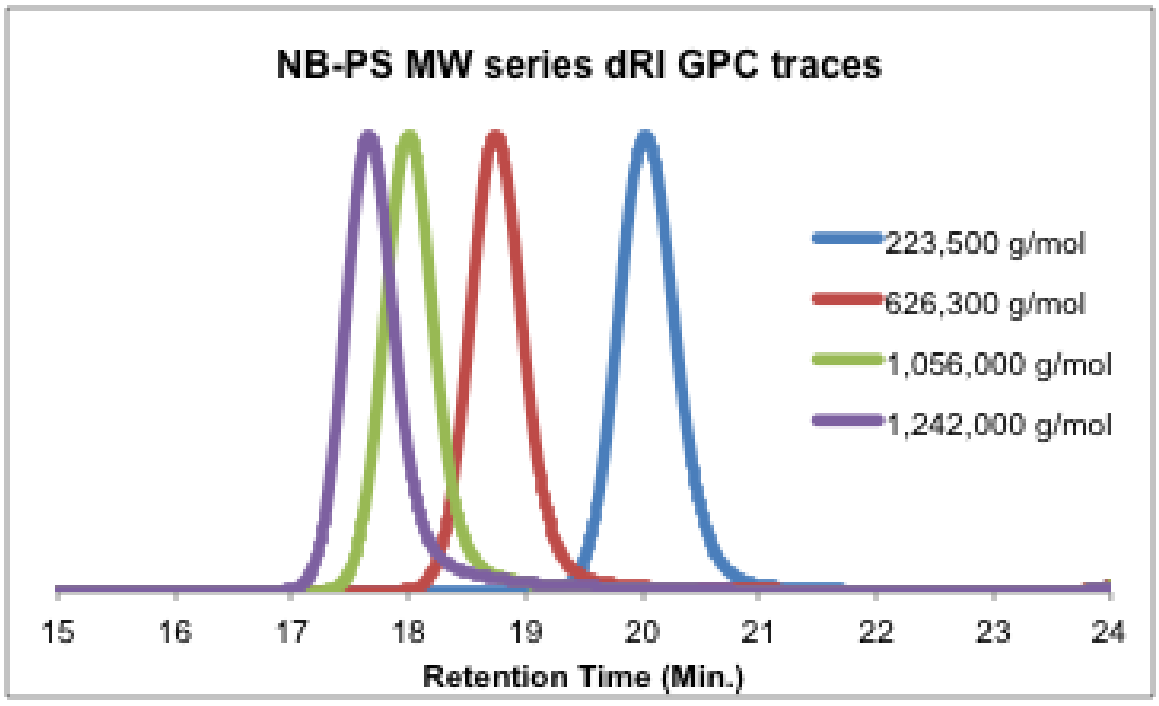

Figure S19. Relative Scaling of GPC RI detector traces for p(NB-PS) MW series.

Table S7. GPC-MALS analysis data of poly(NBI-PS) MW series.

Polymer Sample	GPC M_n (kg/mol)	GPC M_w (kg/mol)	Dispersity (M_w/M_n)	Degree of Polymerization from M_n
p(NBI-PS)-DP53	$1.98x10^2$	$2.00x10^2$	1.01	53
p(NBI-PS)-DP140	$5.28x10^2$	$5.38x10^2$	1.02	140
p(NBI-PS)-DP219	$8.24x10^2$	$8.41x10^2$	1.02	219
p(NBI-PS)-DP298	$1.12x10^3$	$1.16x10^3$	1.04	298

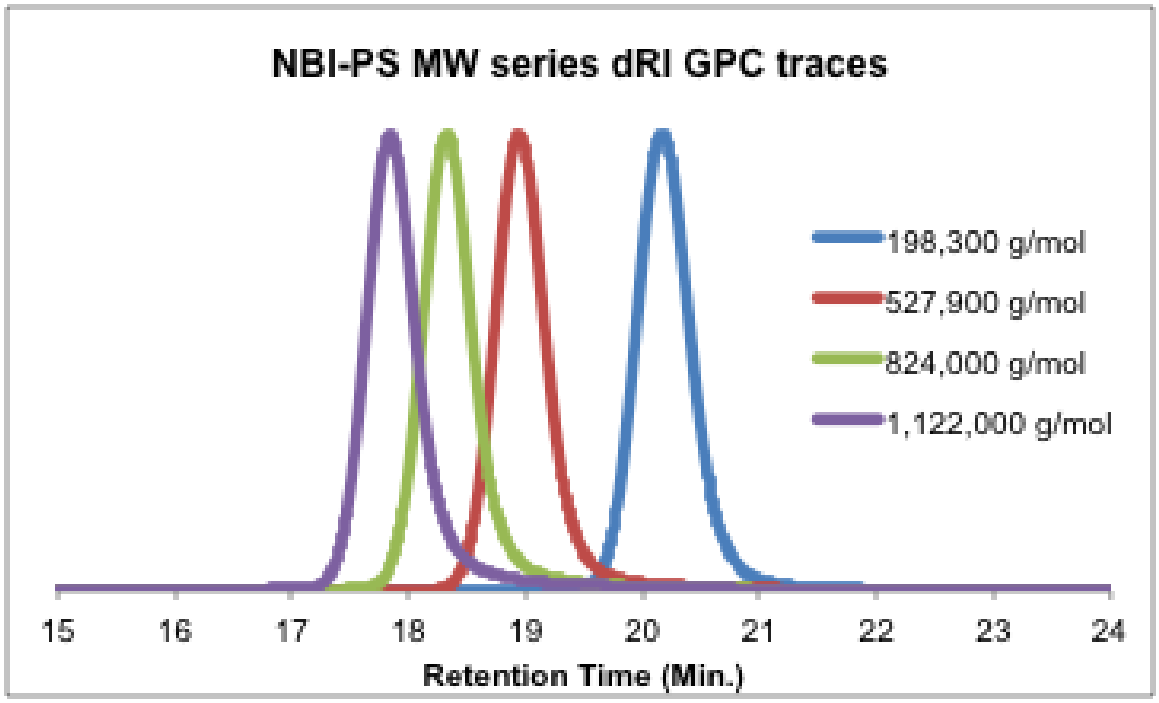

Figure S20. Relative Scaling of GPC RI detector traces for p(NBI-PS) MW series (MM used for this series had an M_n = 3,768 g/mol and a PDI of 1.01).

Characterization of Linear Homopolymer Molecular Conformation from GPC-MALS:

Table S8. Poly(NB-Hep) MW series data obtained from GPC-MALS for the M_n and the Radius of gyration measured with static light scattering (R_z) as long as the polymer was larger than 10 nm in diameter in THF.

Polymer Sample	GPC M_n (kg/mol)	R_z from GPC MALS (nm)	Log M_n	Log R_z
p(NB-Hep)-DP325	76.9	11	4.89	1.0
p(NB-Hep)-DP376	89.0	13	4.95	1.1
p(NB-Hep)-DP437	$1.03x10^2$	15	5.01	1.2
p(NB-Hep)-DP465	$1.10x10^2$	18	5.04	1.2
p(NB-Hep)-DP721	$1.70x10^2$	18	5.23	1.3
p(NB-Hep)-DP996	$2.36x10^2$	21	5.37	1.3
p(NB-Hep)-DP1028	$2.43x10^2$	21	5.39	1.3
p(NB-Hep)-DP1077	$2.55\ x10^2$	25	5.41	1.4

Table S9. Poly(NBI-Hep) MW series data obtained from GPC-MALS for the M_n and the Radius of gyration measured with static light scattering (R_z) as long as the polymer was larger than 10 nm in diameter in THF.

Polymer Sample	GPC M_n (kg/mol)	R_z from GPC MALS (nm)	Log M_n	Log R_z
p(NBI-Hep)-DP360	$1.15x10^2$	11	5.06	1.0
p(NBI-Hep)-DP454	$1.45x10^2$	15	5.16	1.2
p(NBI-Hep)-DP495	$1.58x10^2$	16	5.20	1.2
p(NBI-Hep)-DP618	$1.98x10^2$	19	5.30	1.3
p(NBI-Hep)-DP621	$1.98x10^2$	20	5.30	1.3
p(NBI-Hep)-DP1051	$3.36x10^2$	22	5.53	1.4
p(NBI-Hep)-DP1135	$3.63x10^2$	24	5.56	1.4
p(NBI-Hep)-DP1172	$3.74x10^2$	25	5.57	1.4

Table S10. Poly(NBI-Dec) MW series data obtained from GPC-MALS for the M_n and the Radius of gyration measured with static light scattering (R_z) as long as the polymer was larger than 10 nm in diameter in THF.

Polymer Sample	GPC M_n (kg/mol)	R_z from GPC MALS (nm)	Log M_n	Log R_z
p(NBI-Dec)-DP376	$1.14x10^2$	16	5.06	1.2
p(NBI-Dec)-DP512	$1.56x10^2$	20	5.19	1.3
p(NBI-Dec)-DP863	$2.62x10^2$	21	5.42	1.3
p(NBI-Dec)-DP972	$2.95x10^2$	24	5.47	1.4
p(NBI-Dec)-DP1575	$4.78x10^2$	37	5.68	1.6
p(NBI-Dec)-DP2261	$6.86x10^2$	48	5.84	1.7
p(NBI-Dec)-DP2570	$7.80x10^2$	56	5.89	1.8

Static Light Scattering Scaling Relationship:

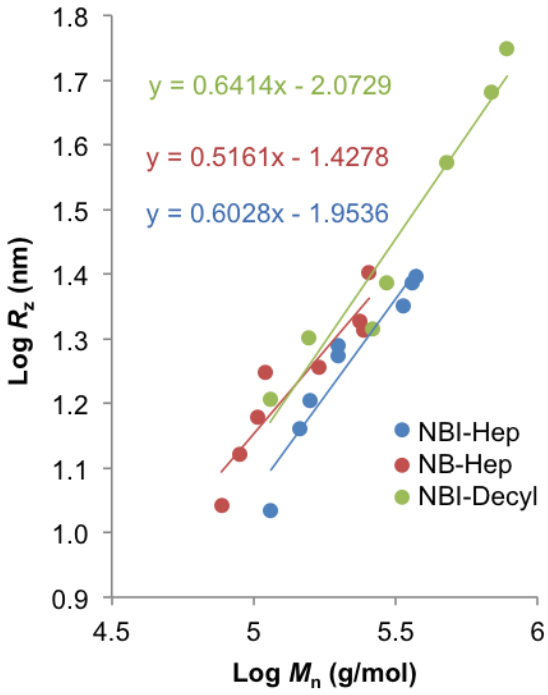

Figure S21. A graph of the z-average radius of gyration of the linear polymers in tetrahydrofuran vs. the number average molecular weight of the polymers (scaling factor = 0.64 for NBI-Decyl, 0.52 for NB-Hep, and 0.60 for NBI-Hep).

General Block Copolymer Synthesis:

In a nitrogen-filled glovebox, a 20 mL vial was charged with a stir bar and 0.1 g of PLA macromonomer that was then diluted to 0.05 M with anhydrous THF. With rapid stirring, the appropriate amount of G3 catalyst completely dissolved in THF was quickly added via syringe. As conversion stopped determined by GPC, the molar equivalent amount of PS macromonomer at a concentration of 0.05 M in anhydrous THF was added quickly. Also dissolved in the second block mixture was pyridine (20 mM for the BBCPs with the NB-PS MM or 30 mM for the BBCPs with the NBI-PS MM). After 3 hours (for the NB-PS containing BBCPs) or 20 hours (for the NBI-PS containing BBCPs) from the addition of the 2nd block, the polymerization was quenched by the addition of 0.5 mL of ethyl vinyl ether. The polymer was precipitated out into 20 mL of methanol at room temperature, after which the polymer was isolated, washed with excess methanol, and dried under reduced pressure at 70 °C to a constant weight. Yield is recorded below with the GPC-MALS data.

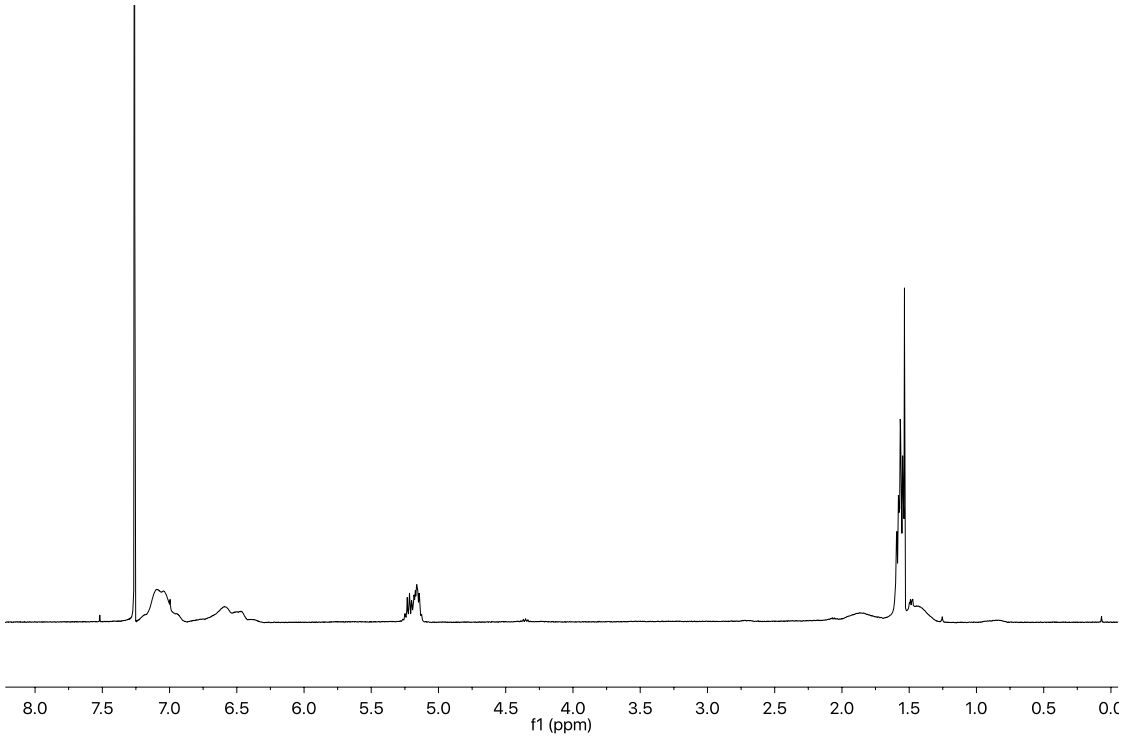

Figure S22. Isolated and representative p(NBI-PLA)-*b*-p(NBI-PS) (polymer shown M_n = 1.56x10^3 kg/mol) 1H NMR (400 MHz, CDCl3): δ 7.08 (m), 6.58 (m), 5.17 (m), 4.35 (m), 1.88 (bs), 1.53 (m), 1.26 (s), 0.91 (bs), [Water singlet from CDCl3 at 1.55 ppm].

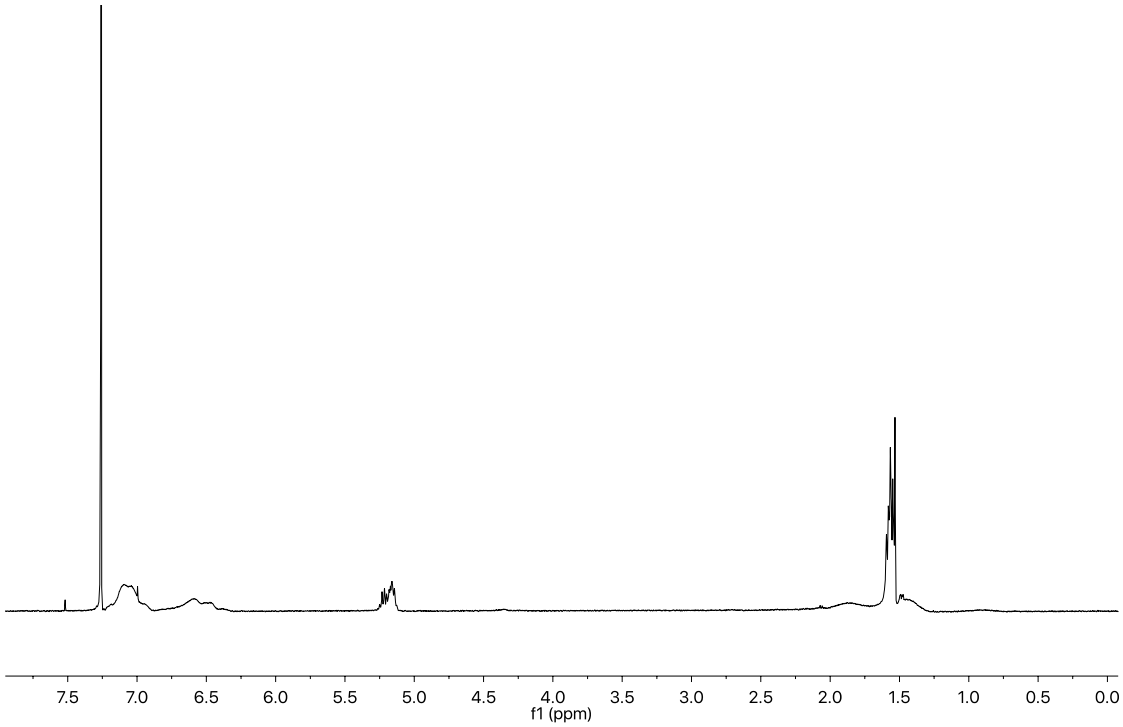

Figure S23. Isolated and representative p(NBI-PLA)-*b*-p(NB-PS) (polymer shown M_n = 2.60x10^3 kg/mol) 1H NMR (400 MHz, CDCl3): δ 7.08 (m), 6.58 (m), 5.17 (m), 4.35 (m), 1.88 (bs), 1.53 (m), 1.26 (s), 0.91 (bs), 0.71 (m) [Water singlet from CDCl3 at 1.55 ppm].

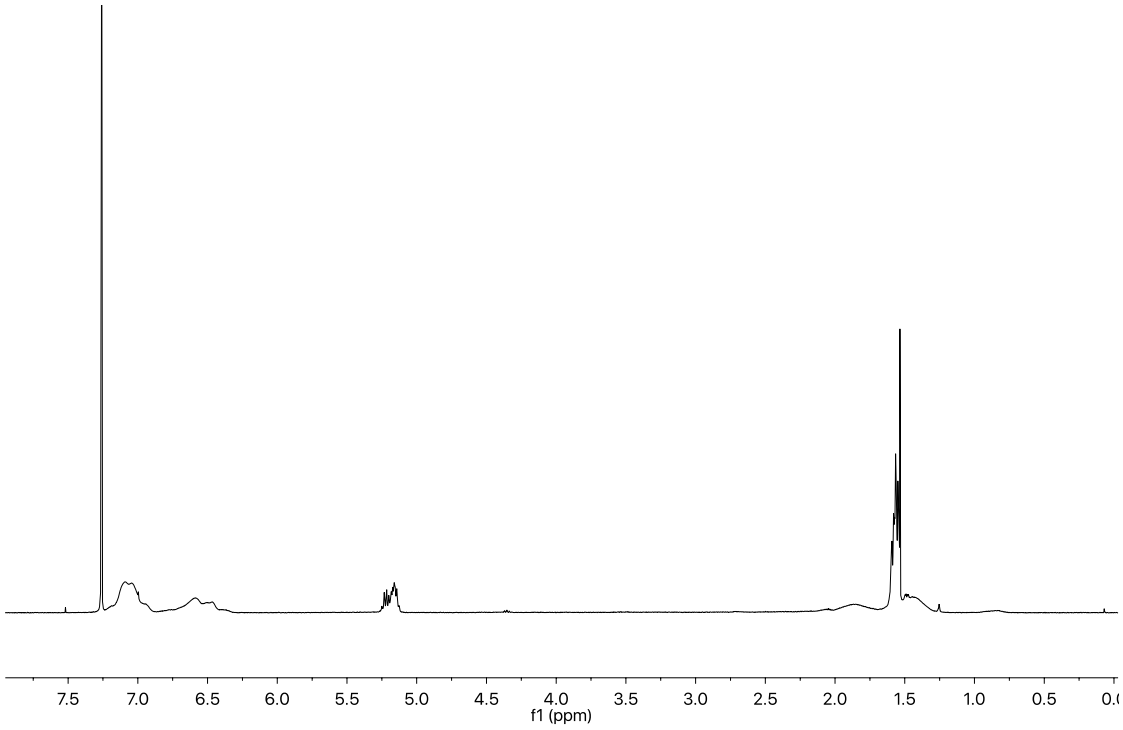

Figure S24. Isolated and representative p(NB-PLA)-*b*-p(NBI-PS) (polymer shown M_n = 2.13x10^3 kg/mol) 1H NMR (400 MHz, CDCl3): δ 7.08 (m), 6.58 (m), 5.17 (m), 4.35 (m), 1.88 (bs), 1.53 (m), 1.26 (s), 0.91 (bs) [Water singlet from CDCl3 at 1.55 ppm].

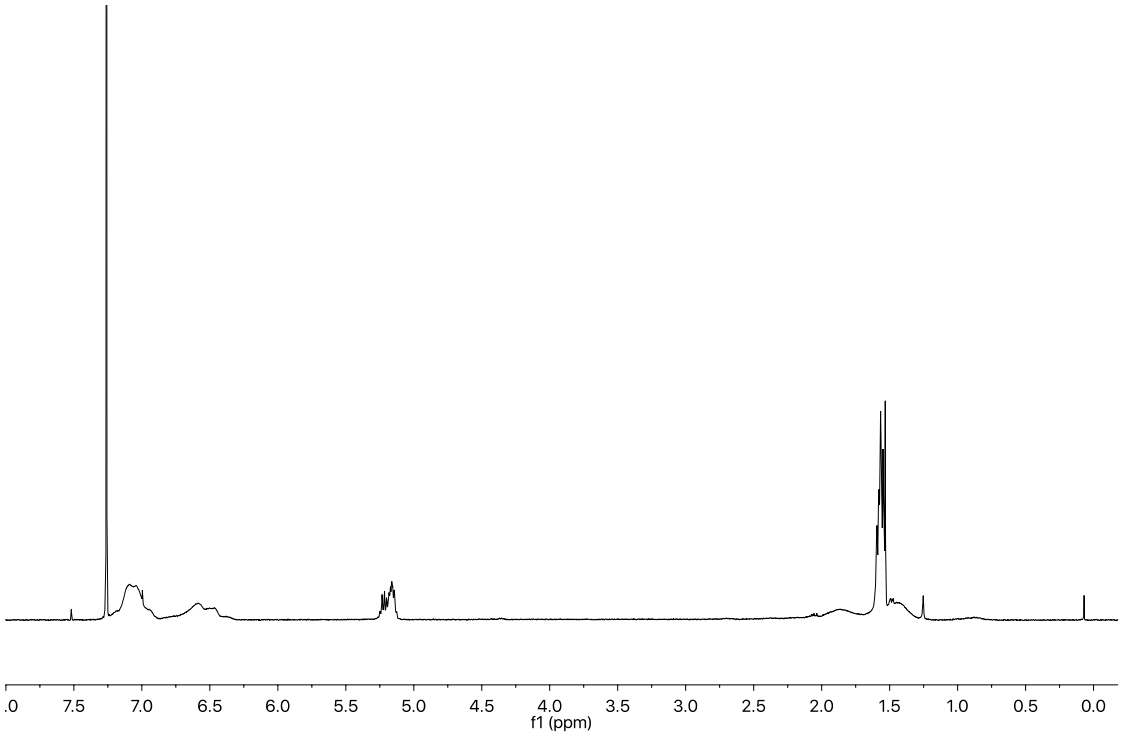

Figure S25. Isolated and representative p(NB-PLA)-*b*-p(NB-PS) (polymer shown M_n = 2.30x10^3 kg/mol) 1H NMR (400 MHz, CDCl3): δ 7.08 (m), 6.58 (m), 5.17 (m), 4.35 (m), 1.88 (bs), 1.53 (m), 1.26 (s), 0.91 (bs), 0.71 (m) [Water singlet from CDCl3 at 1.55 ppm].

Block Copolymer Characterization via Gel Permeation – Multi Angle Light Scattering Traces (GPC-MALS) and Isolated Yield:

Table S11. p(NBI-PLA)-*b*-p(NBI-PS) MW series data obtained from GPC-MALS and isolated yield.

p(NBI-PLA)-*b*-p(NBI-PS) Sample	M_n (kg/mol)	M_w (kg/mol)	Dispersity (M_w/M_n)	Isolated Yield (%)
1	$4.55x10^2$	$5.02x10^2$	1.10	69
2	$5.20x10^2$	$5.38x10^2$	1.03	67
3	$8.50x10^2$	$1.02x10^3$	1.20	76
4	$1.31x10^3$	$1.47x10^3$	1.12	72
5	$1.42x10^3$	$1.74x10^3$	1.22	81
6	$1.43x10^3$	$1.89x10^3$	1.31	77
7	$1.56x10^3$	$1.96x10^3$	1.25	76

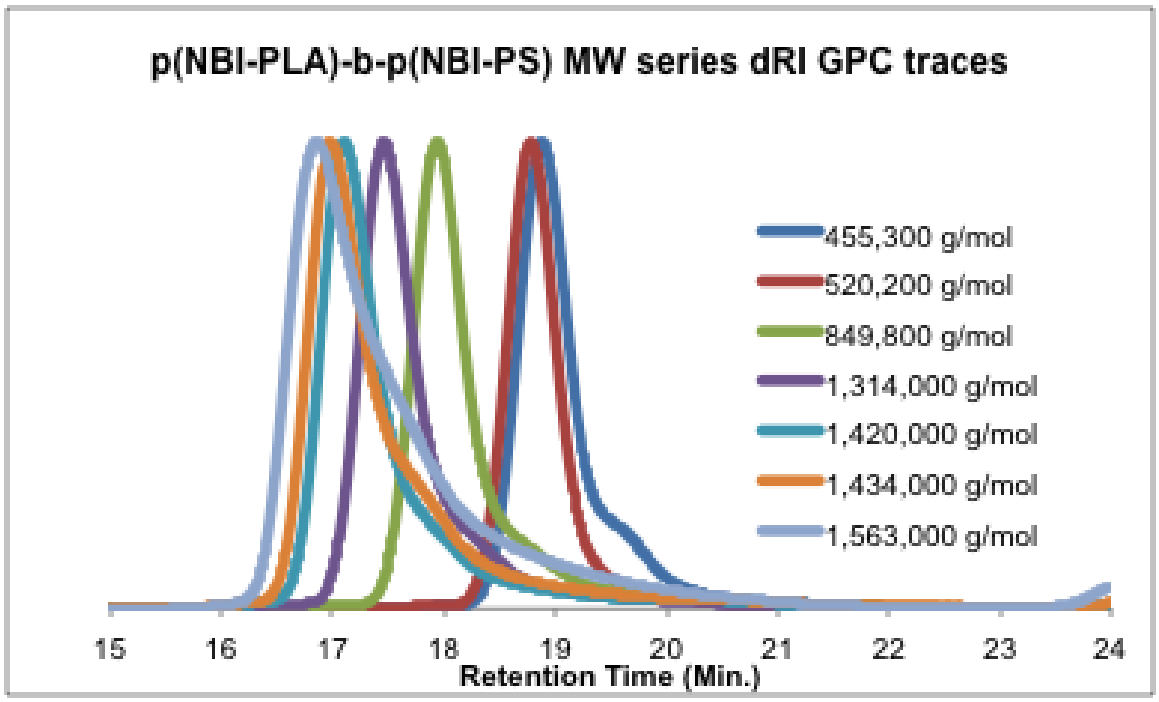

Figure S26. Relative Scaling of GPC RI detector traces for p(NBI-PLA)-b-p(NBI-PS) MW series.

Table S12. p(NBI-PLA)-*b*-p(NB-PS) MW series data obtained from GPC-MALS and isolated yield.

p(NBI-PLA)-*b*-p(NB-PS) Sample	M_n (kg/mol)	M_w (kg/mol)	Dispersity (M_w/M_n)	Isolated Yield (%)
1	$6.13x10^2$	$6.61x10^2$	1.08	74
2	$7.66x10^2$	$7.95x10^2$	1.04	72
3	$1.11x10^3$	$1.18x10^3$	1.07	83
4	$1.52x10^3$	$1.61x10^3$	1.05	76
5	$1.66x10^3$	$1.70x10^3$	1.03	77
6	$2.60x10^3$	$2.71x10^3$	1.04	74

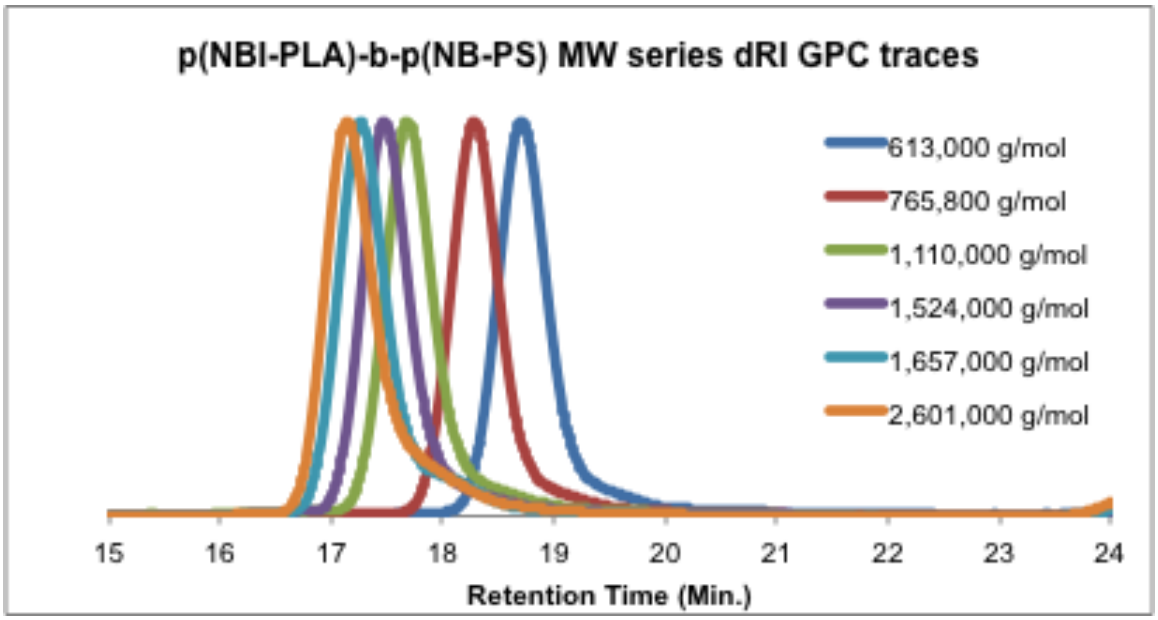

Figure S27. Relative Scaling of GPC RI detector traces for p(NBI-PLA)-b-p(NB-PS) MW series.

Table S13. p(NB-PLA)-*b*-p(NBI-PS) MW series data obtained from GPC-MALS and isolated yield.

p(NB-PLA)-*b*-p(NBI-PS) Sample	M_n (kg/mol)	M_w (kg/mol)	Dispersity (M_w/M_n)	Isolated Yield (%)
1	$5.24x10^2$	$5.40x10^2$	1.03	81
2	$9.18x10^2$	$9.69x10^2$	1.06	79
3	$1.44x10^3$	$1.52x10^3$	1.06	83
4	$1.88x10^3$	$1.97x10^3$	1.05	83
5	$1.90x10^3$	$2.03x10^3$	1.07	78
6	$2.13x10^3$	$2.42x10^3$	1.14	82

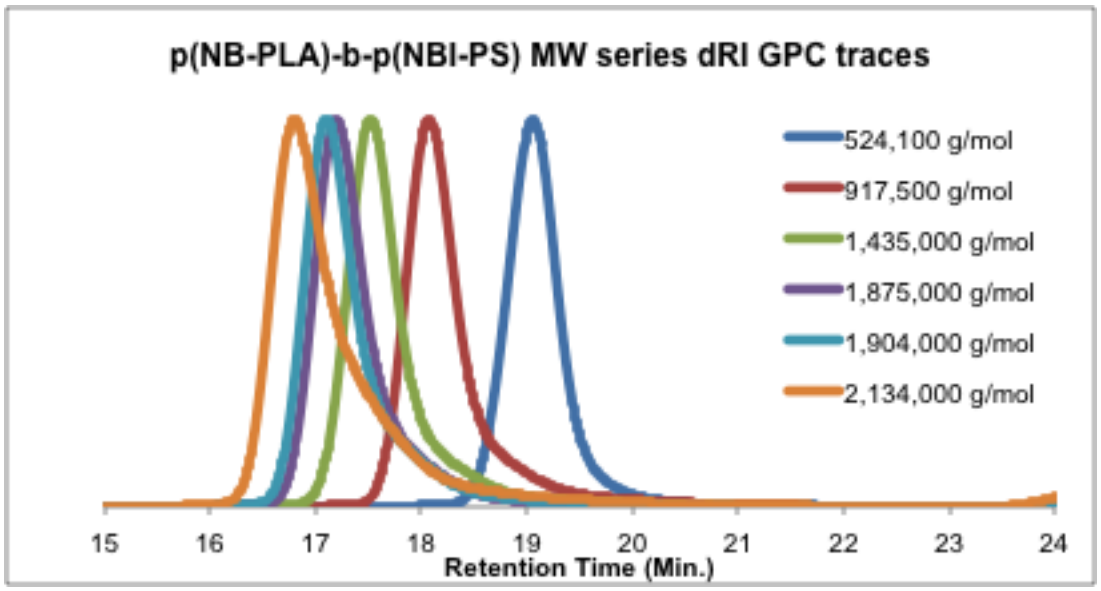

Figure S28. Relative Scaling of GPC RI detector traces for p(NB-PLA)-b-p(NBI-PS) MW series.

Table S14. p(NB-PLA)-*b*-p(NB-PS) MW series data obtained from GPC-MALS and isolated yield.

p(NB-PLA)-*b*-p(NB-PS) Sample	M_n (kg/mol)	M_w (kg/mol)	Dispersity (M_w/M_n)	Isolated Yield (%)
1	$4.14x10^2$	$4.20x10^2$	1.02	63
2	$7.87x10^2$	$8.04x10^2$	1.02	69
3	$1.31x10^3$	$1.34x10^3$	1.03	73
4	$1.73x10^3$	$1.80x10^3$	1.04	82
5	$1.70x10^3$	$1.75x10^3$	1.03	82
6	$2.30x10^3$	$2.40x10^3$	1.04	75

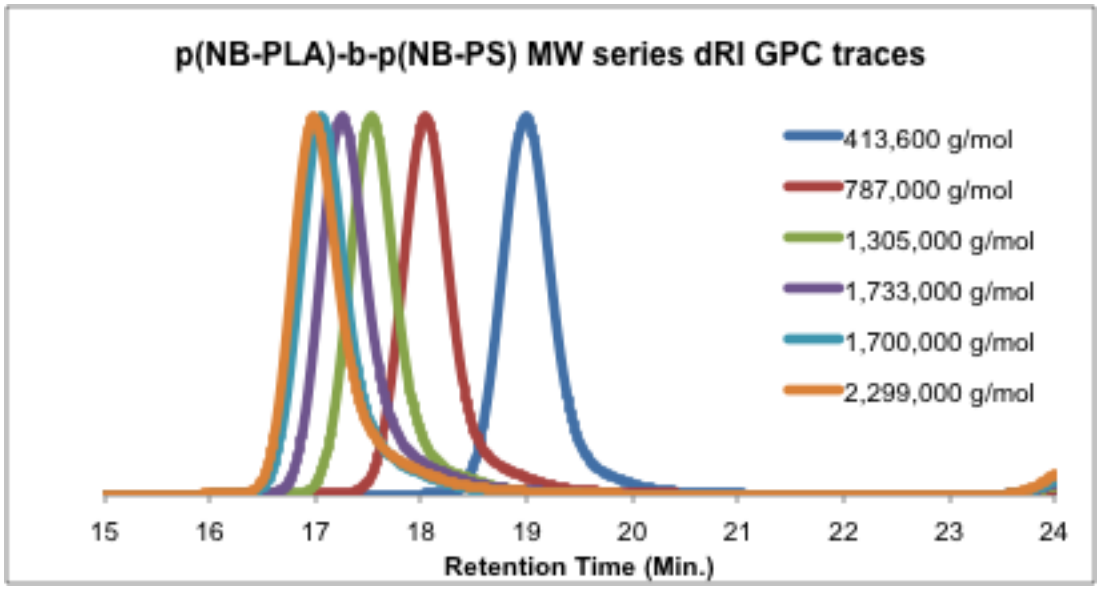

Figure S29. Relative Scaling of GPC RI detector traces for p(NB-PLA)-b-p(NB-PS) MW series.

Characterization of Block Copolymer Composition by NMR:

^{1}H NMR spectroscopy was conducted on each brush block copolymer to observe the degree of polymerization of each block in each of the copolymers. The molar ratios of the styrene repeat unit to the lactide repeat unit were estimated from the integration value of the peak at δ 6.29-7.25 ppm (for styrene) and δ 5.03-5.25 ppm (for lactide). The styrene peaks were integrated to a value of 1 and divided by 5 to produce a molar ratio of 0.2 for styrene in the BBCP. The lactide peak was then integrated and the resulting integration value was divided by 2 to provide the molar amount of lactide in the BBCP.

Then, using the experimentally measured M_n from the GPC for the macromonomer used in the copolymer, the norbornene chain-end group was subtracted out to be able to calculate the number of moles using the MW of each repeat unit of either styrene or lactide within a macromonomer.

With both sets of molar ratios calculated above, it was then possible to divide the respective BBCP molar ratio by the amount of moles of the styrene or lactide within a macromonomer repeat unit to get an empirical value of the respective macromonomer degree of polymerization in the BBCP. Using these empirical values, a percent of the styrene or lactide macromonomer was calculated based on the sum of the two empirical values. This percent was then used to multiply into the GPC-derived M_n value for the BBCP. The resulting MW value was then divided by the respective experimentally measured M_n of the macromonomer to get an estimate of the degree of polymerization of each macromonomer within a block. The results of the above calculations are shown in the following table below.

Table S15. Summary of block degree of polymerization calculations and data obtained from GPC-MALS and NMR.

	BBCP M_n (kg/mol)	NMR Molar ratio (styrene : lactide)	Moles of Sty./ MM unit	Moles of Lac./ MM unit	Empirical MM ratio (sty. MM : lac. MM)	% Sty. in BBCP	% Lac. in BBCP	DP of Sty. Block	DP of Lac. Block
p(NBI-PLA)-*b*-p(NBI-PS)									
1	$5.20x10^2$	0.2 : 0.17	0.0305	0.0447	6.55 : 3.69	64	36	88	55
2	$8.50x10^2$	0.2 : 0.14	0.0256	0.0447	7.81 : 3.13	71	29	136	72
3	$1.31x10^3$	0.2 : 0.13	0.0256	0.0447	7.81 : 2.91	73	27	217	104
4	$1.42x10^3$	0.2 : 0.15	0.0256	0.0447	7.81 : 3.24	71	29	228	120
5	$1.43x10^3$	0.2 : 0.14	0.0256	0.0447	7.81 : 3.02	72	28	235	117
6	$1.56x10^3$	0.2 : 0.14	0.0256	0.0447	7.81 : 3.13	71	29	251	132
p(NBI-PLA)-*b*-p(NB-PS)									
1	$6.13x10^2$	0.2 : 0.16	0.0309	0.0447	6.48 : 3.47	65	35	109	63
2	$7.66x10^2$	0.2 : 0.15	0.0309	0.0447	6.48 : 3.24	67	33	140	74
3	$1.11x10^3$	0.2 : 0.13	0.0309	0.0447	6.48 : 2.91	69	31	210	100
4	$1.52x10^3$	0.2 : 0.15	0.0309	0.0447	6.48 : 3.36	66	34	276	151
5	$1.66x10^3$	0.2 : 0.14	0.0309	0.0447	6.48 : 3.02	68	32	309	155
6	$2.60x10^3$	0.2 : 0.14	0.0309	0.0447	6.48 : 3.02	68	32	485	243
p(NB-PLA)-*b*-p(NBI-PS)									
1	$5.24x10^2$	0.2 : 0.13	0.0256	0.0460	7.81 : 2.72	74	26	88	42
2	$9.18x10^2$	0.2 : 0.13	0.0256	0.0460	7.81 : 2.72	74	26	154	73
3	$1.44x10^3$	0.2 : 0.12	0.0256	0.0460	7.81 : 2.61	75	25	243	110
4	$1.88x10^3$	0.2 : 0.11	0.0256	0.0460	7.81 : 2.39	77	23	325	135
5	$1.90x10^3$	0.2 : 0.13	0.0256	0.0460	7.81 : 2.72	74	26	319	152
6	$2.13x10^3$	0.2 : 0.12	0.0256	0.0460	7.81 : 2.50	76	24	367	158
p(NB-PLA)-*b*-p(NB-PS)									
1	$4.14x10^2$	0.2 : 0.16	0.0309	0.0460	6.48 : 3.48	65	35	74	45
2	$7.87x10^2$	0.2 : 0.14	0.0309	0.0460	6.48 : 2.93	69	31	149	75
3	$1.31x10^3$	0.2 : 0.14	0.0309	0.0460	6.48 : 2.93	69	31	247	124
4	$1.73x10^3$	0.2 : 0.13	0.0309	0.0460	6.48 : 2.82	70	30	332	160
5	$1.70x10^3$	0.2 : 0.15	0.0309	0.0460	6.48 : 3.26	66	34	308	178
6	$2.30x10^3$	0.2 : 0.13	0.0309	0.0460	6.48 : 2.82	70	30	441	212

Photographs of BBCP Films:

p(NBI-PLA)-b-p(NBI-PS):

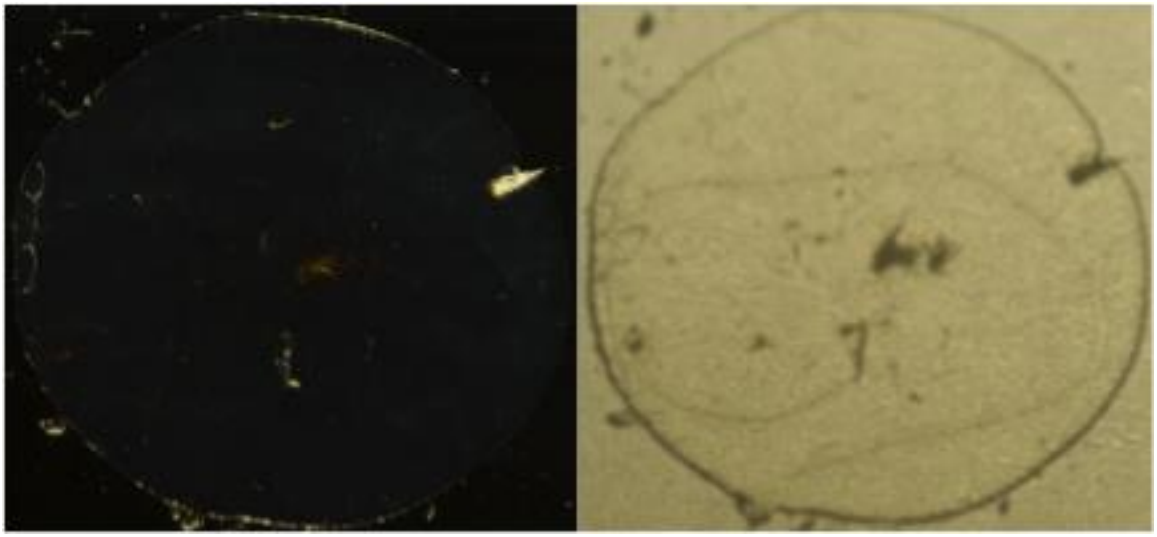

Figure S30. Photographs of the reflection (left) and transmission (right) of the p(NBI-PLA)-b-p(NBI-PS) (M_n = 455,300 g/mol) film.

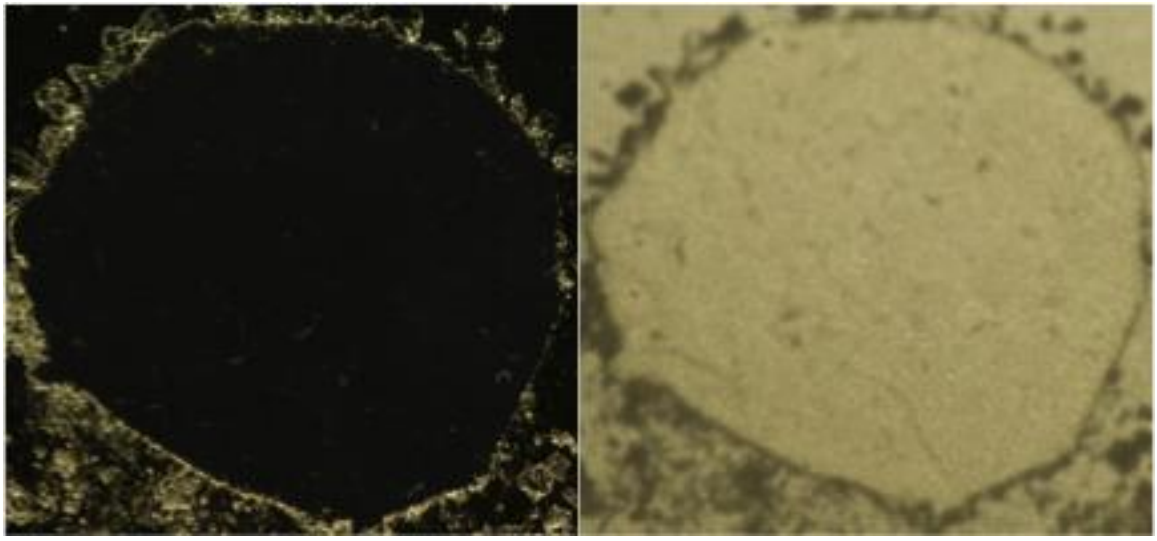

Figure S31. Photographs of the reflection (left) and transmission (right) of the p(NBI-PLA)-b-p(NBI-PS) (M_n = 520,200 g/mol) film.

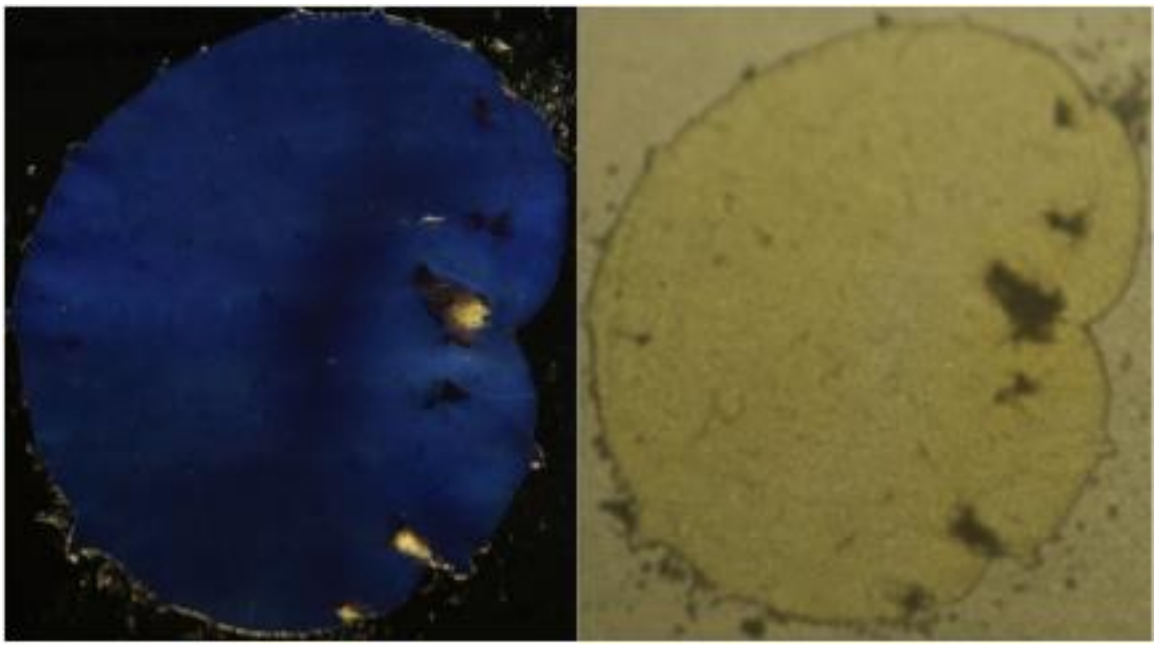

Figure S32. Photographs of the reflection (left) and transmission (right) of the p(NBI-PLA)-b-p(NBI-PS) (M_n = 849,800 g/mol) film.

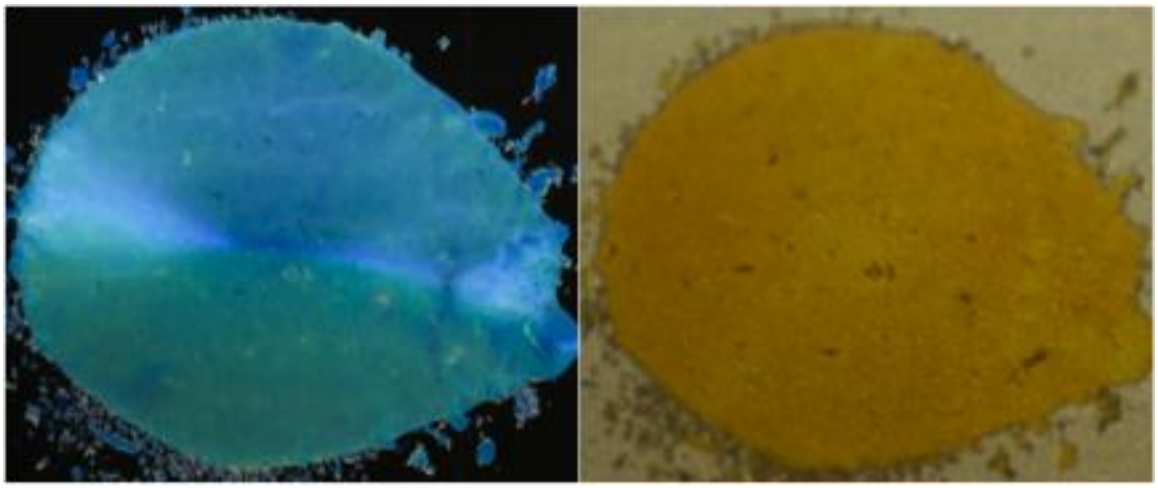

Figure S33. Photographs of the reflection (left) and transmission (right) of the p(NBI-PLA)-b-p(NBI-PS) (M_n = 1,314,000 g/mol) film.

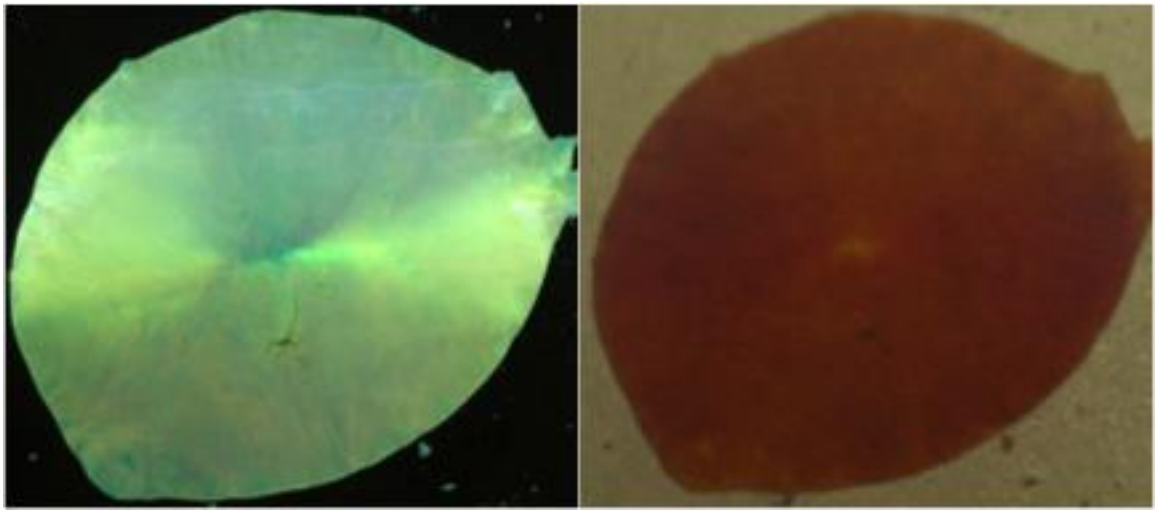

Figure S34. Photographs of the reflection (left) and transmission (right) of the p(NBI-PLA)-b-p(NBI-PS) (M_n = 1,420,000 g/mol) film.

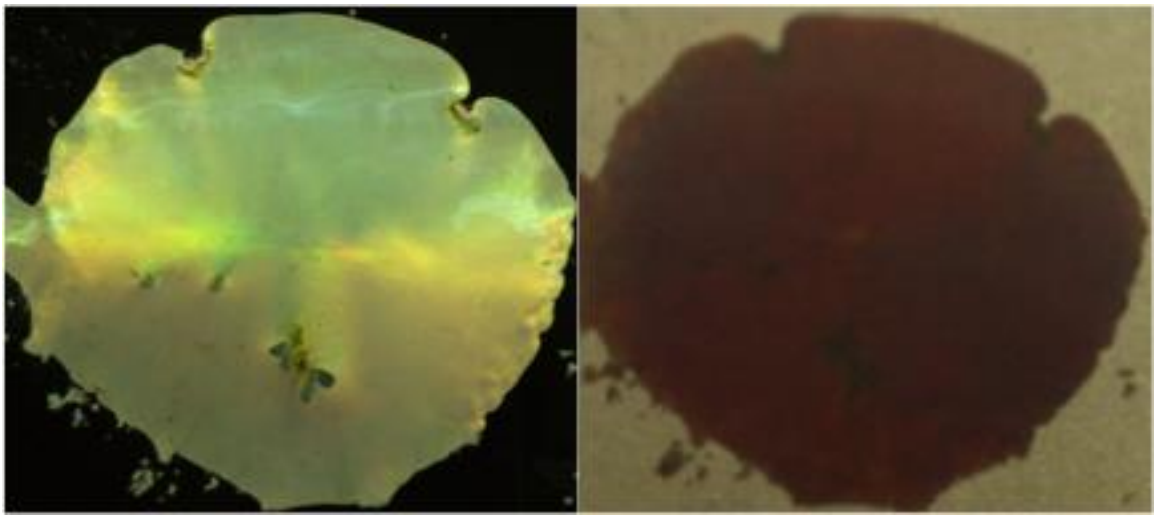

Figure S35. Photographs of the reflection (left) and transmission (right) of the p(NBI-PLA)-b-p(NBI-PS) (M_n = 1,434,000 g/mol) film.

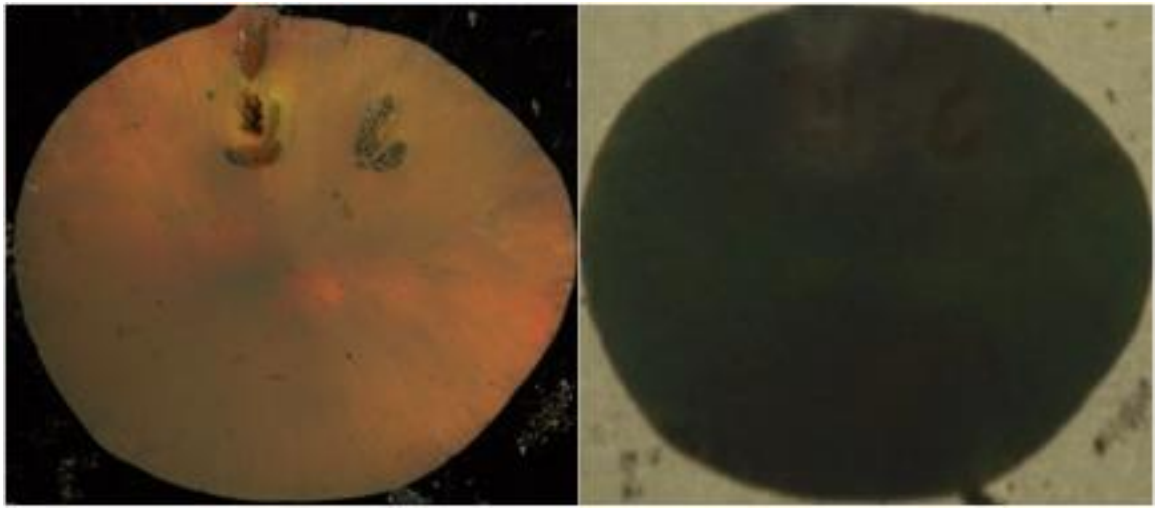

Figure S36. Photographs of the reflection (left) and transmission (right) of the p(NBI-PLA)-b-p(NBI-PS) (M_n = 1,563,000 g/mol) film.

p(NBI-PLA)-b-p(NB-PS):

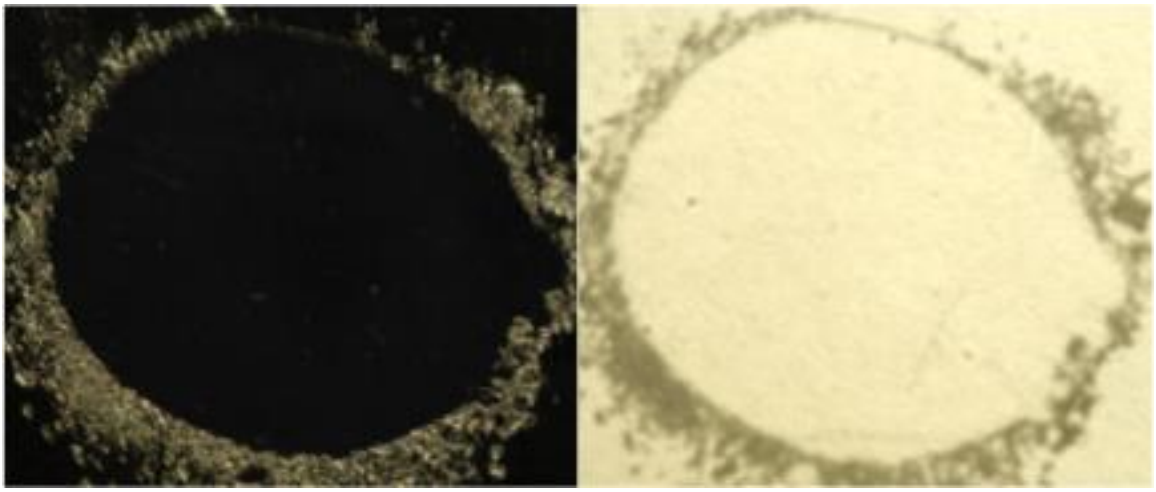

Figure S37. Photographs of the reflection (left) and transmission (right) of the p(NBI-PLA)-b-p(NB-PS) (M_n = 613,000 g/mol) film.

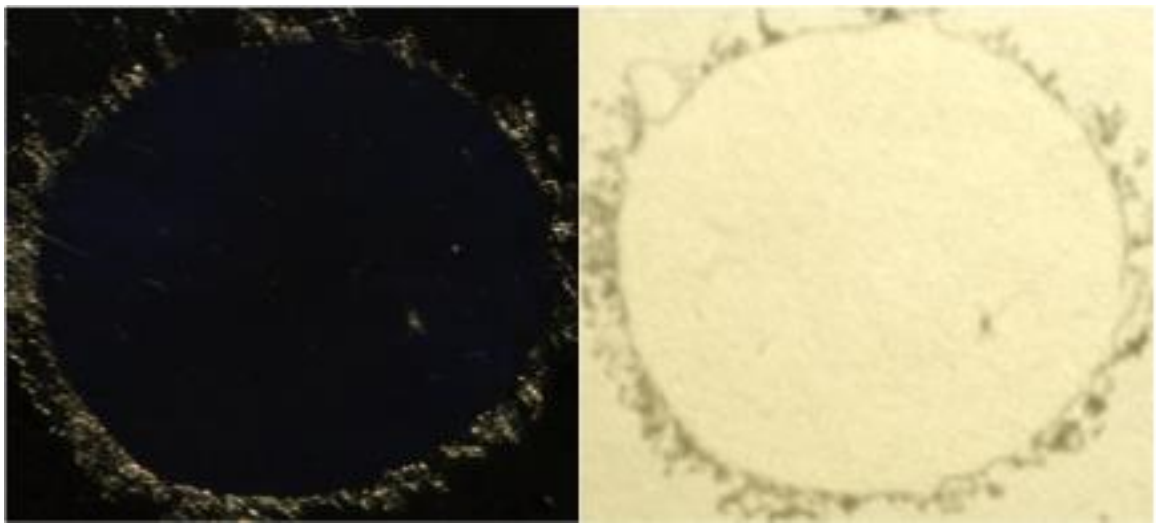

Figure S38. Photographs of the reflection (left) and transmission (right) of the p(NBI-PLA)-b-p(NB-PS) (M_n = 765,800 g/mol) film.

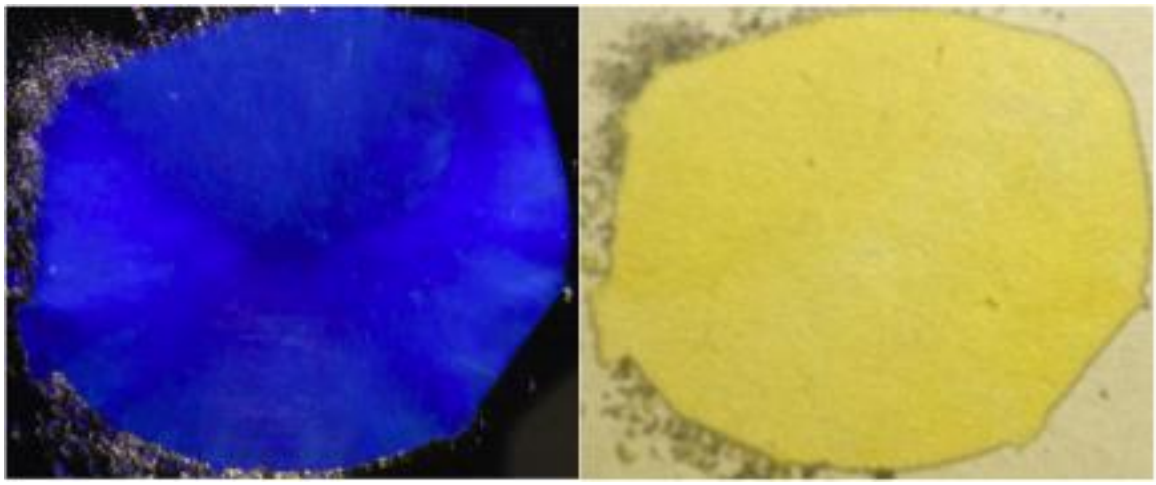

Figure S39. Photographs of the reflection (left) and transmission (right) of the p(NBI-PLA)-b-p(NB-PS) (M_n = 1,110,000 g/mol) film.

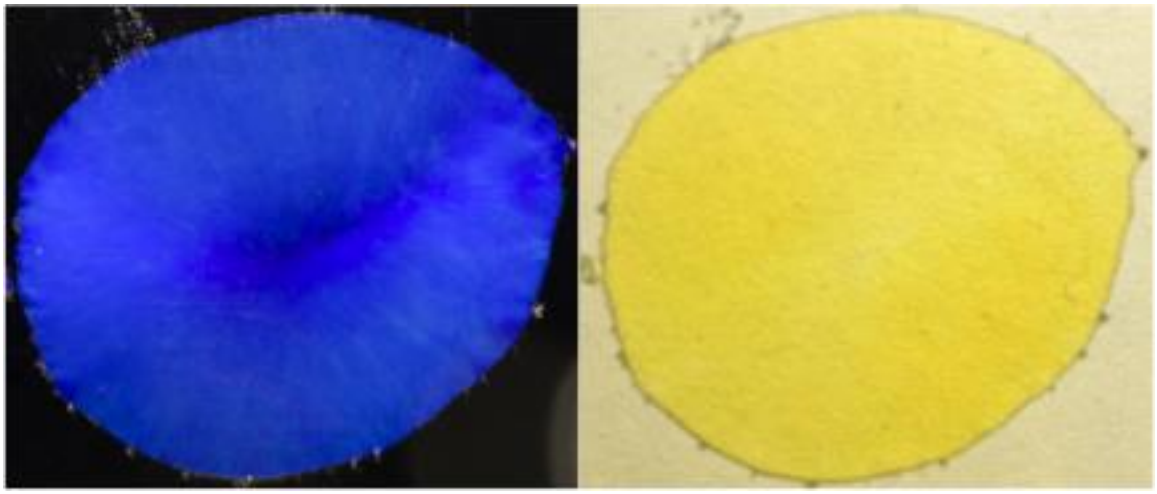

Figure S40. Photographs of the reflection (left) and transmission (right) of the p(NBI-PLA)-b-p(NB-PS) (M_n = 1,524,000 g/mol) film.

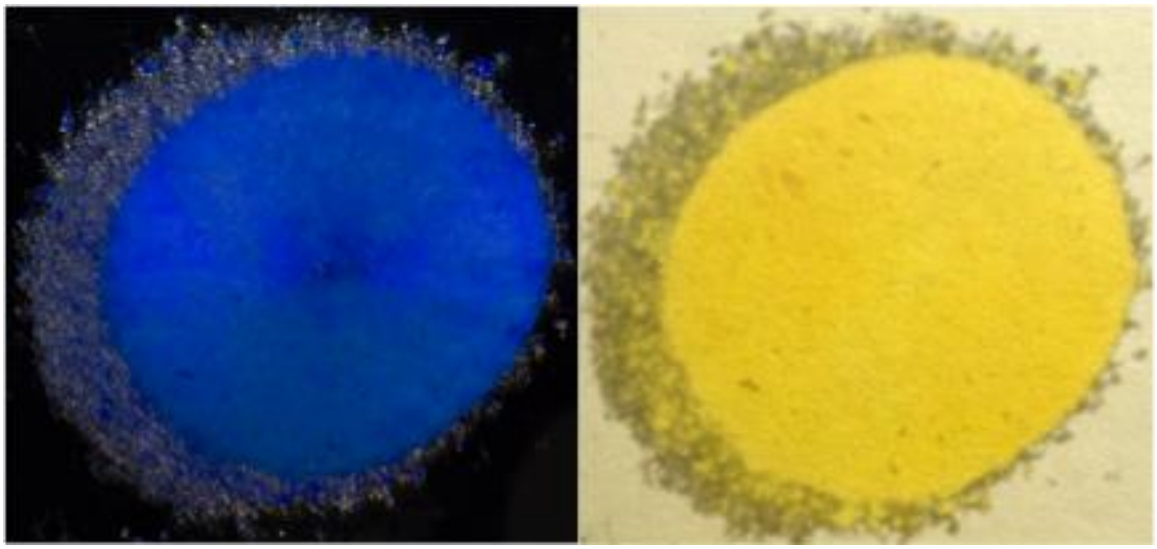

Figure S41. Photographs of the reflection (left) and transmission (right) of the p(NBI-PLA)-b-p(NB-PS) (M_n = 1,657,000 g/mol) film.

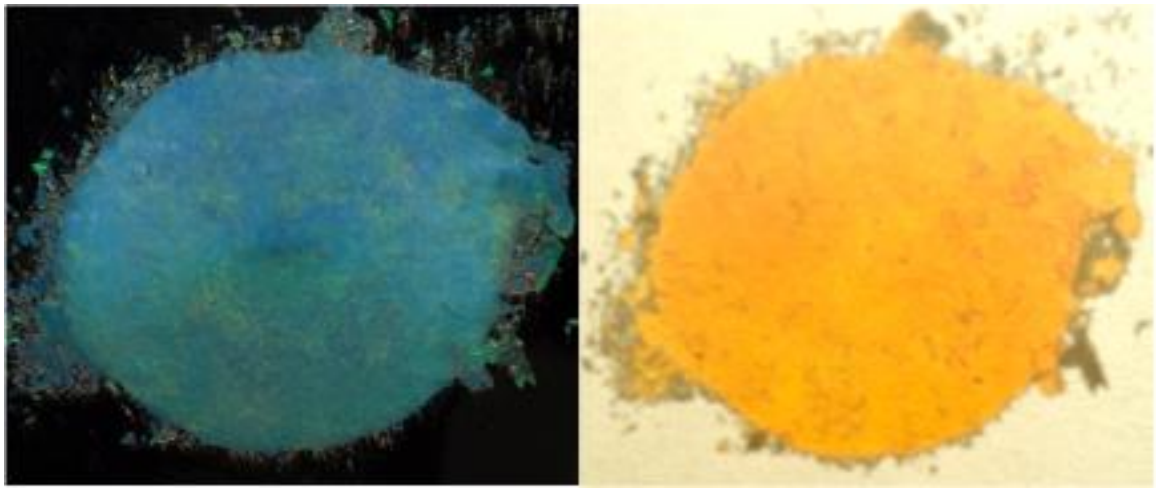

Figure S42. Photographs of the reflection (left) and transmission (right) of the p(NBI-PLA)-b-p(NB-PS) (M_n = 2,601,000 g/mol) film.

p(NB-PLA)-b-p(NBI-PS):

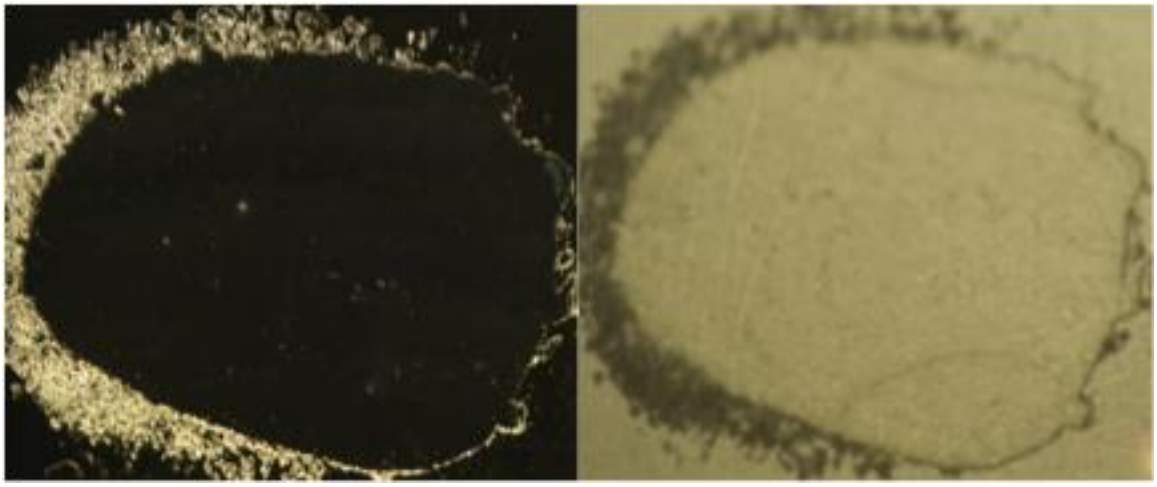

Figure S43. Photographs of the reflection (left) and transmission (right) of the p(NB-PLA)-b-p(NBI-PS) (M_n = 524,100 g/mol) film.

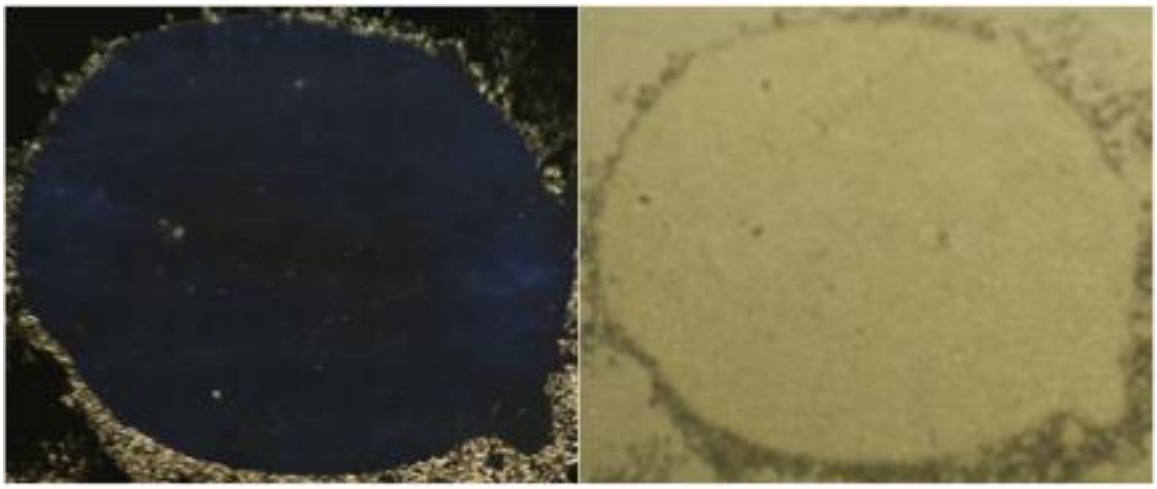

Figure S44. Photographs of the reflection (left) and transmission (right) of the p(NB-PLA)-b-p(NBI-PS) (M_n = 917,500 g/mol) film.

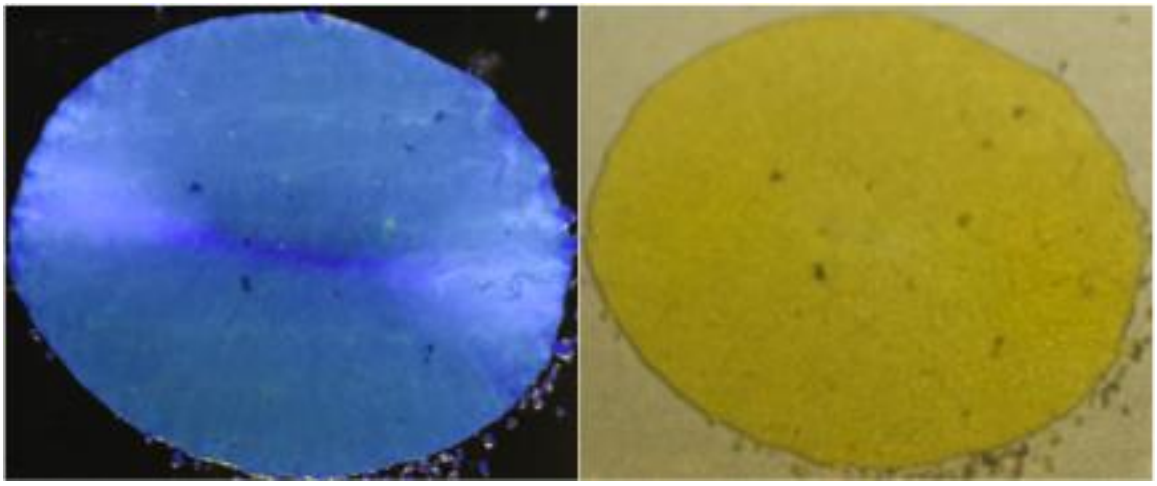

Figure S45. Photographs of the reflection (left) and transmission (right) of the p(NB-PLA)-b-p(NBI-PS) (M_n = 1,435,000 g/mol) film.

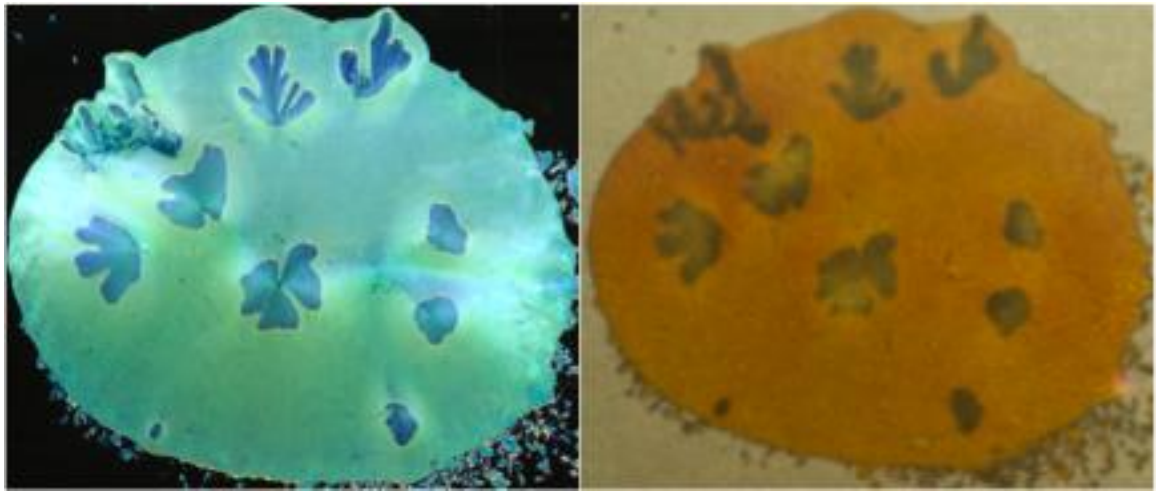

Figure S46. Photographs of the reflection (left) and transmission (right) of the p(NB-PLA)-b-p(NBI-PS) (M_n = 1,875,000 g/mol) film.

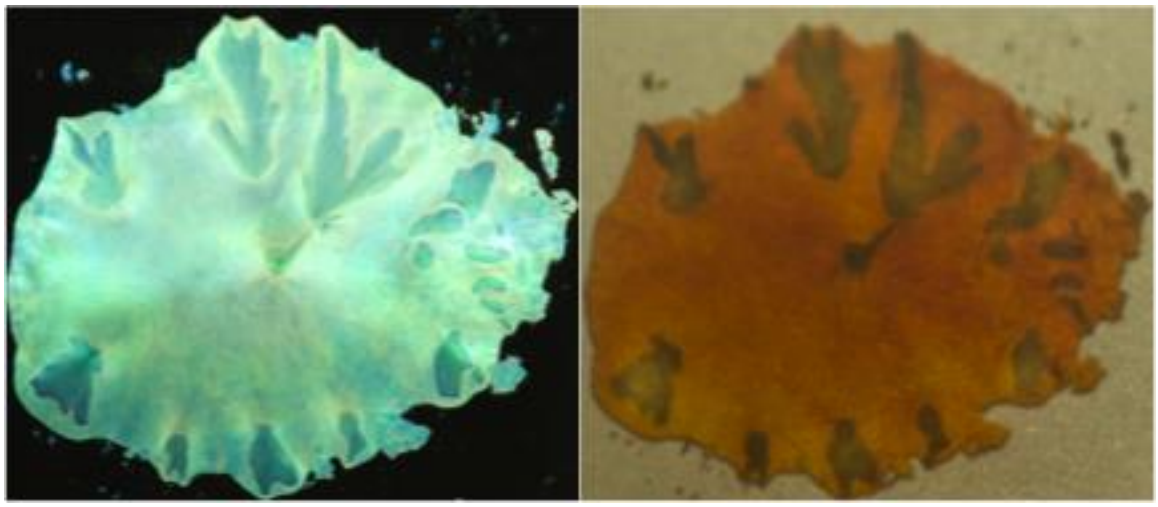

Figure S47. Photographs of the reflection (left) and transmission (right) of the p(NB-PLA)-b-p(NBI-PS) (M_n = 1,904,000 g/mol) film.

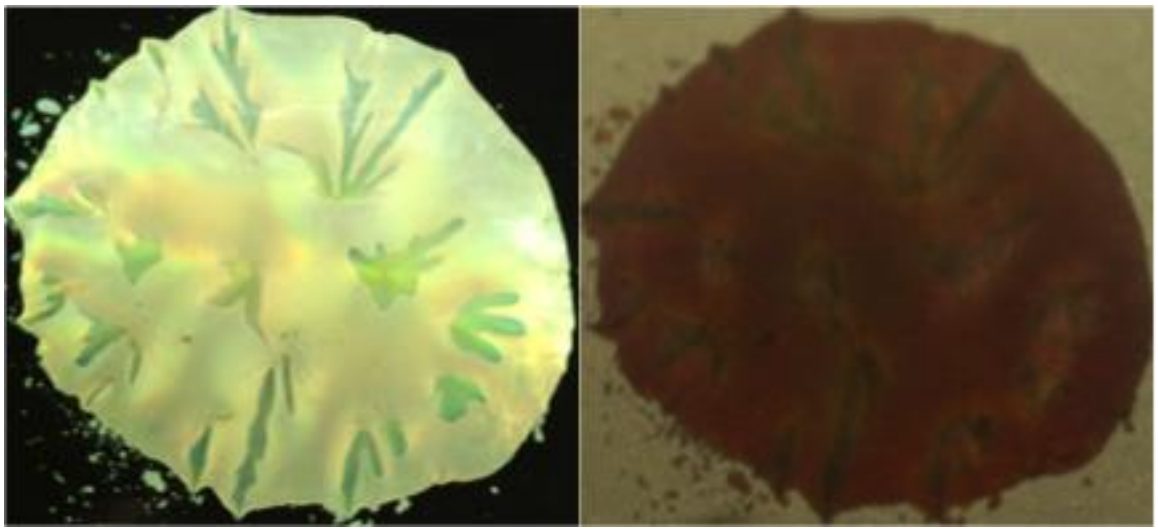

Figure S48. Photographs of the reflection (left) and transmission (right) of the p(NB-PLA)-b-p(NBI-PS) (M_n = 2,134,000 g/mol) film.

p(NB-PLA)-b-p(NB-PS):

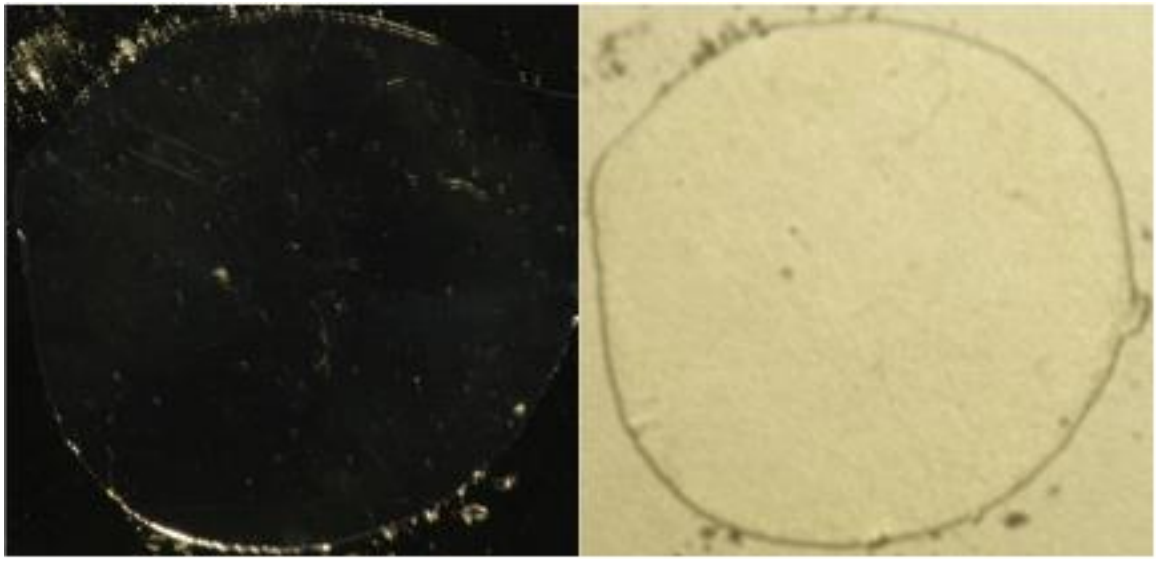

Figure S49. Photographs of the reflection (left) and transmission (right) of the p(NB-PLA)-b-p(NB-PS) (M_n = 413,600 g/mol) film.

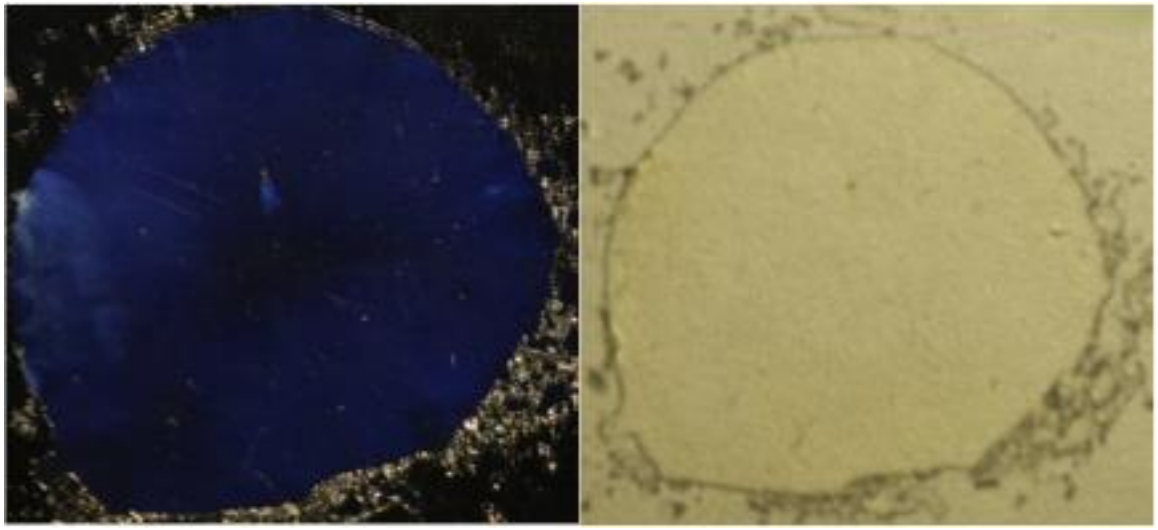

Figure S50. Photographs of the reflection (left) and transmission (right) of the p(NB-PLA)-b-p(NB-PS) (M_n = 787,000 g/mol) film.

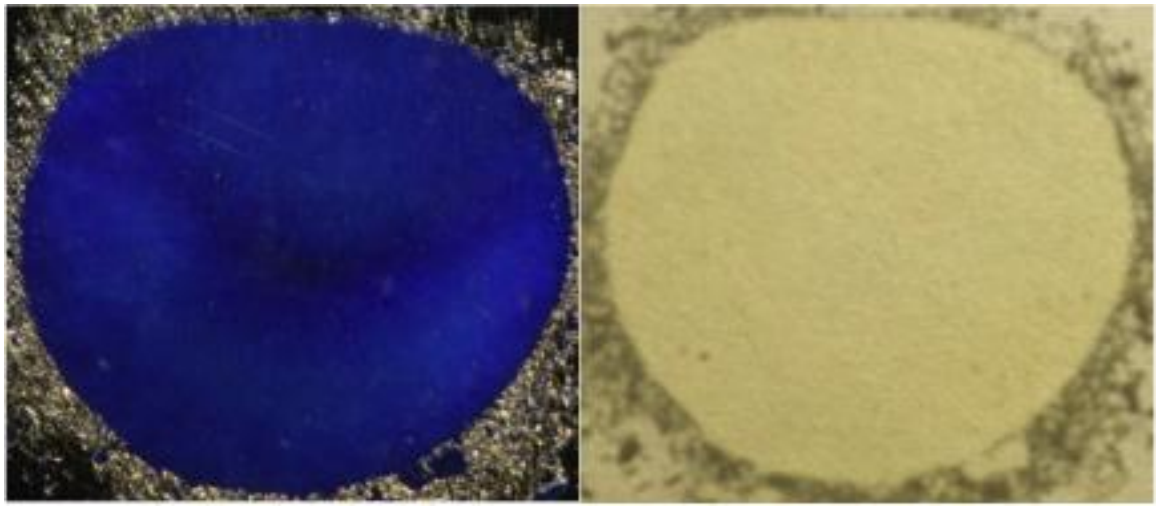

Figure S51. Photographs of the reflection (left) and transmission (right) of the p(NB-PLA)-b-p(NB-PS) (M_n = 1,305,000 g/mol) film.

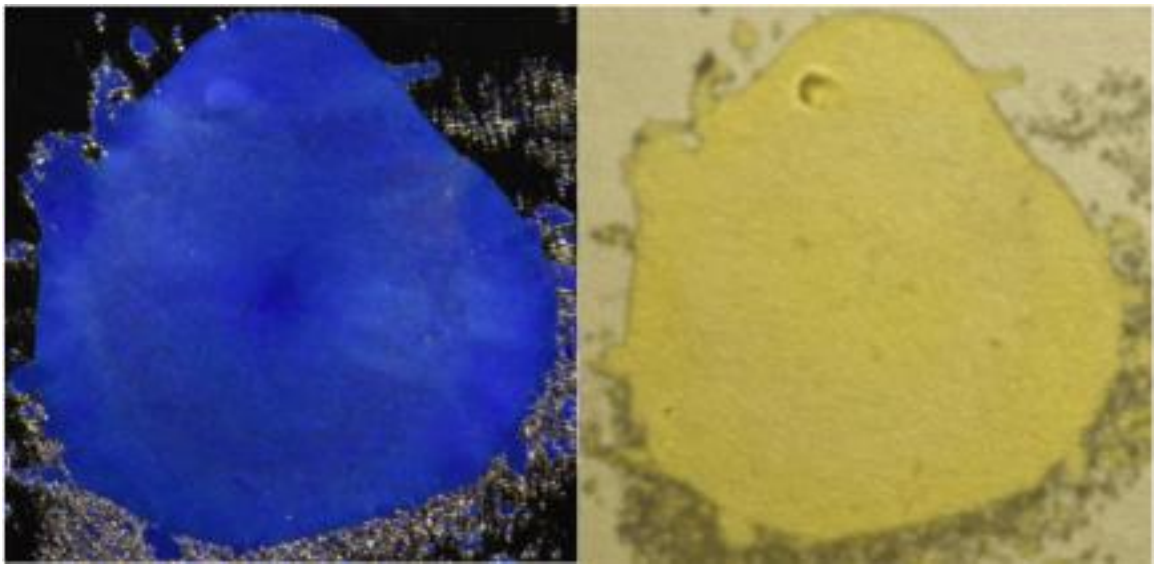

Figure S52. Photographs of the reflection (left) and transmission (right) of the p(NB-PLA)-b-p(NB-PS) (M_n = 1,733,000 g/mol) film.

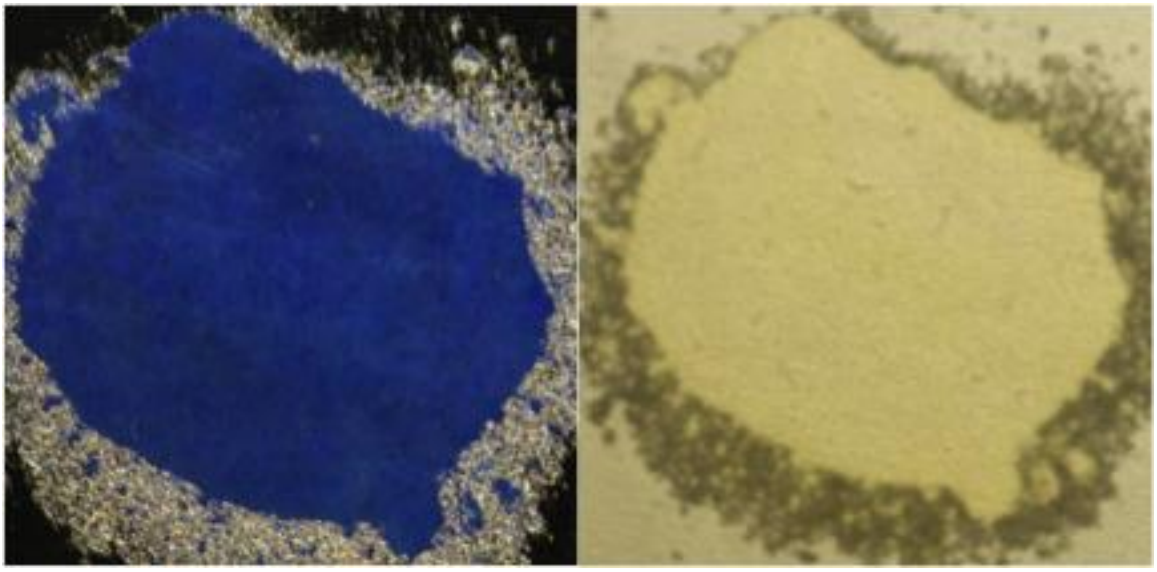

Figure S53. Photographs of the reflection (left) and transmission (right) of the p(NB-PLA)-b-p(NB-PS) (M_n = 1,700,000 g/mol) film.

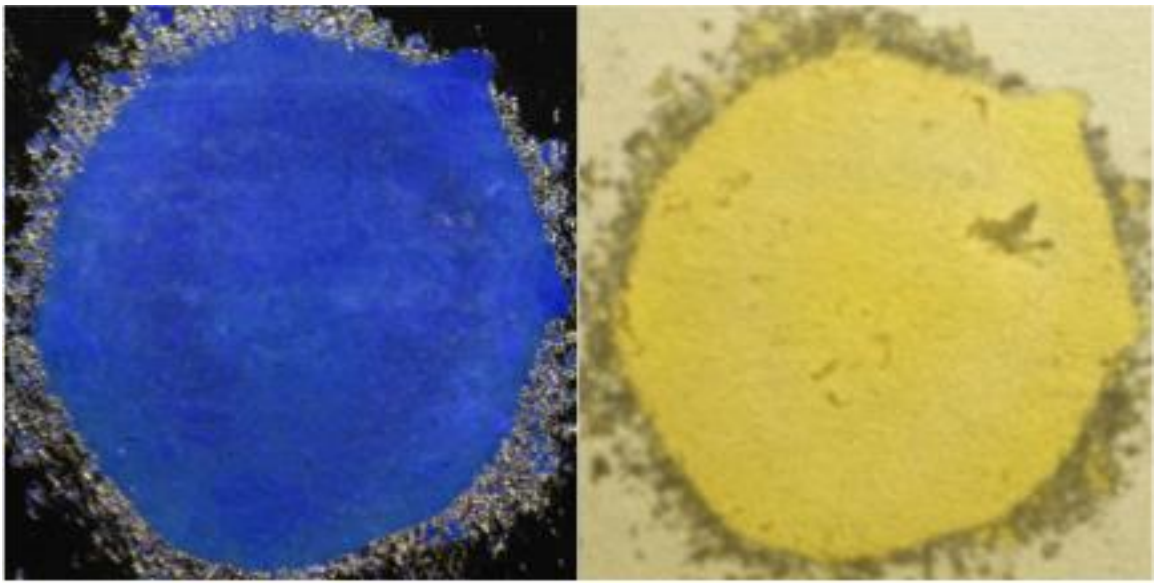

Figure S54. Photographs of the reflection (left) and transmission (right) of the p(NB-PLA)-b-p(NB-PS) (M_n = 2,299,000 g/mol) film.

UV-Vis DRA reflection traces:

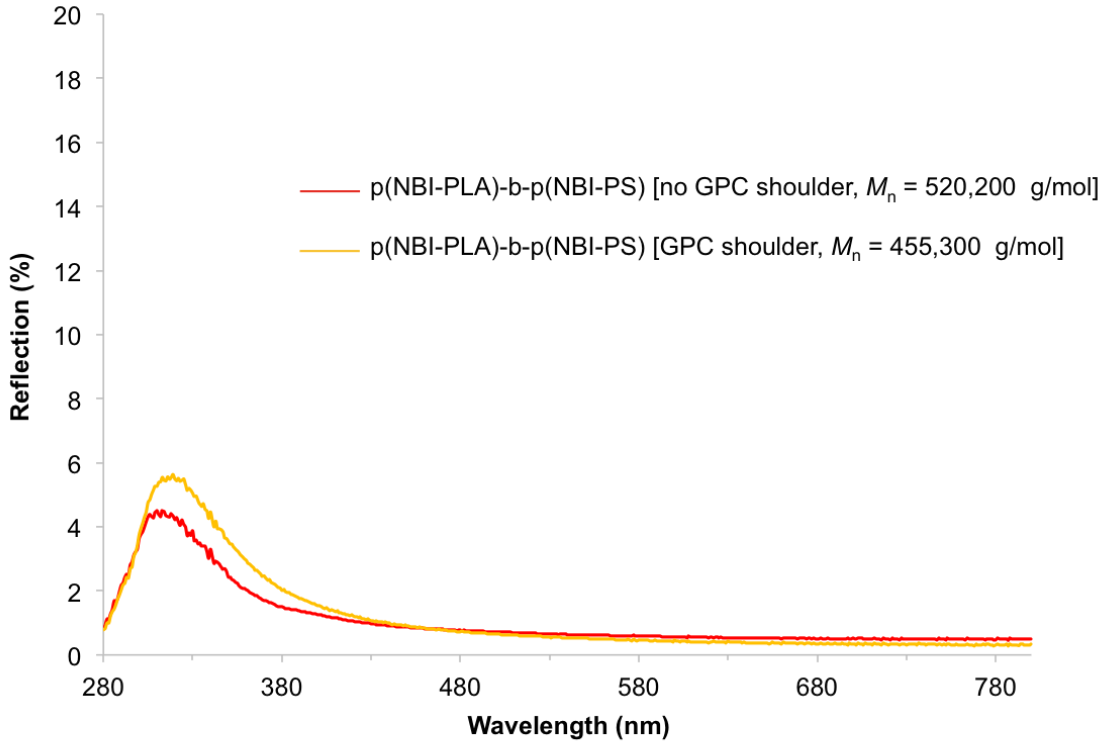

Figure S55. Reflection traces of 2 thin films of similar MW (with and without a small MW shoulder in GPC trace) between two glass slides on a UV-Vis diffuse reflectance accessory.

SEM Micrographs of BBCP Films:

p(NBI-PLA)-b-p(NBI-PS):

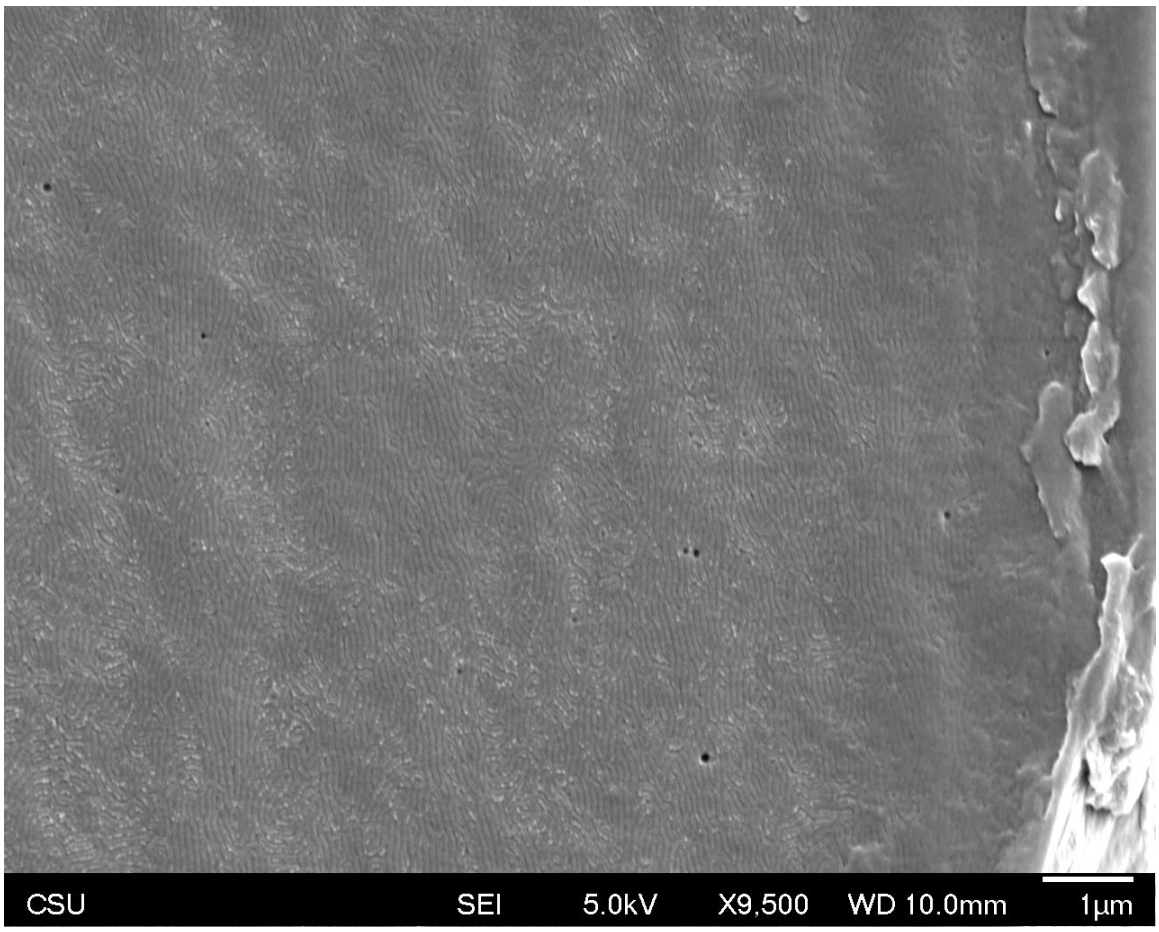

Figure S56. Representative SEM micrograph of the p(NBI-PLA)-b-p(NBI-PS) (M_n = 455,300 g/mol) film.

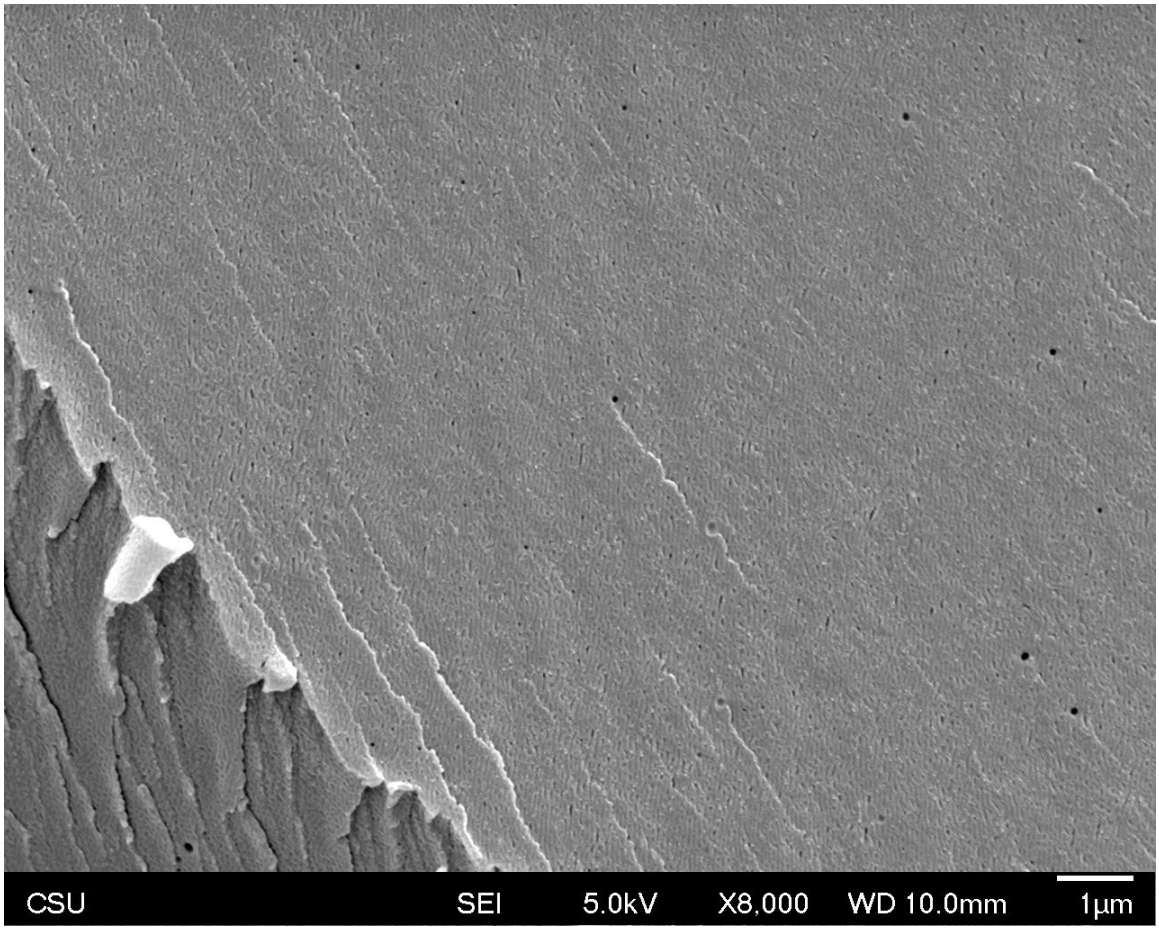

Figure S57. Representative SEM micrograph of the p(NBI-PLA)-b-p(NBI-PS) (M_n = 520,200 g/mol) film.

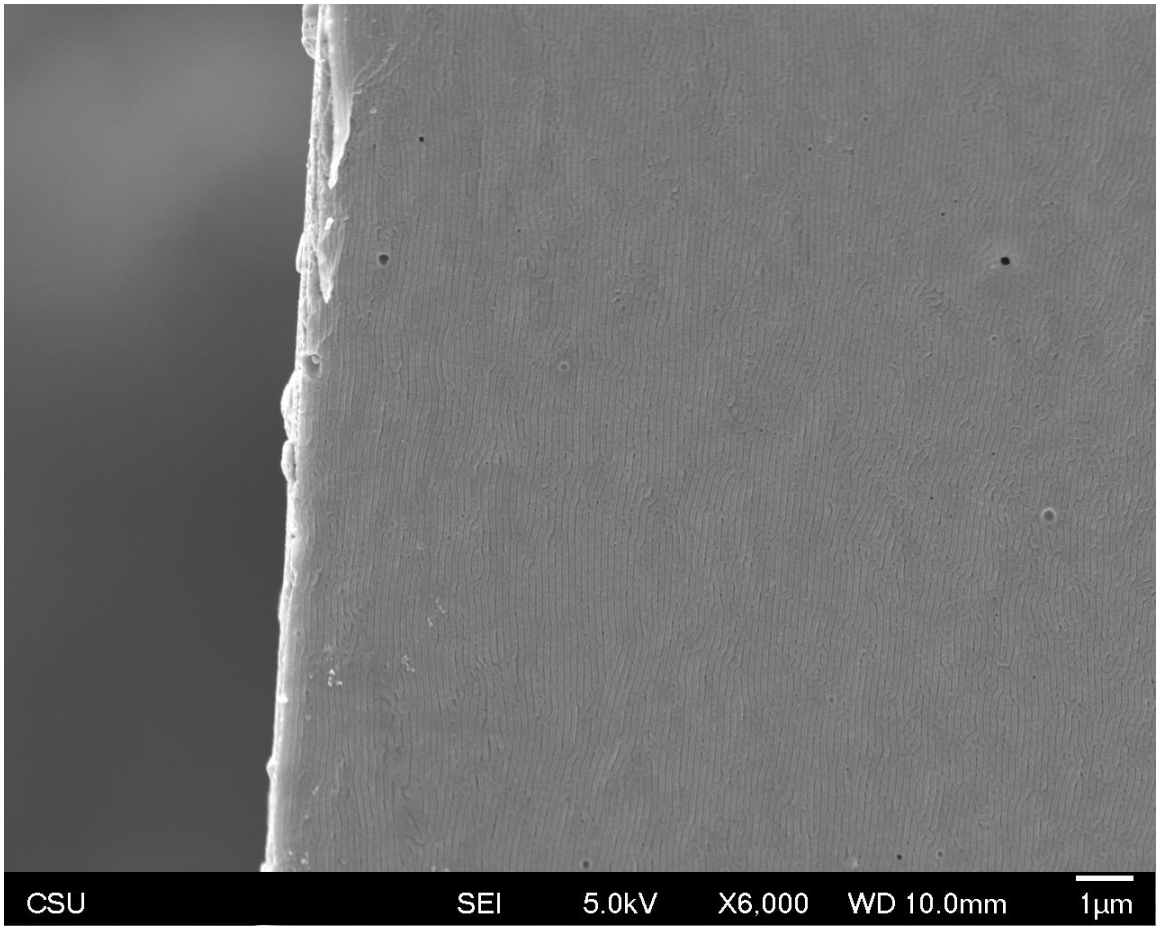

Figure S58. Representative SEM micrograph of the p(NBI-PLA)-b-p(NBI-PS) (M_n = 849,800 g/mol) film.

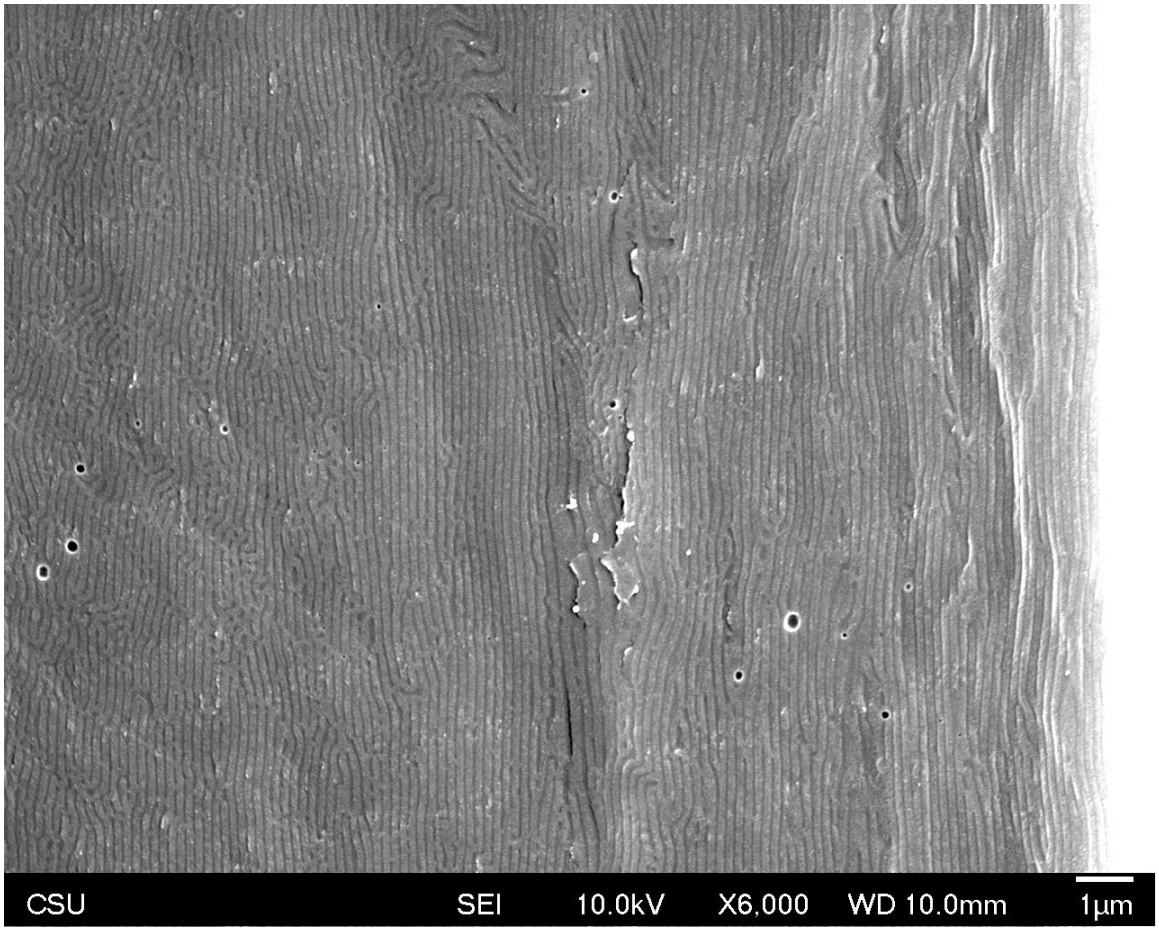

Figure S59. Representative SEM micrograph of the p(NBI-PLA)-b-p(NBI-PS) (M_n = 1,314,000 g/mol) film.

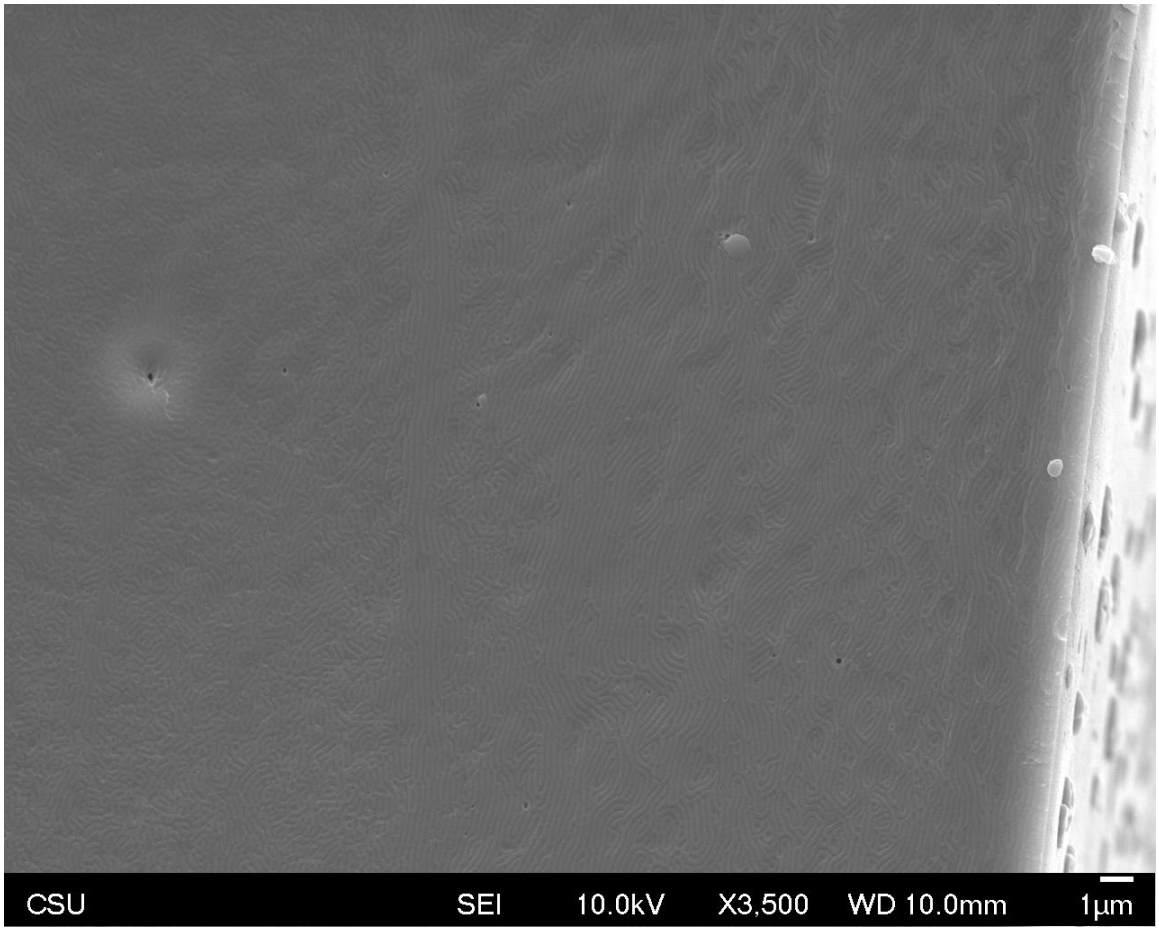

Figure S60. Representative SEM micrograph of the p(NBI-PLA)-b-p(NBI-PS) (M_n = 1,420,000 g/mol) film.

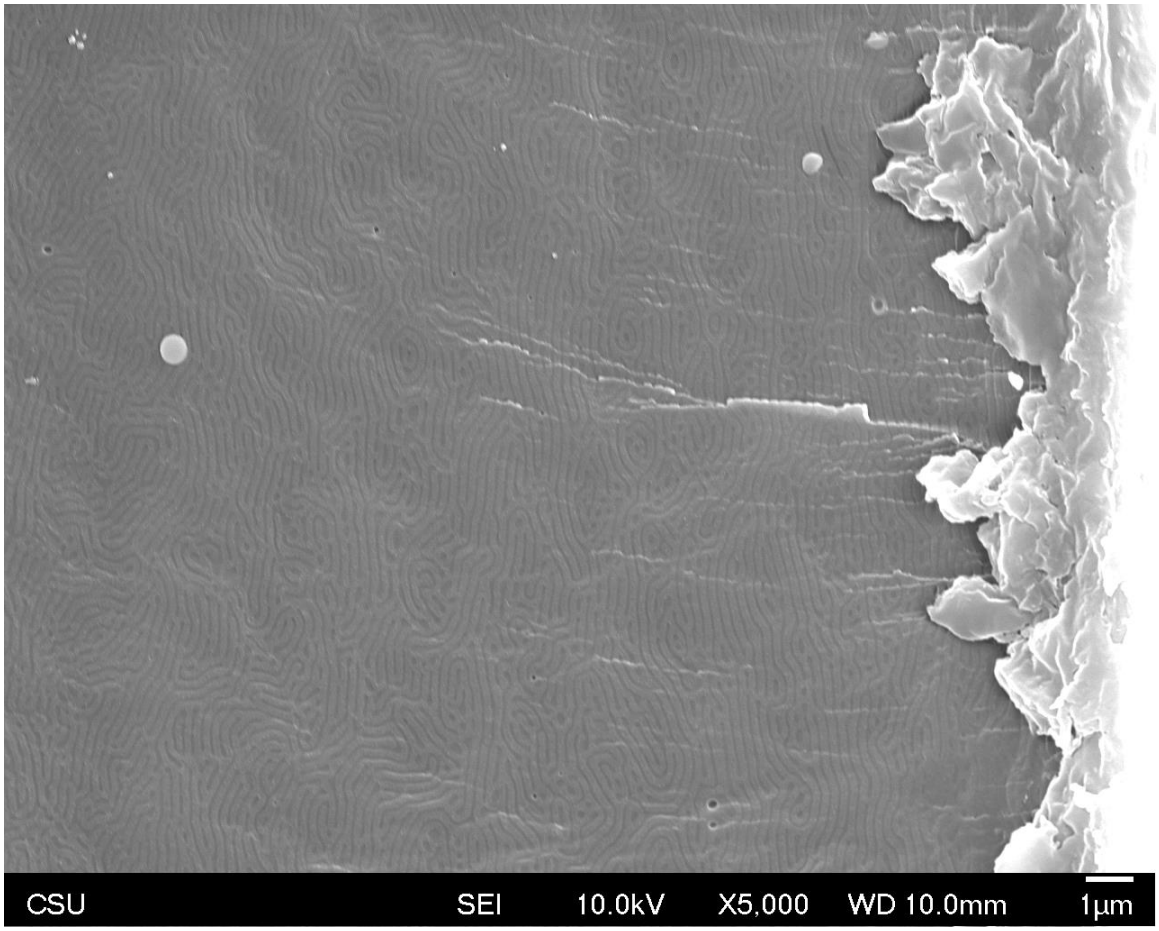

Figure S61. Representative SEM micrograph of the p(NBI-PLA)-b-p(NBI-PS) (M_n = 1,434,000 g/mol) film.

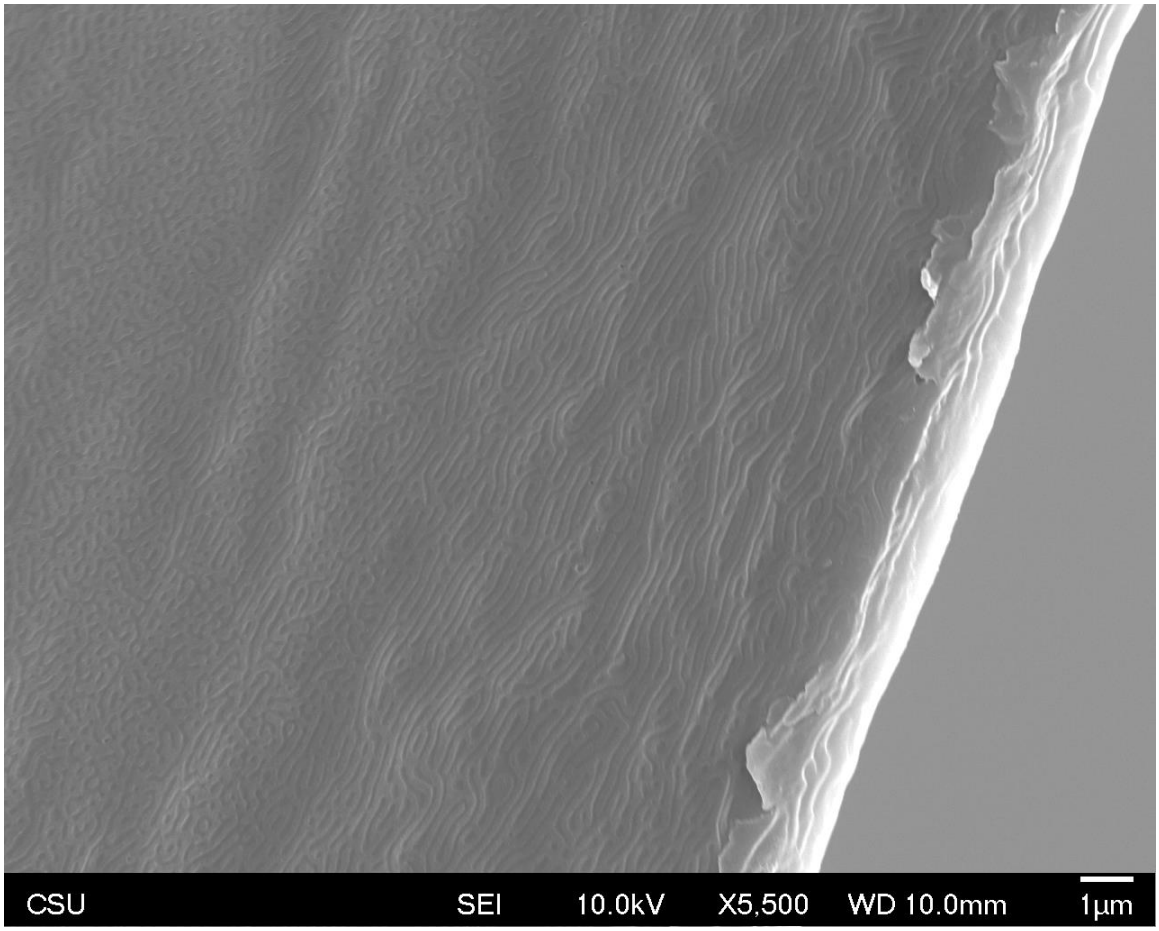

Figure S62. Representative SEM micrograph of the p(NBI-PLA)-b-p(NBI-PS) (M_n = 1,563,000 g/mol) film.

p(NBI-PLA)-b-p(NB-PS):

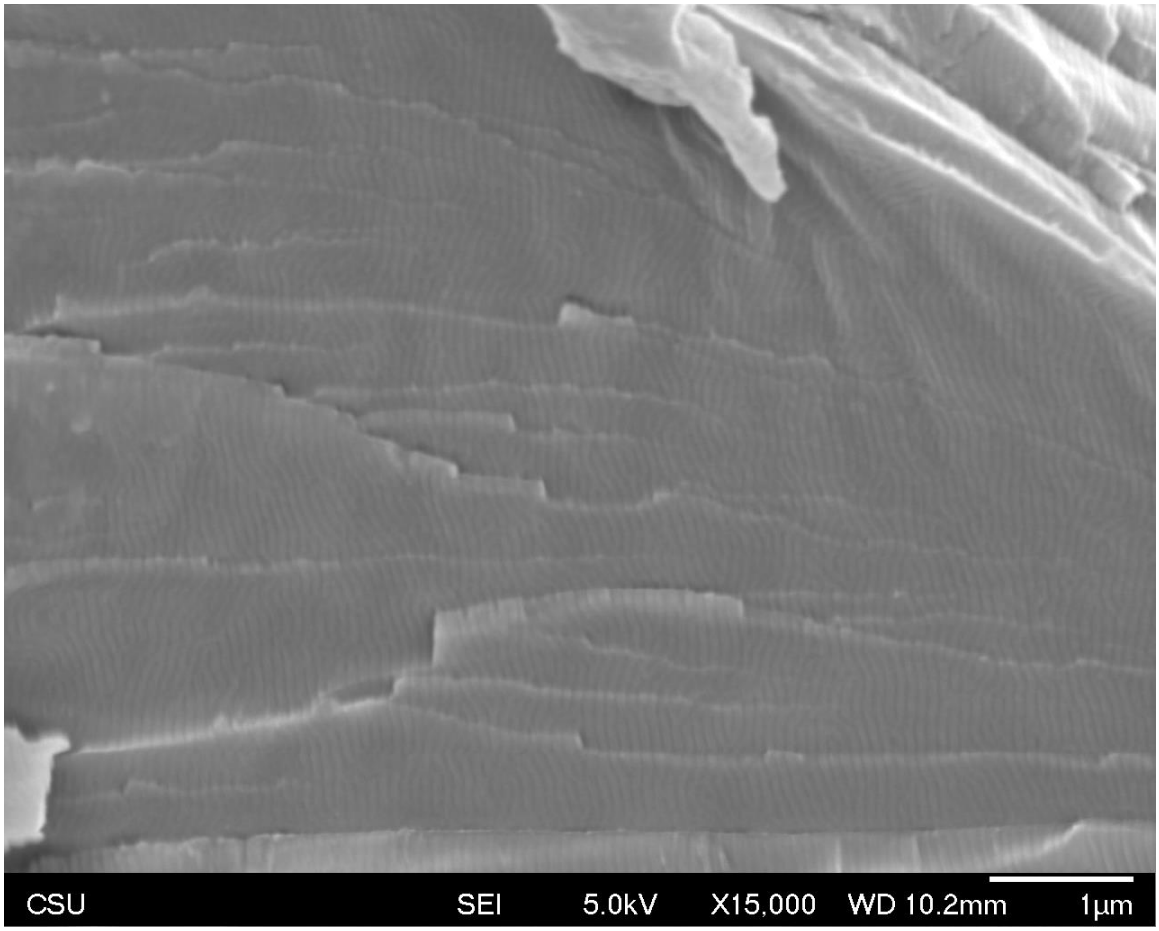

Figure S63. Representative SEM micrograph of the p(NBI-PLA)-b-p(NB-PS) (M_n = 613,000 g/mol) film.

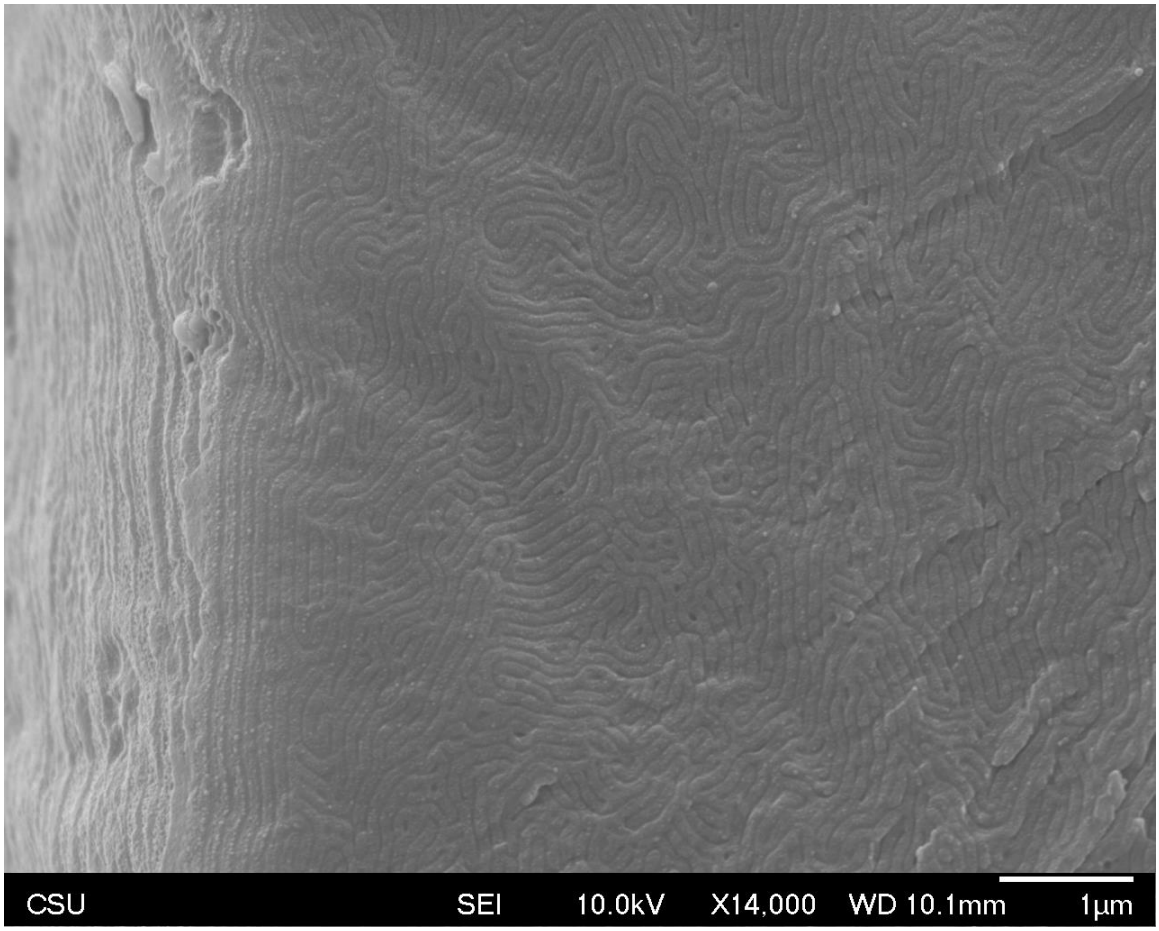

Figure S64. Representative SEM micrograph of the p(NBI-PLA)-b-p(NB-PS) (M_n = 765,800 g/mol) film.

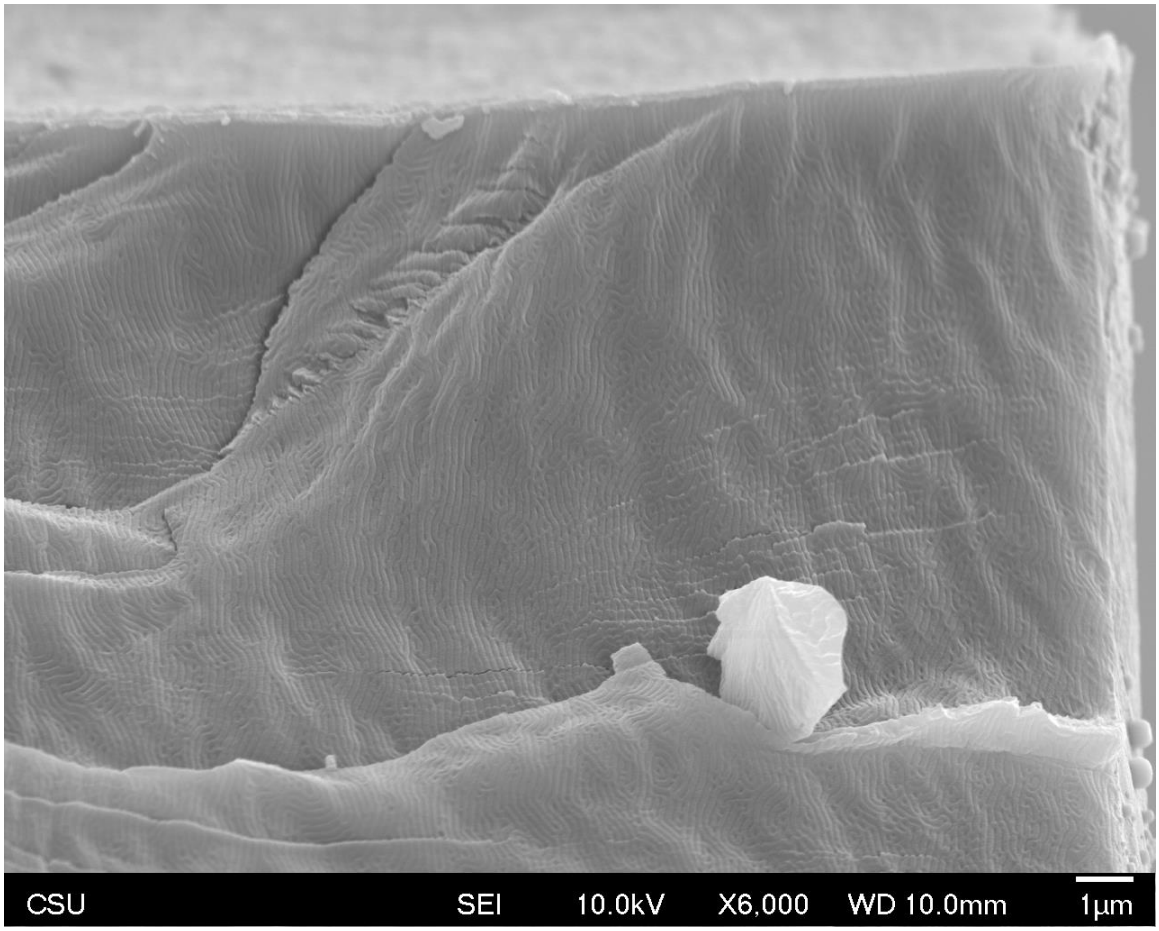

Figure S65. Representative SEM micrograph of the p(NBI-PLA)-b-p(NB-PS) (M_n = 1,110,000 g/mol) film.

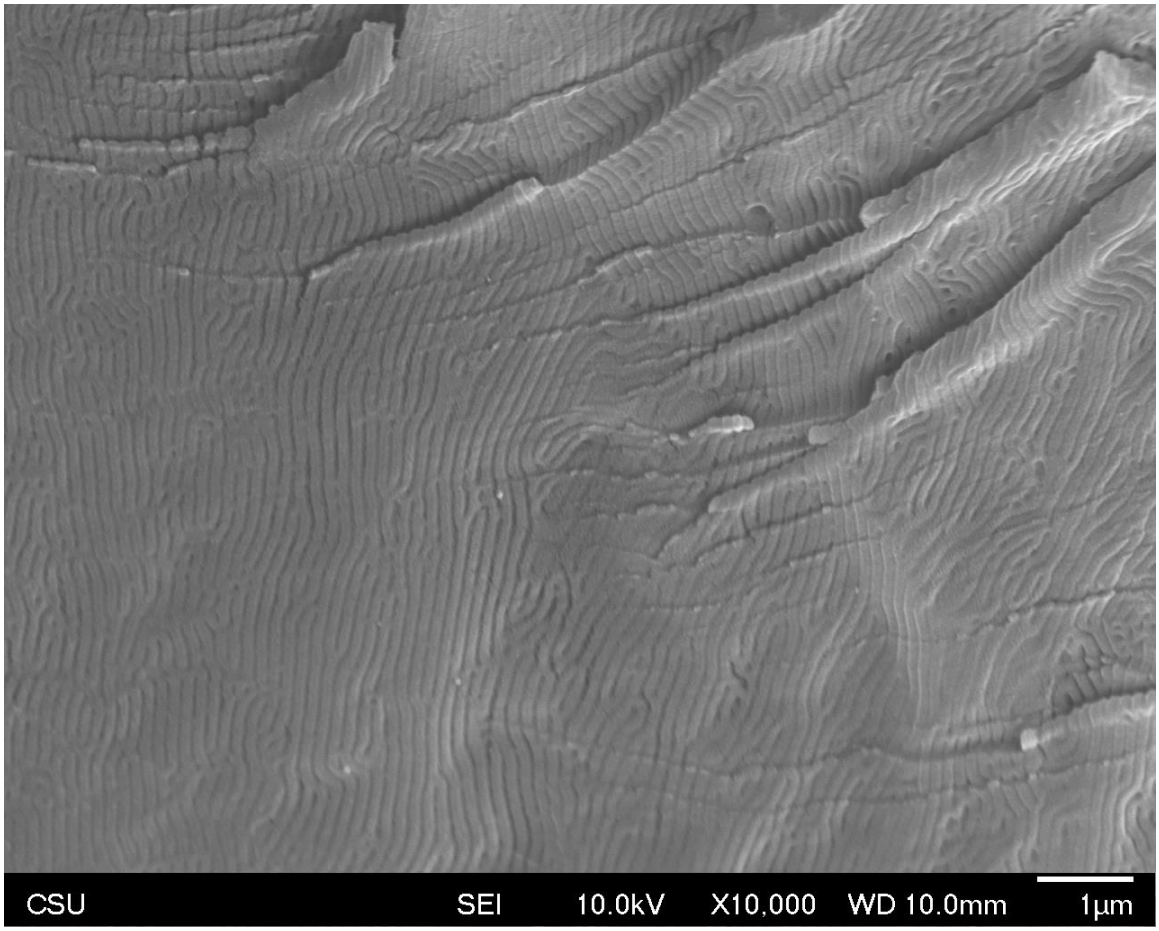

Figure S66. Representative SEM micrograph of the p(NBI-PLA)-b-p(NB-PS) (M_n = 1,524,000 g/mol) film.

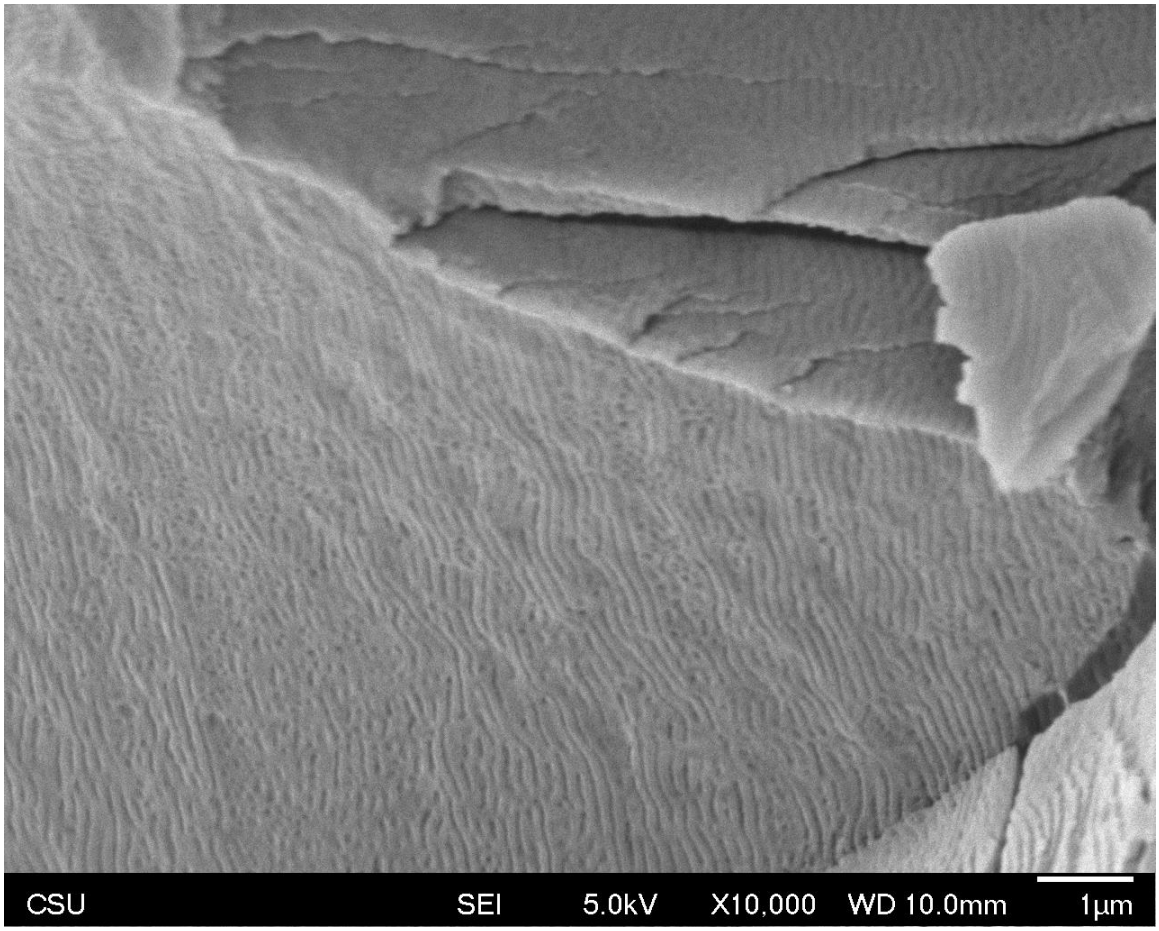

Figure S67. Representative SEM micrograph of the p(NBI-PLA)-b-p(NB-PS) (M_n = 1,657,000 g/mol) film.

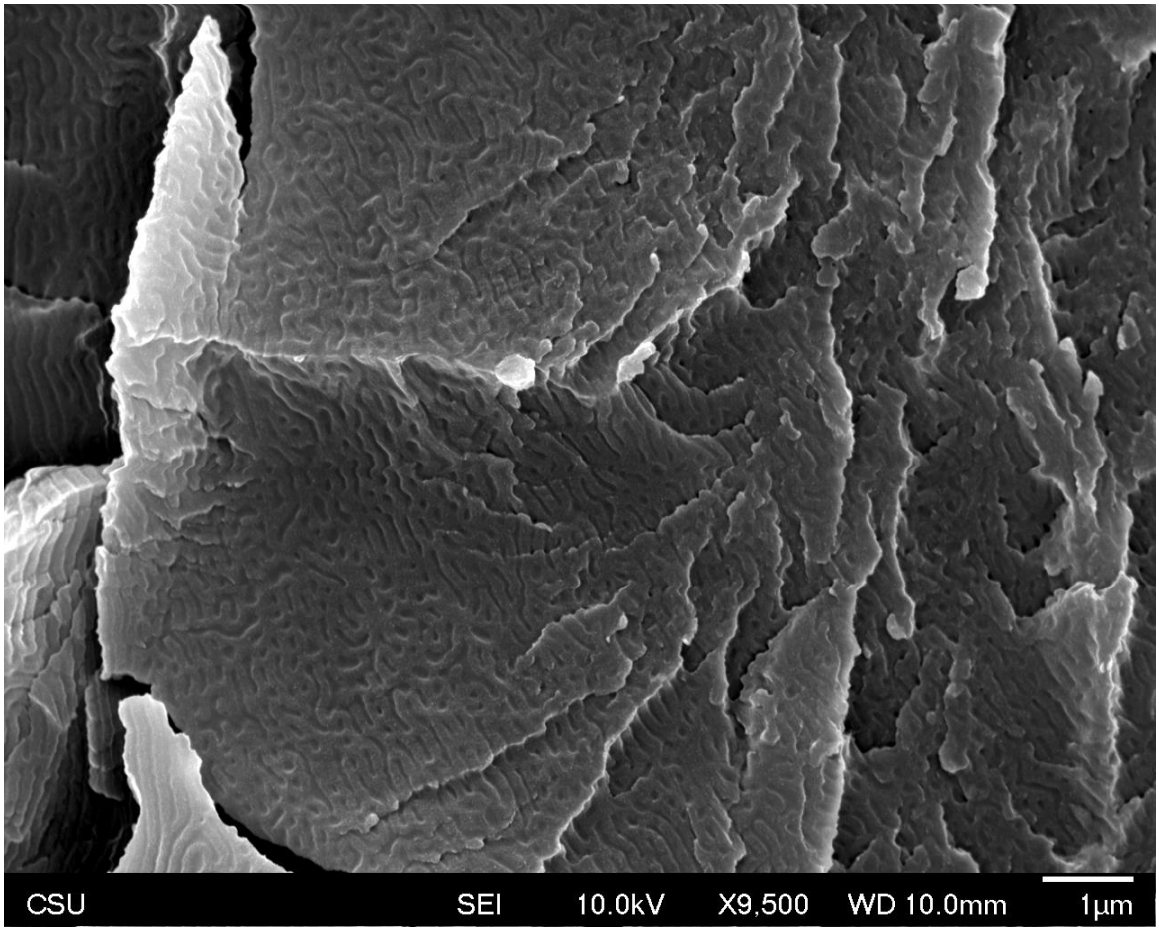

Figure S68. Representative SEM micrograph of the p(NBI-PLA)-b-p(NB-PS) (M_n = 2,601,000 g/mol) film.

p(NB-PLA)-b-p(NBI-PS):

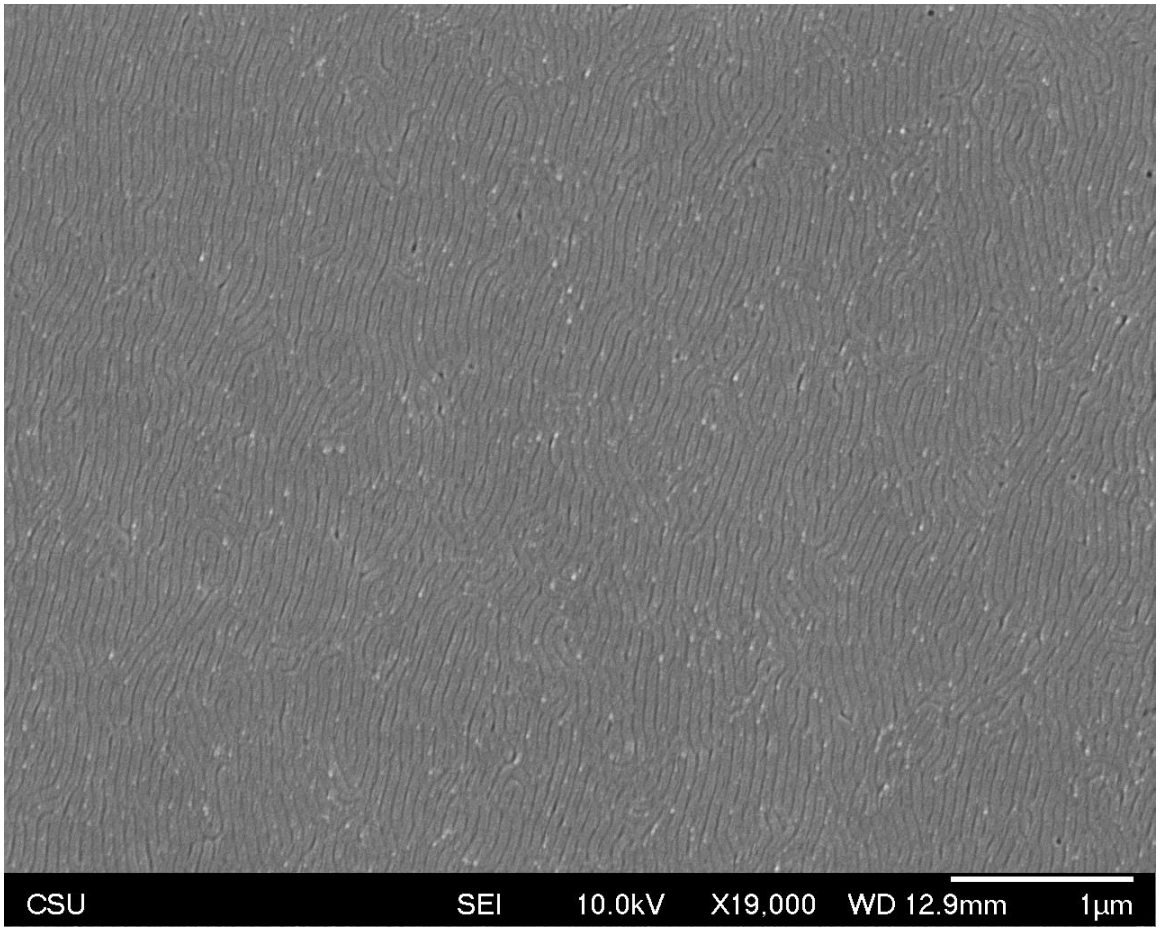

Figure S69. Representative SEM micrograph of the p(NB-PLA)-b-p(NBI-PS) (M_n = 524,100 g/mol) film.

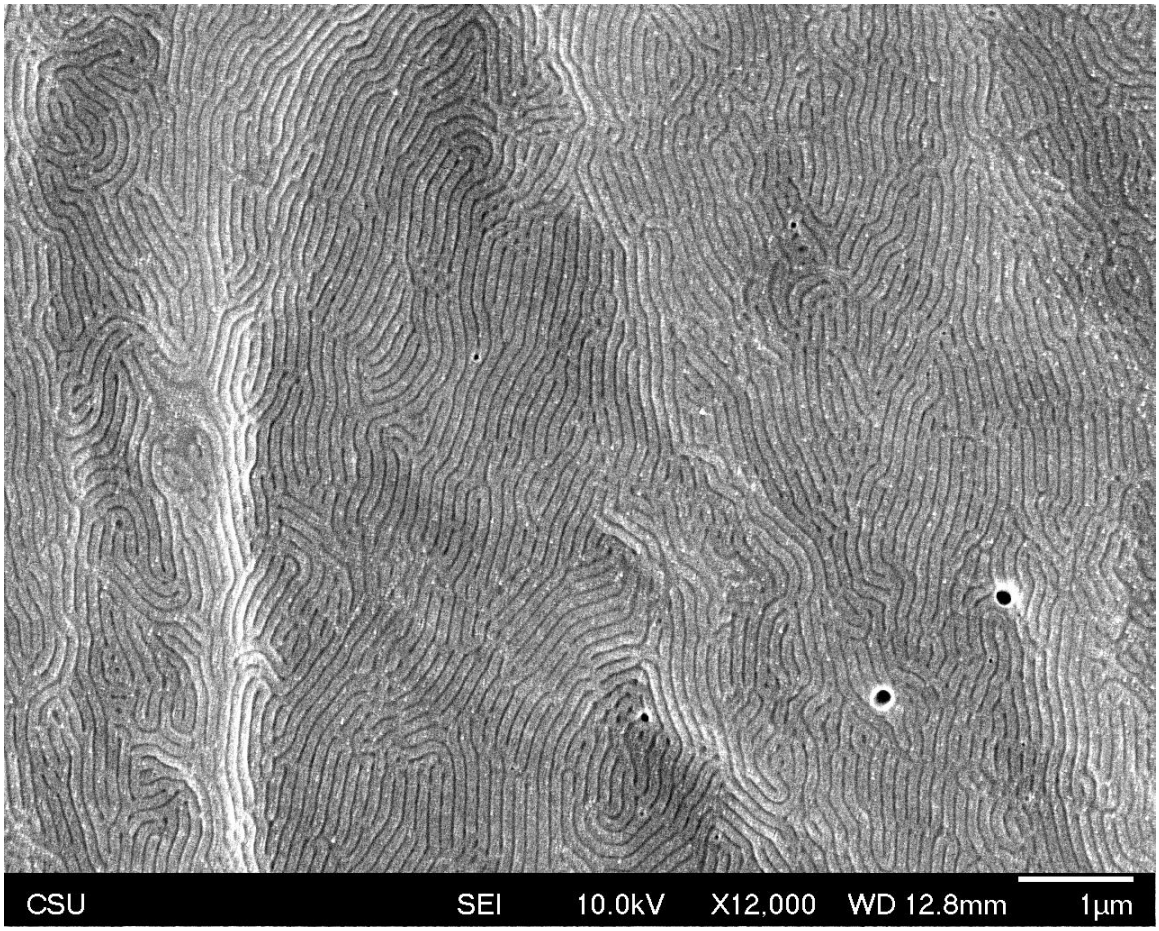

Figure S70. Representative SEM micrograph of the p(NB-PLA)-b-p(NBI-PS) (M_n = 917,500 g/mol) film.

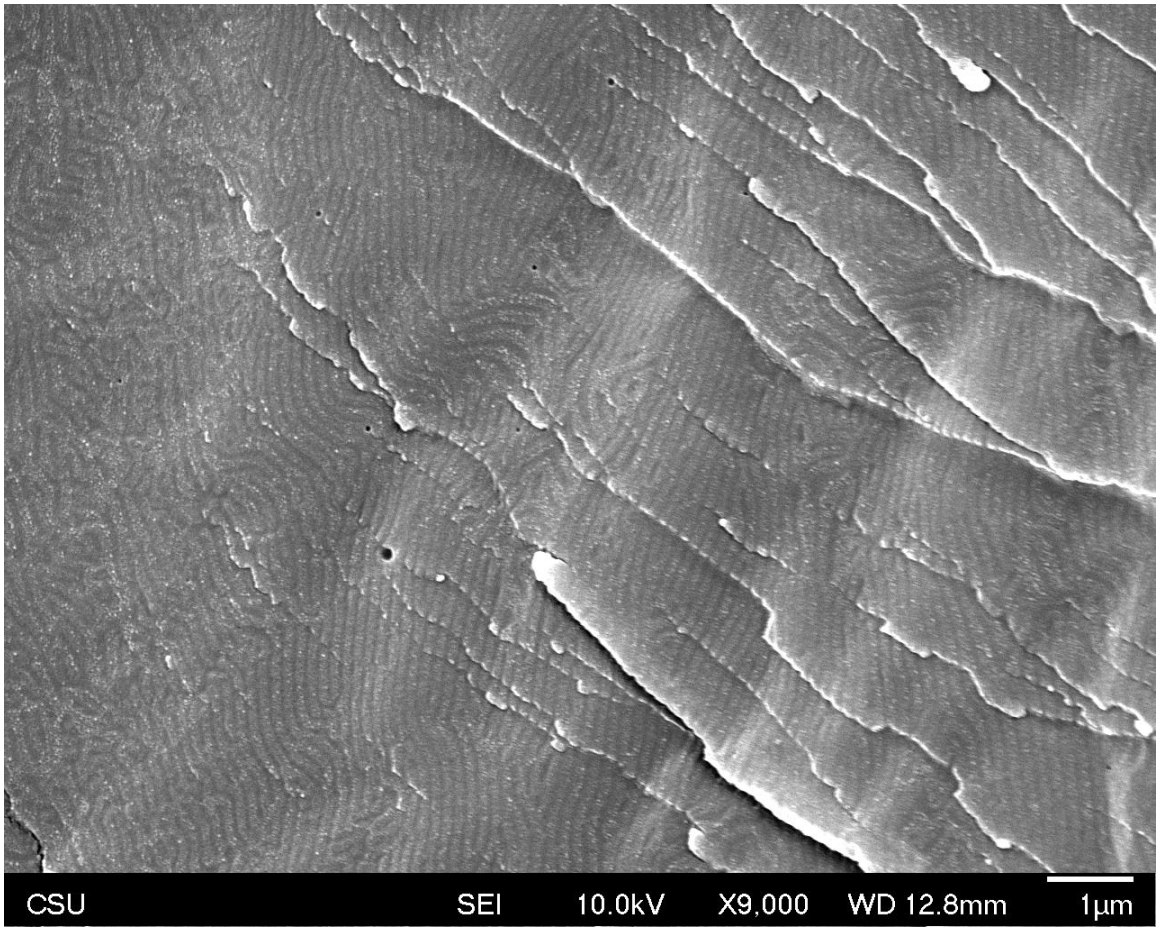

Figure S71. Representative SEM micrograph of the p(NB-PLA)-b-p(NBI-PS) (M_n = 1,435,000 g/mol) film.

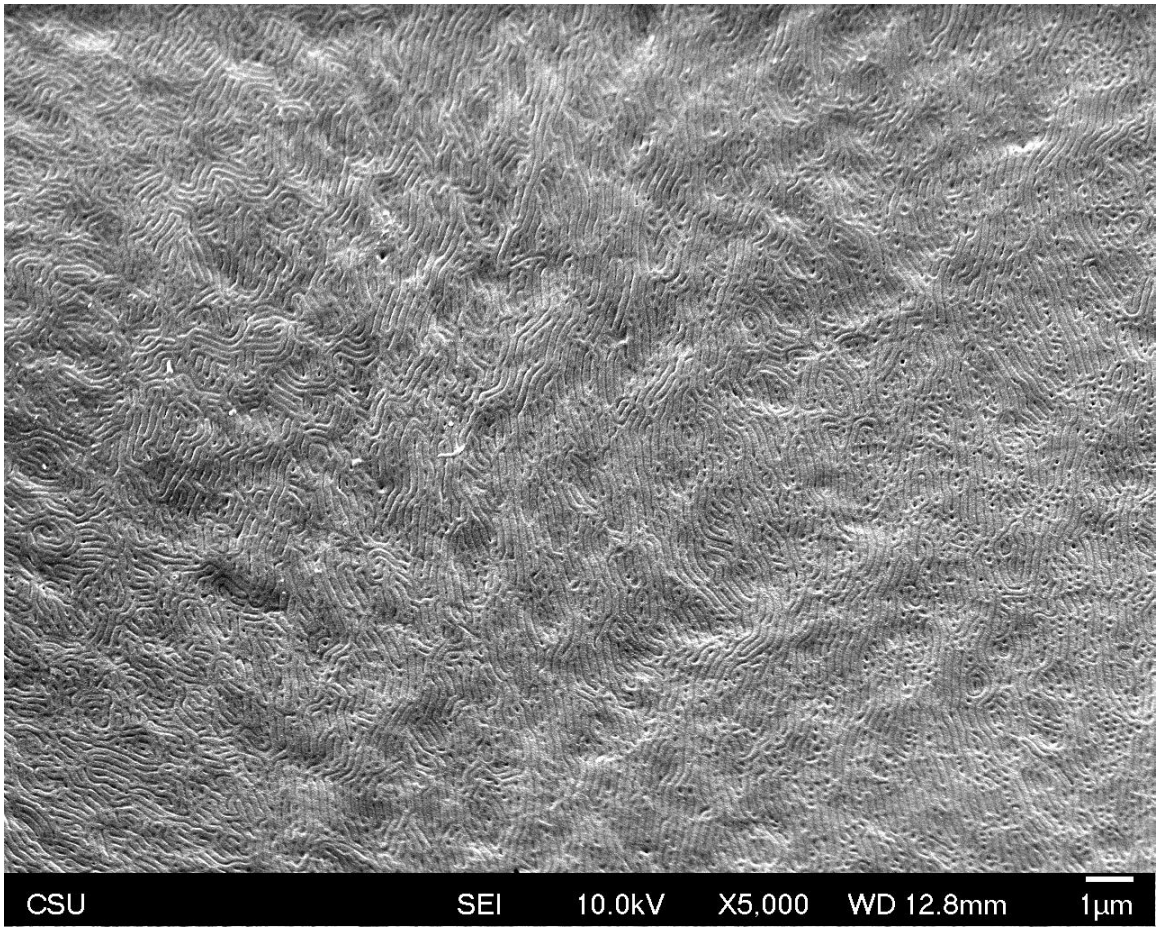

Figure S72. Representative SEM micrograph of the p(NB-PLA)-b-p(NBI-PS) (M_n = 1,875,000 g/mol) film.

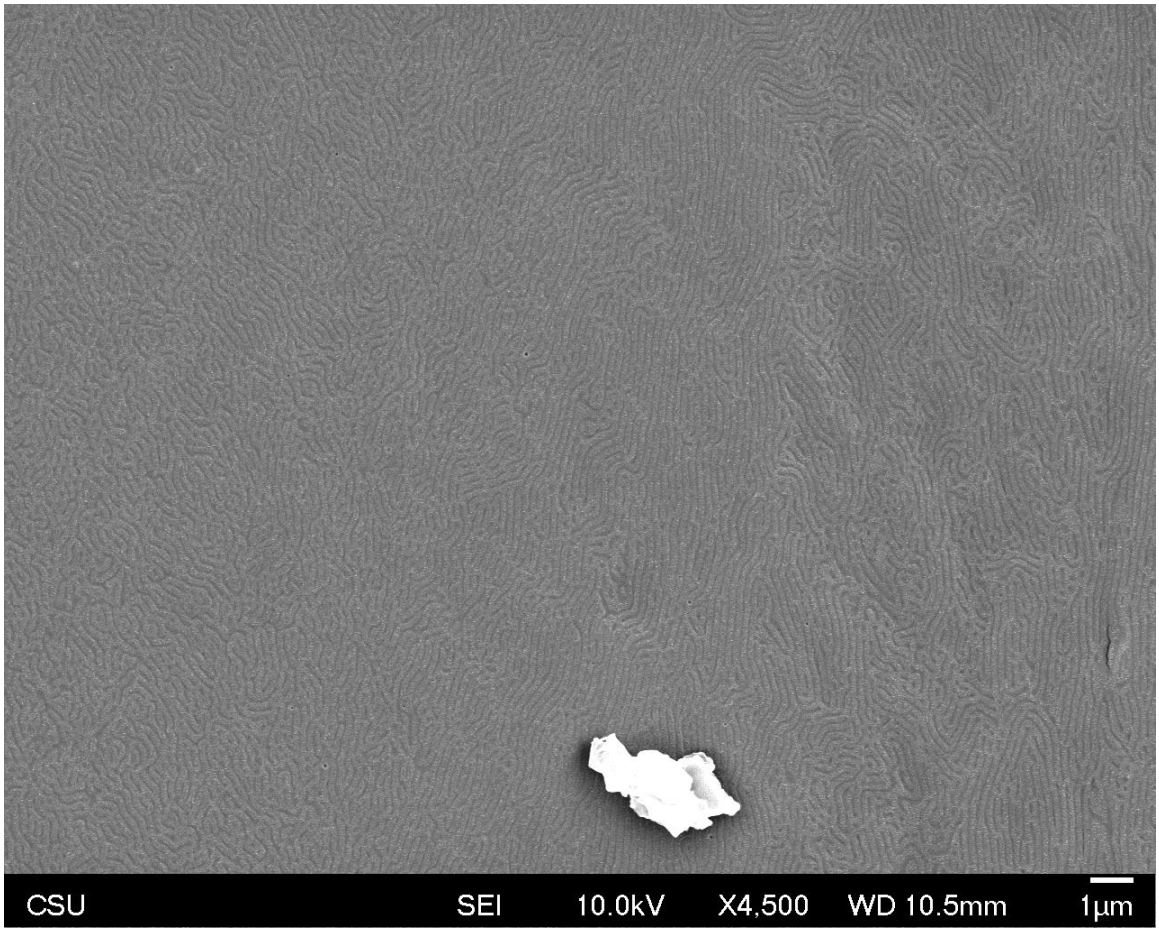

Figure S73. Representative SEM micrograph of the p(NB-PLA)-b-p(NBI-PS) (M_n = 1,904,000 g/mol) film.

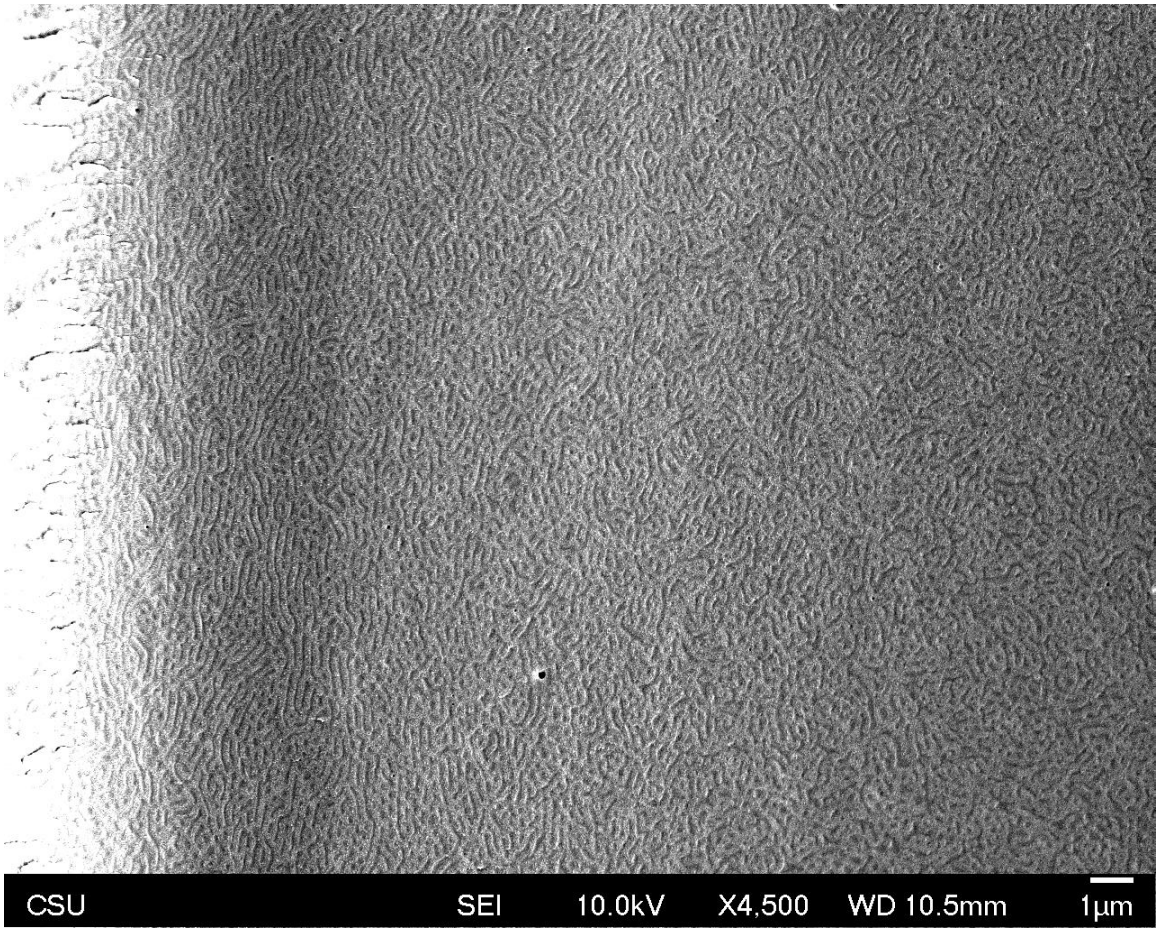

Figure S74. Representative SEM micrograph of the p(NB-PLA)-b-p(NBI-PS) (M_n = 2,134,000 g/mol) film.

p(NB-PLA)-b-p(NB-PS):

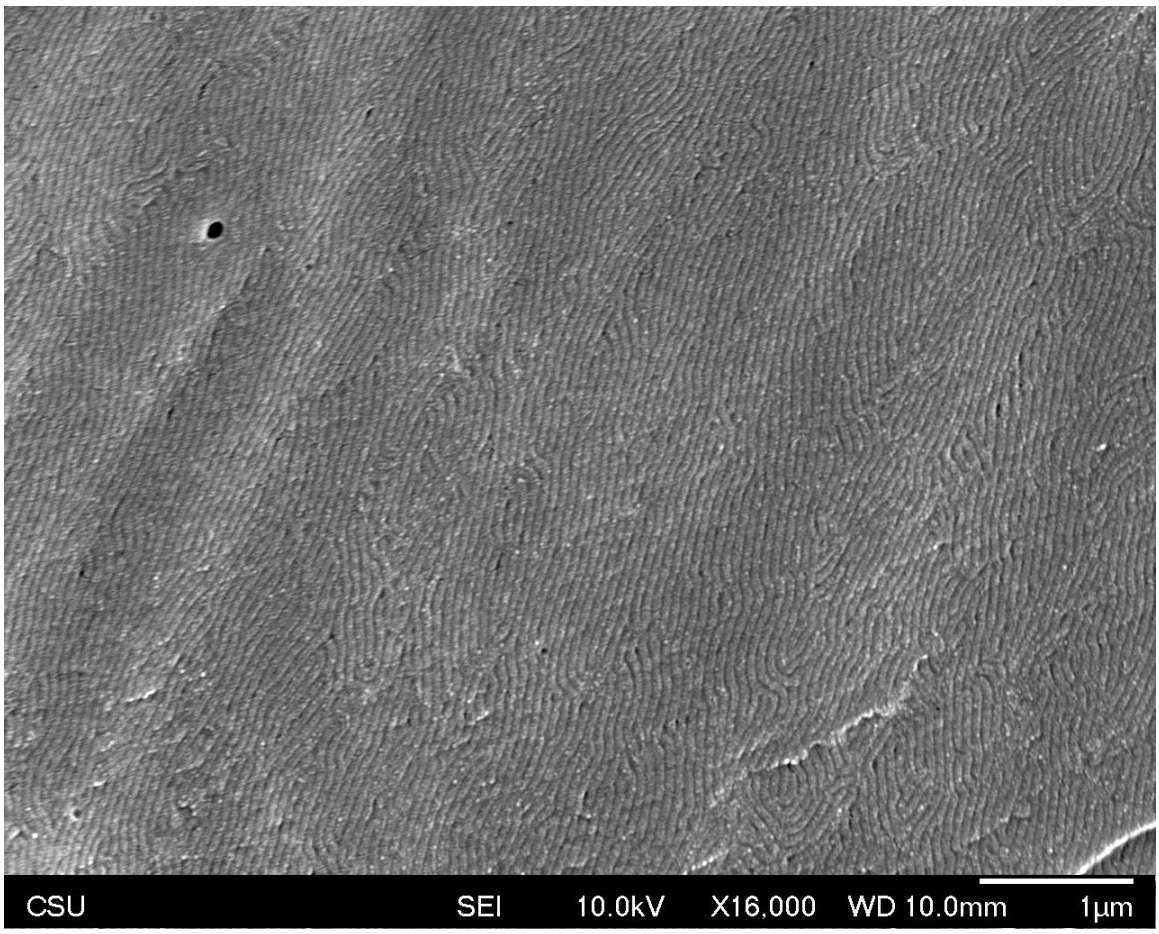

Figure S75. Representative SEM micrograph of the p(NB-PLA)-b-p(NB-PS) (M_n = 413,600 g/mol) film.

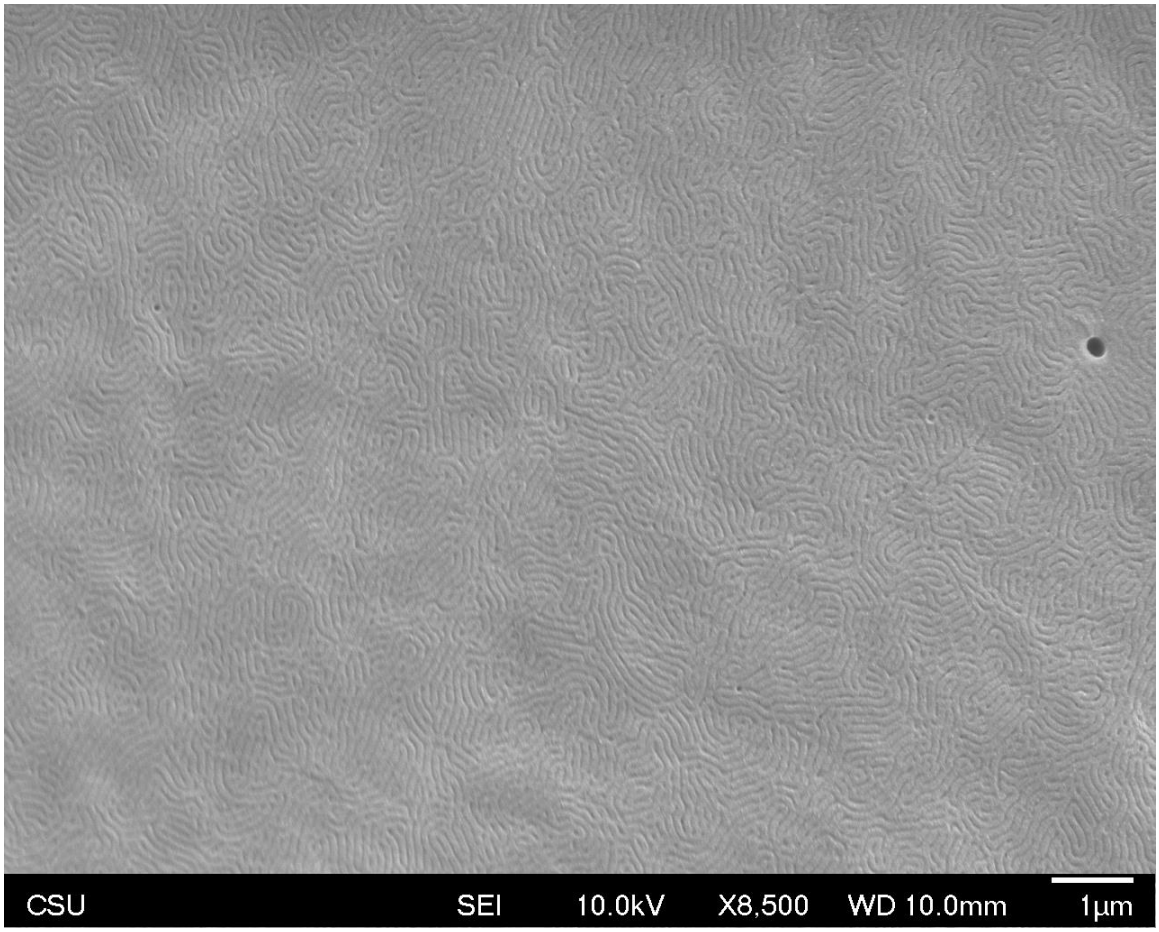

Figure S76. Representative SEM micrograph of the p(NB-PLA)-b-p(NB-PS) (M_n = 787,000 g/mol) film.

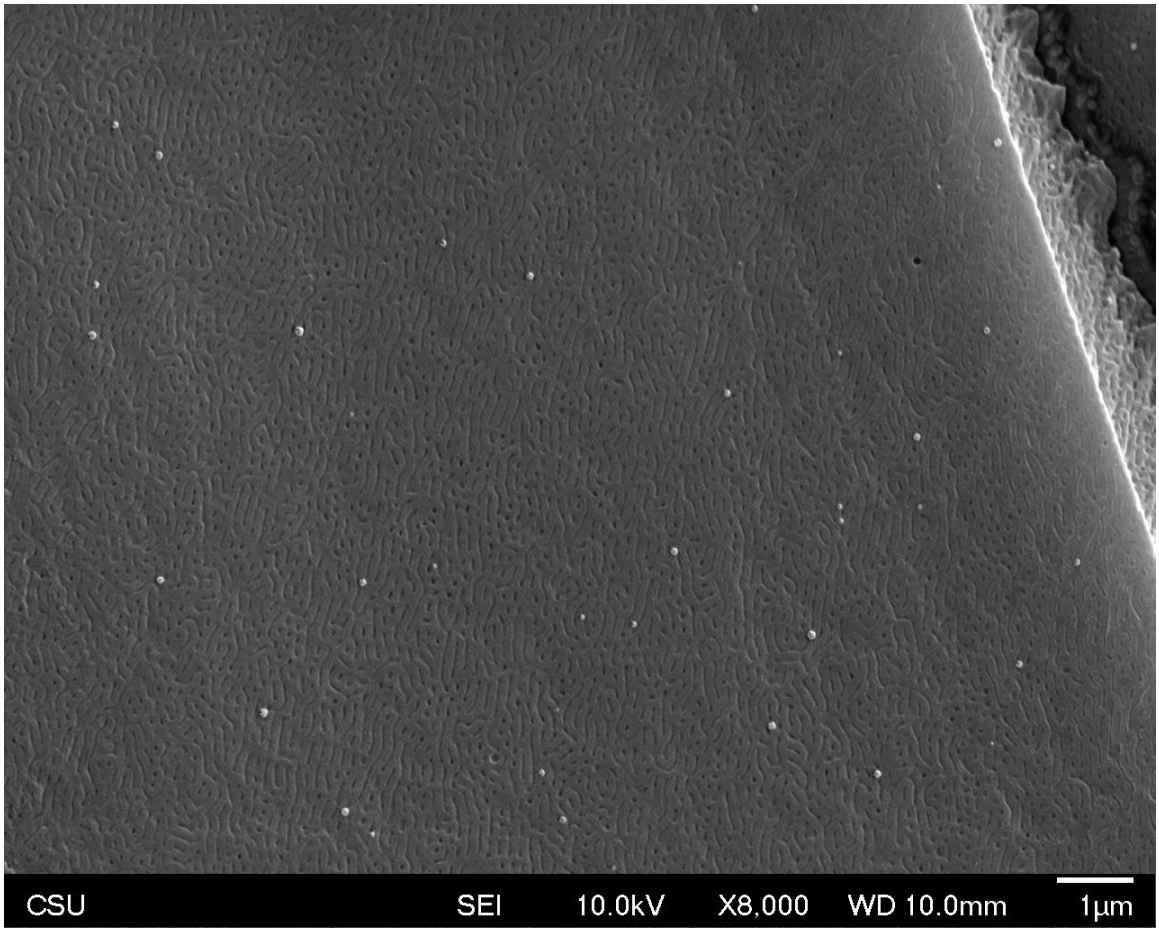

Figure S77. Representative SEM micrograph of the p(NB-PLA)-b-p(NB-PS) (M_n = 1,305,000 g/mol) film.

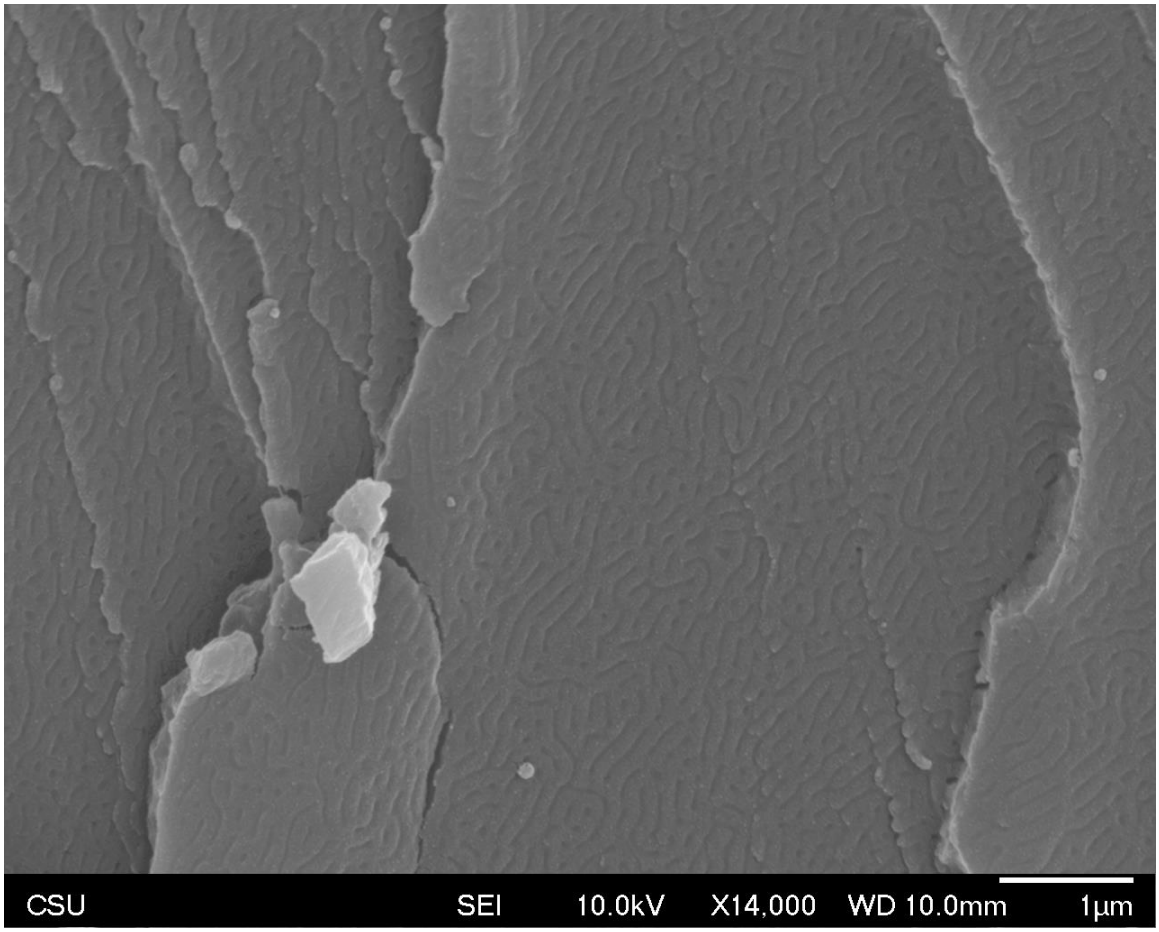

Figure S78. Representative SEM micrograph of the p(NB-PLA)-b-p(NB-PS) (M_n = 1,733,000 g/mol) film.

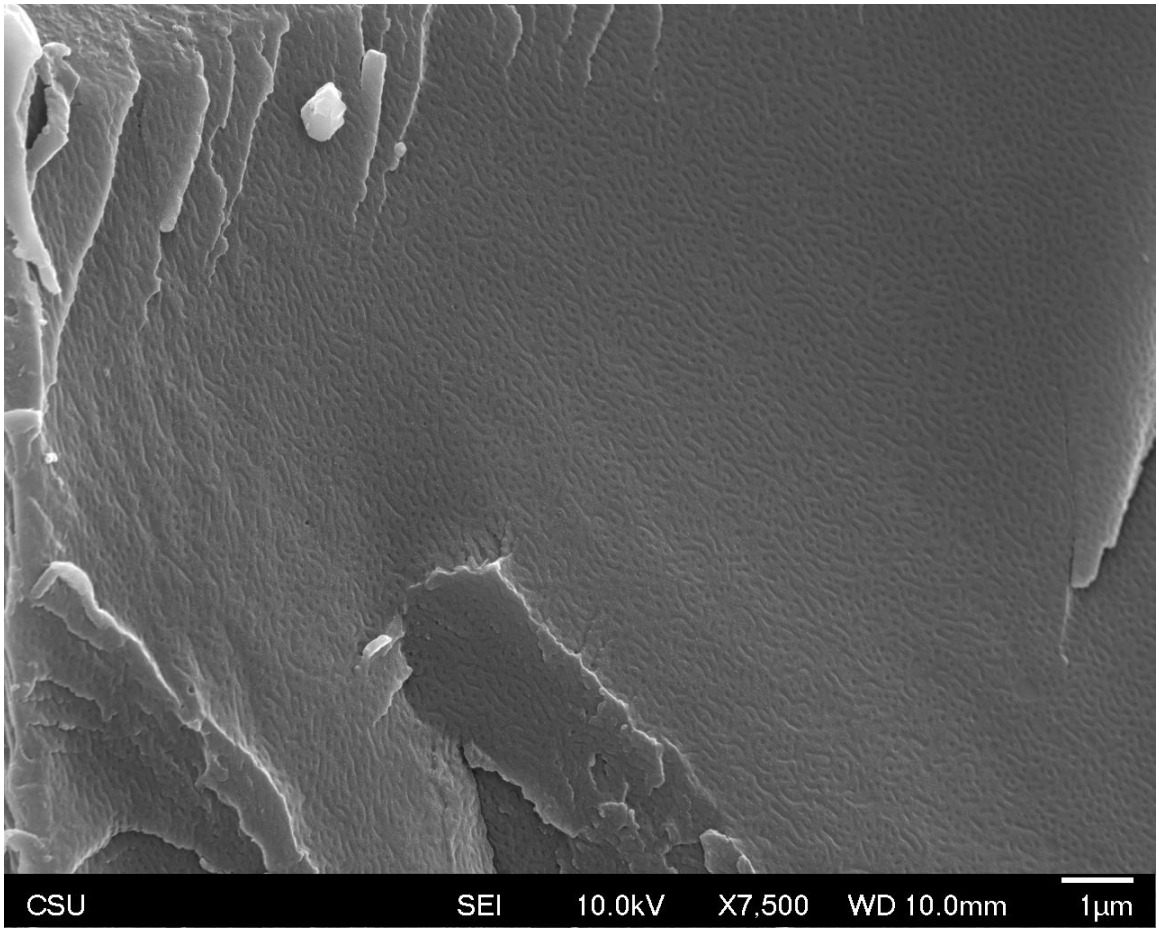

Figure S79. Representative SEM micrograph of the p(NB-PLA)-b-p(NB-PS) (M_n = 1,700,000 g/mol) film.

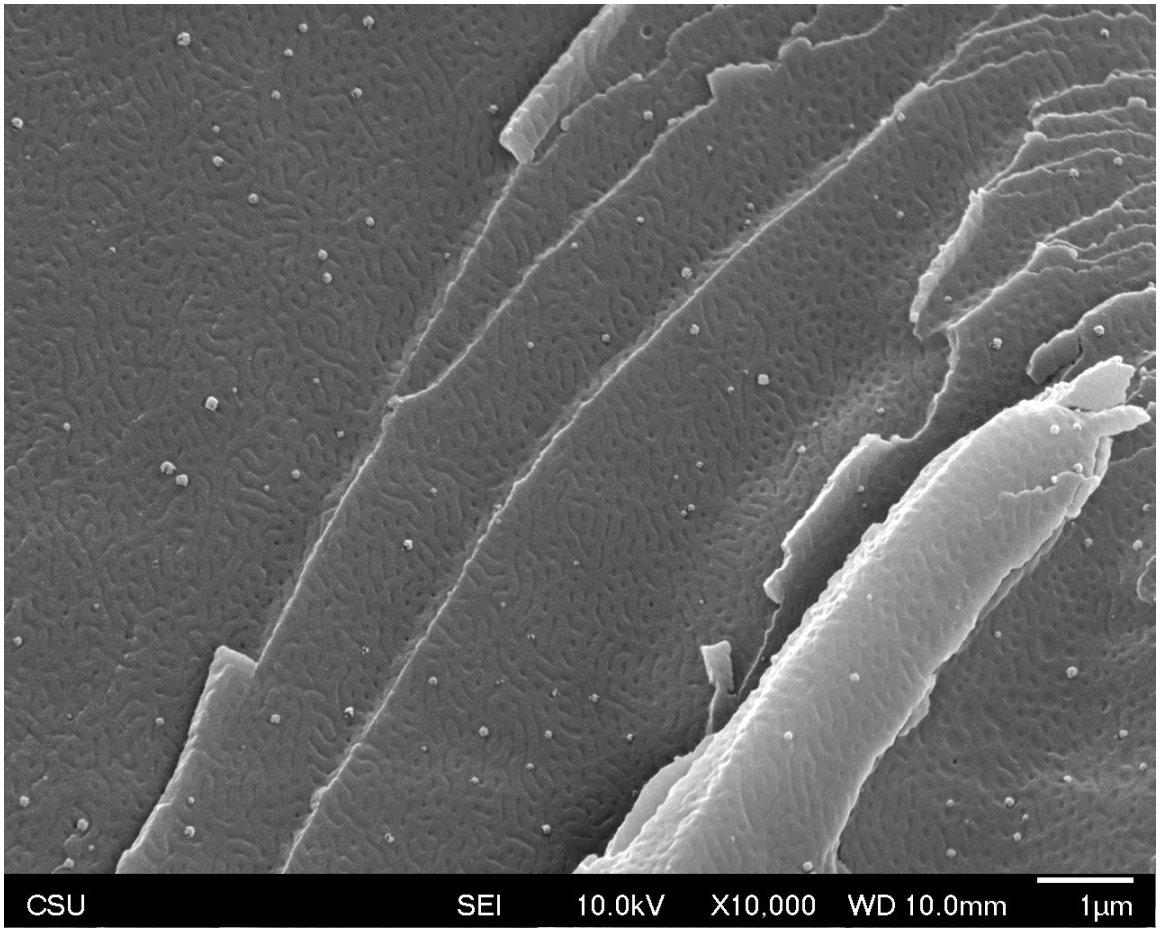

Figure S80. Representative SEM micrograph of the p(NB-PLA)-b-p(NB-PS) (M_n = 2,299,000 g/mol) film.

In-Situ SAXS Measurements:

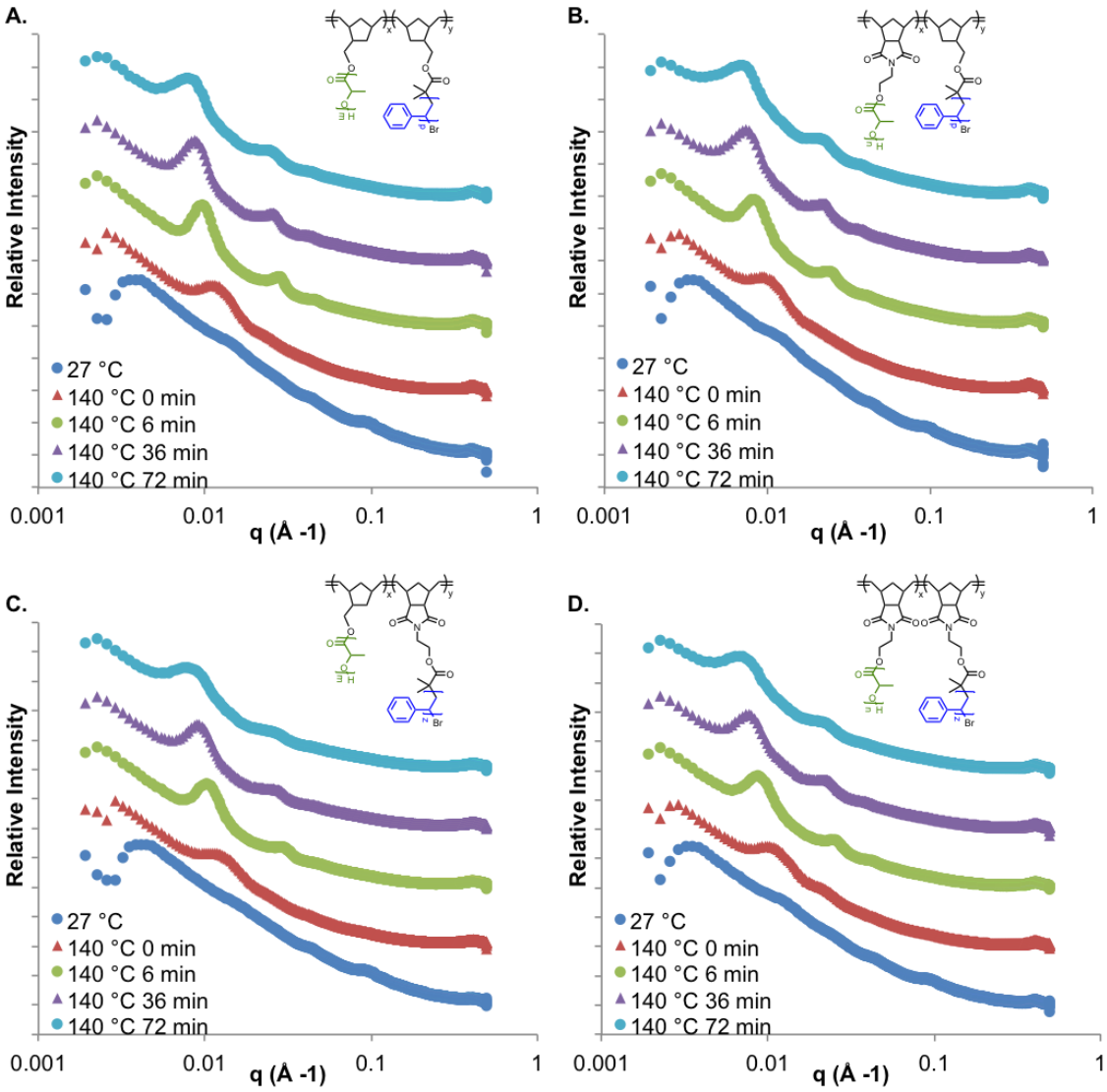

Figure S81. Log-log *in-situ* SAXS profiles for each of the four lowest MW BBCP assembled films (*p*(NB-PLA)-*b*-*p*(NB-PS) (A), *p*(NBI-PLA)-*b*-*p*(NB-PS) (B), *p*(NB-PLA)-*b*-*p*(NBI-PS) (C), and *p*(NBI-PLA)-*b*-*p*(NBI-PS) (D)). Spectra are vertically shifted for clarity.

Thermal Properties:

Thermal Gravimetric Analysis (TGA)

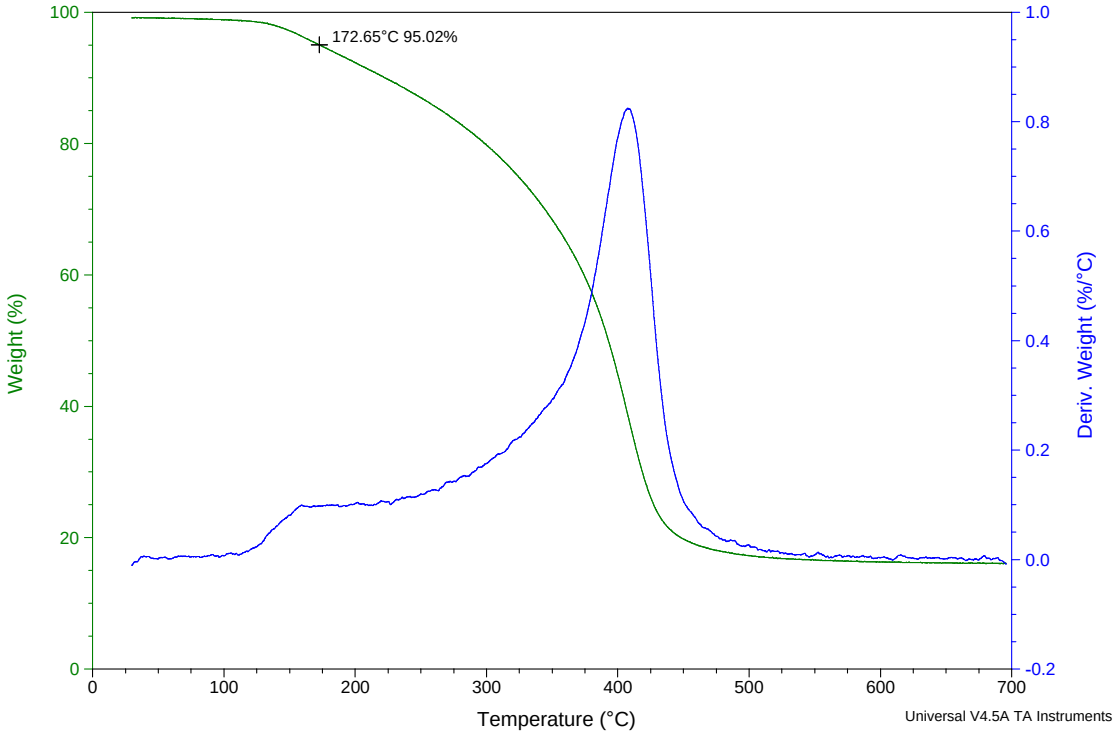

Figure S82. TGA trace of p(NB-Hep) (M_n = 242,900 g/mol). Decomposition temperature at 5% weight loss is 172.7 °C.

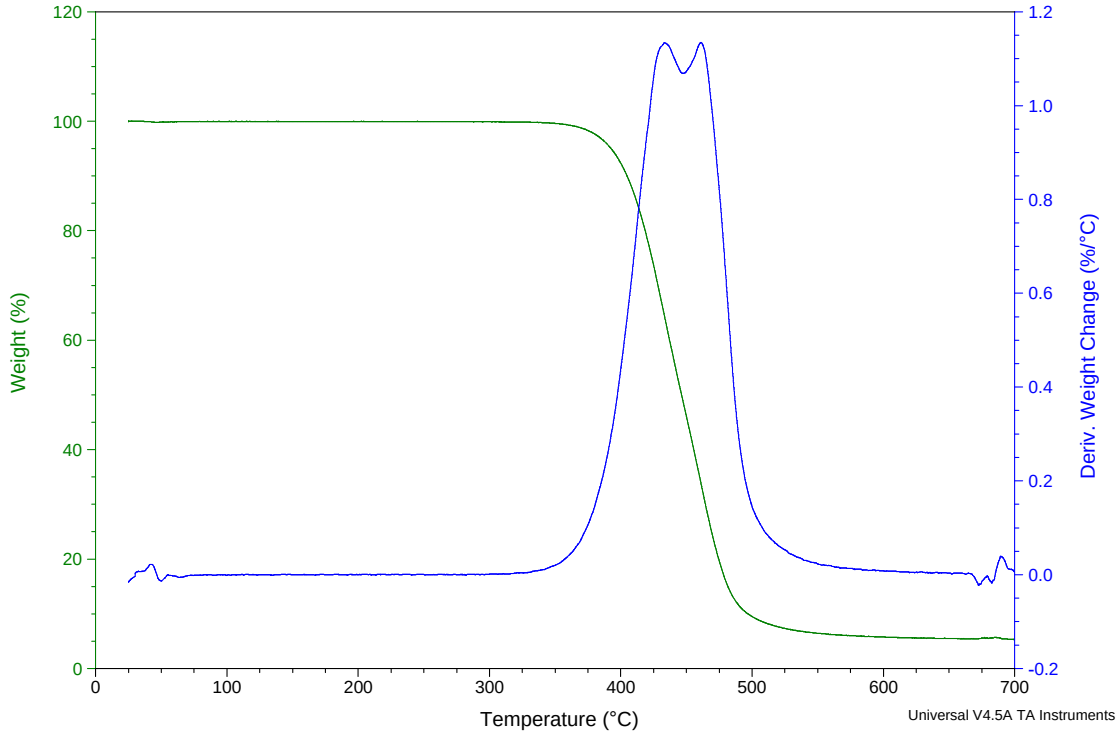

Figure S83. TGA trace of p(NBI-Hep) (M_n = 114,900 g/mol). Decomposition temperature at 5% weight loss is 392.7 °C.

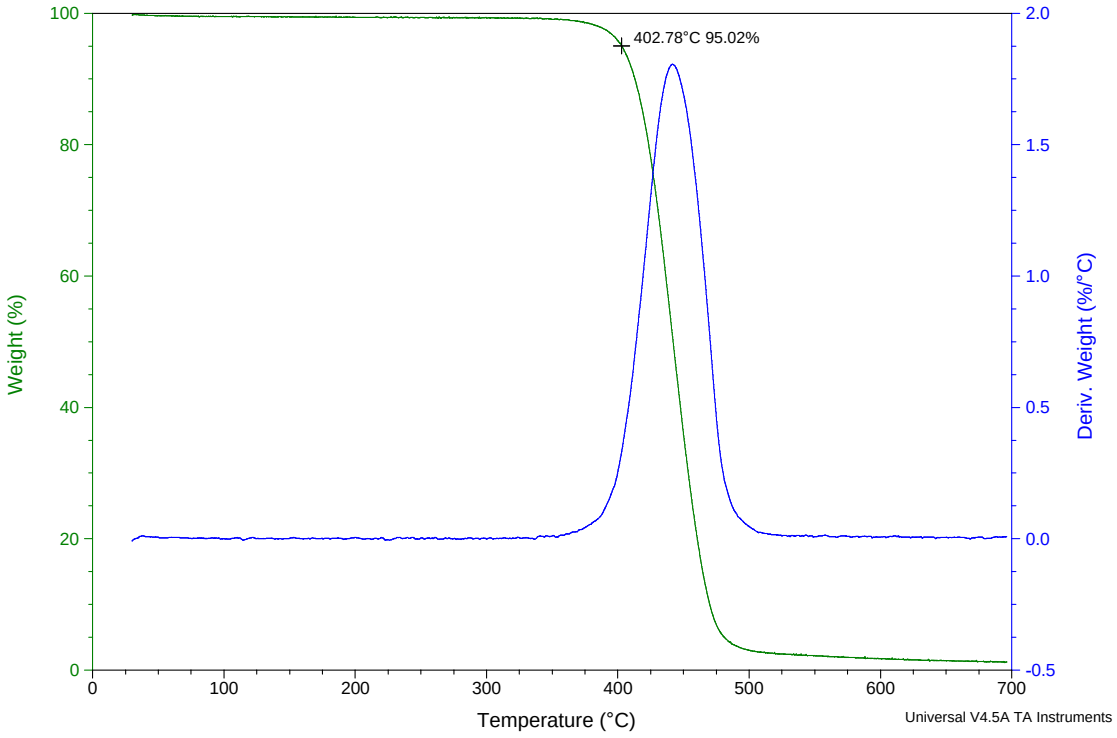

Figure S84. TGA trace of p(NBI-Dec) (M_n = 779,700 g/mol). Decomposition temperature at 5% weight loss is 402.78 °C.

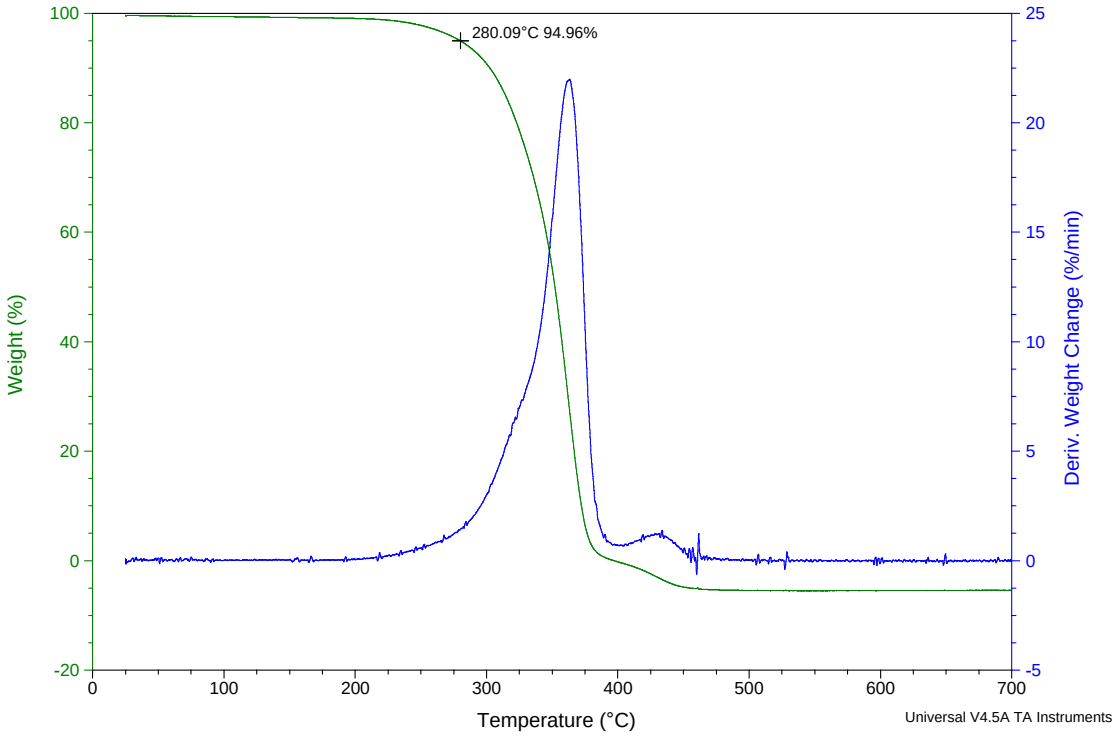

Figure S85. TGA trace of p(NB-PLA) (M_n = 209,600 g/mol). Decomposition temperature at 5% weight loss is 280.0 °C.

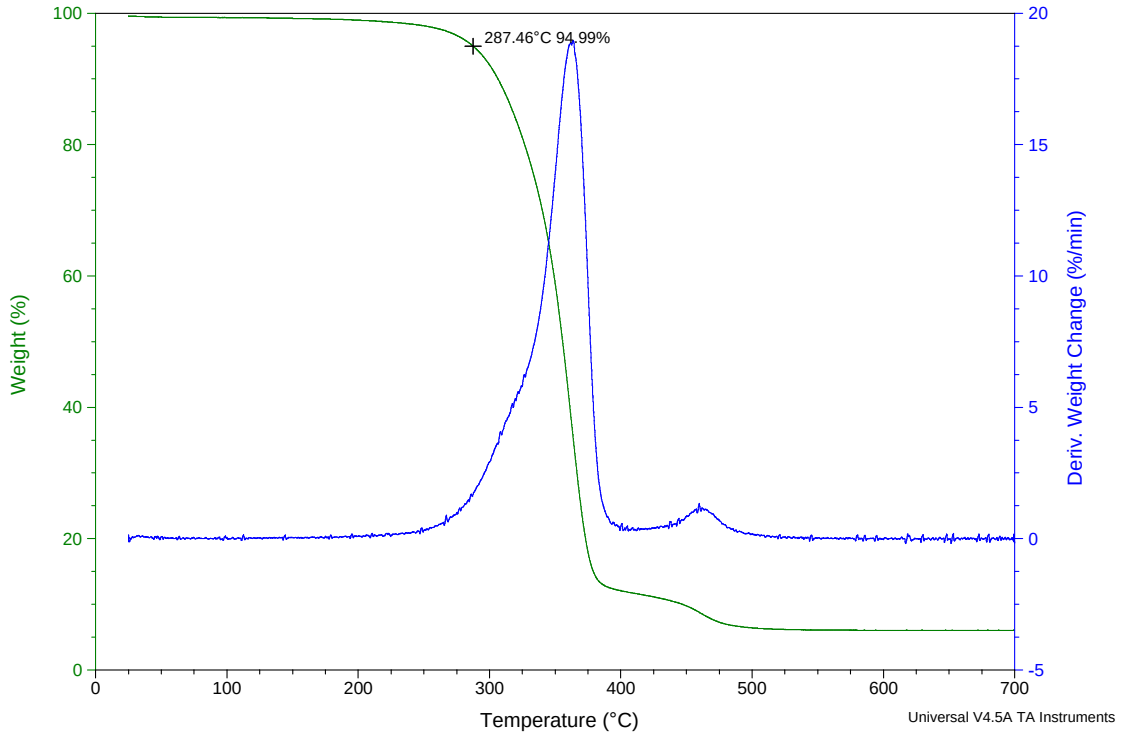

Figure S86. TGA trace of p(NBI-PLA) (M_n = 254,500 g/mol). Decomposition temperature at 5% weight loss is 287.5 °C.

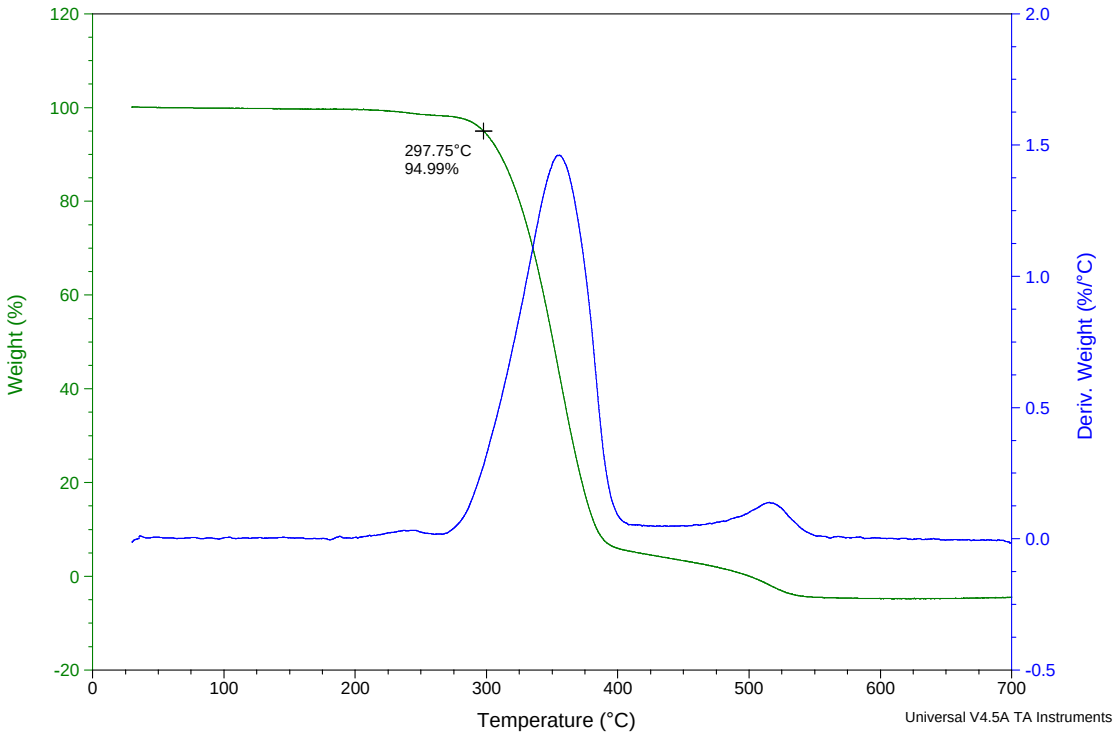

Figure S87. TGA trace of p(NB-PS) (M_n = 1,242,000 g/mol). Decomposition temperature at 5% weight loss is 297.8 °C.

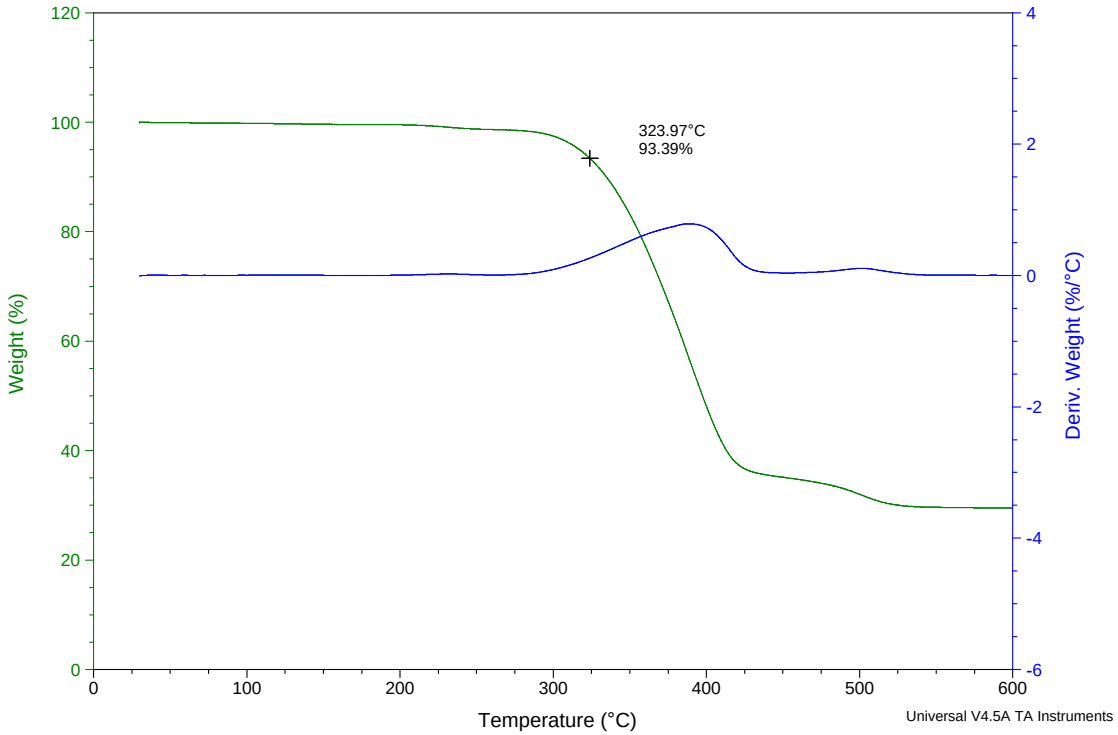

Figure S88. TGA trace of p(NBI-PS) (M_n = 1,122,000 g/mol). Decomposition temperature at 5% weight loss is 324 °C.

Differential Scanning Calorimetry (DSC)

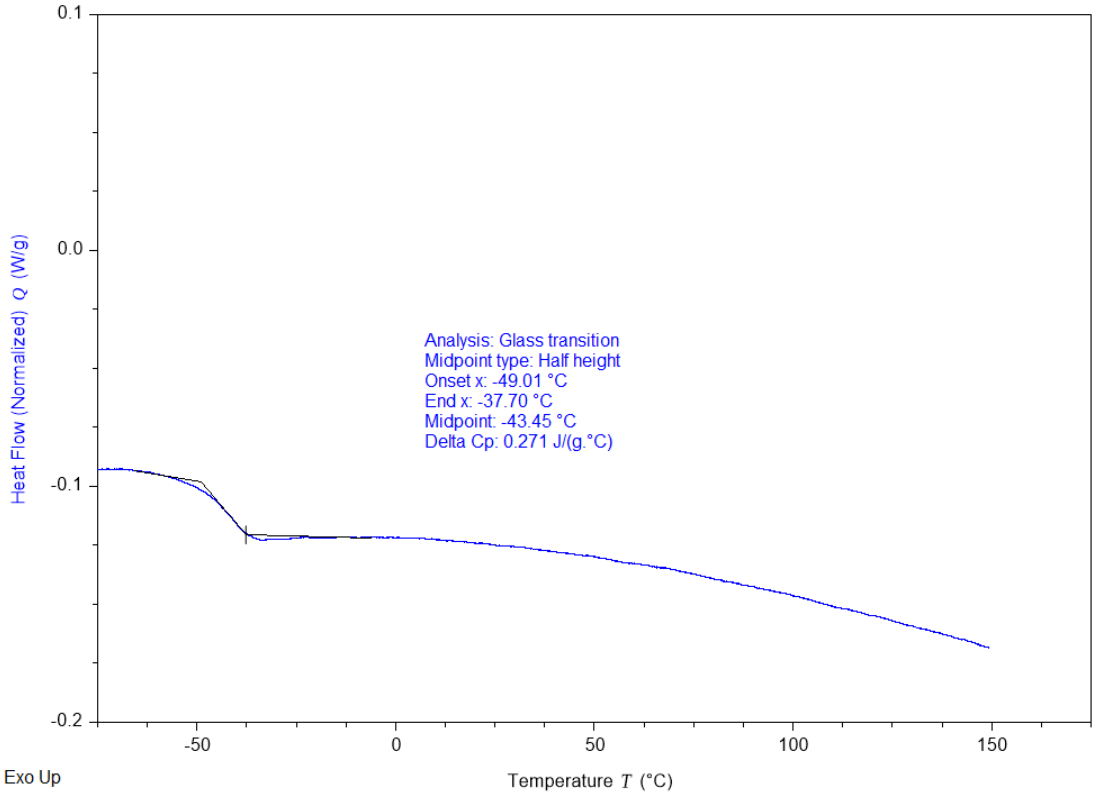

Figure S89. Representative and isolated DSC 2nd heat trace for p(NB-Hep) (M_n = 242,900 g/mol).

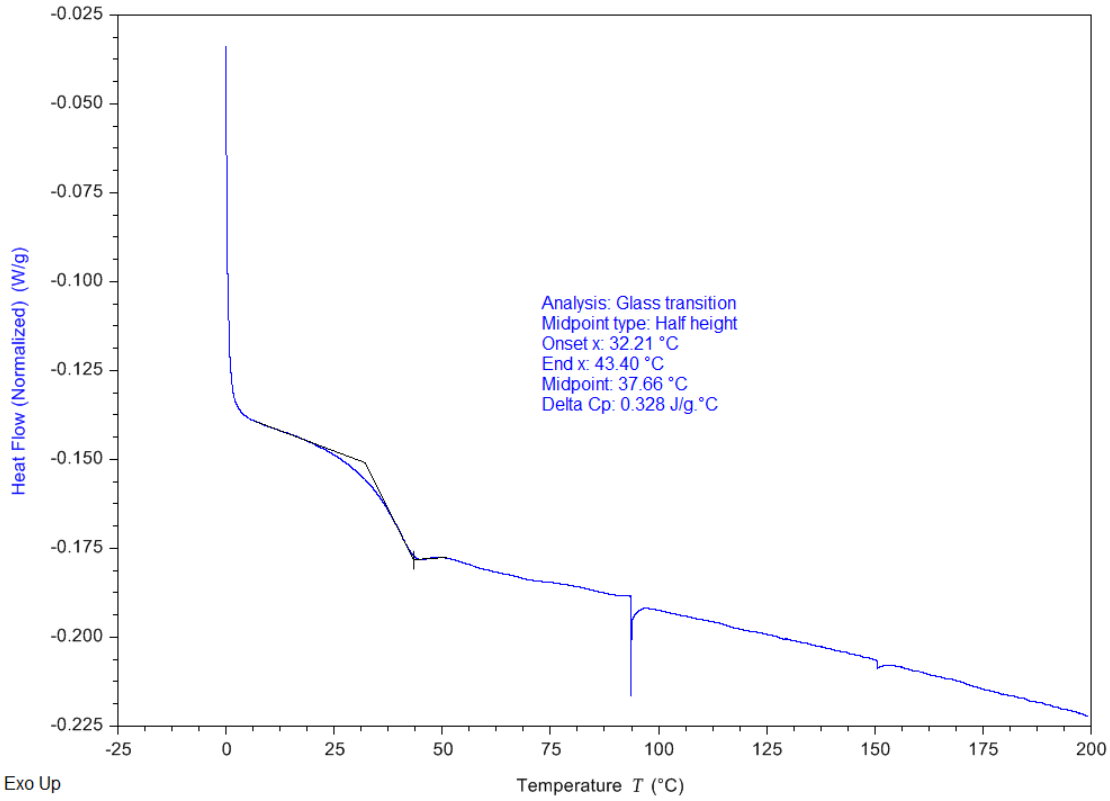

Figure S90. Representative and isolated DSC 2nd heat trace for p(NBI-Hep) (M_n = 114,900 g/mol).

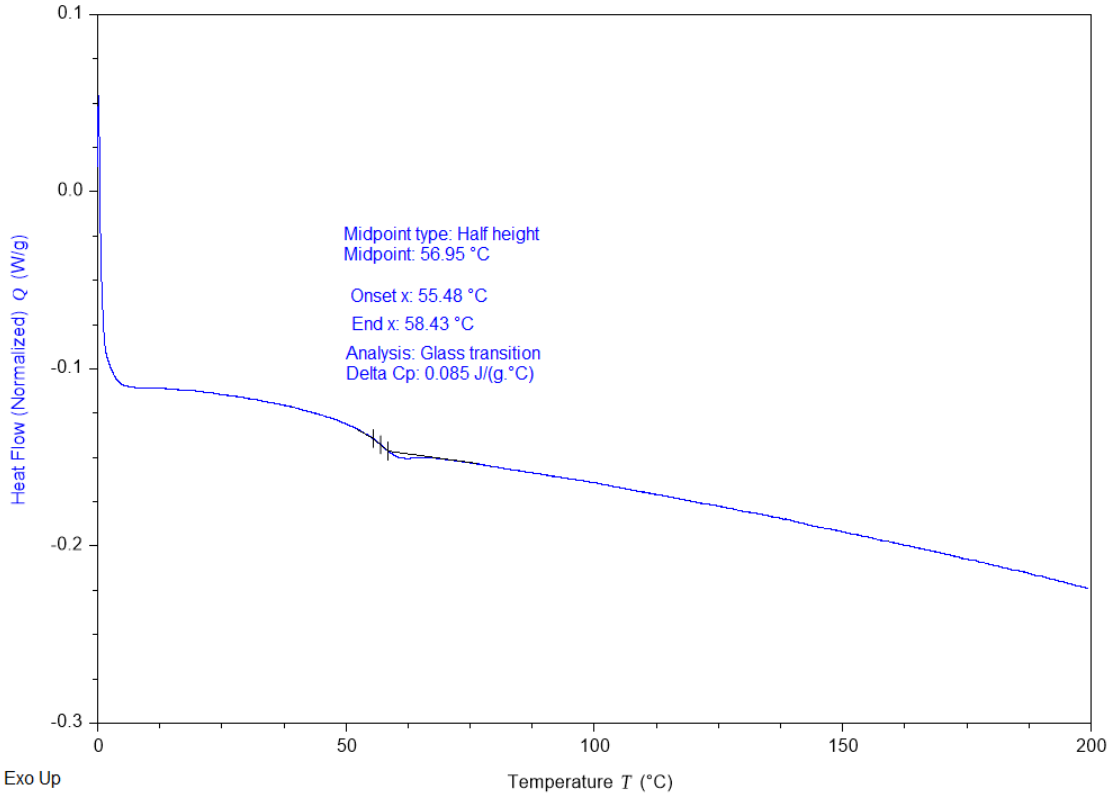

Figure S91. Representative and isolated DSC 2nd heat trace for p(NBI-Dec) (M_n = 779,700 g/mol).

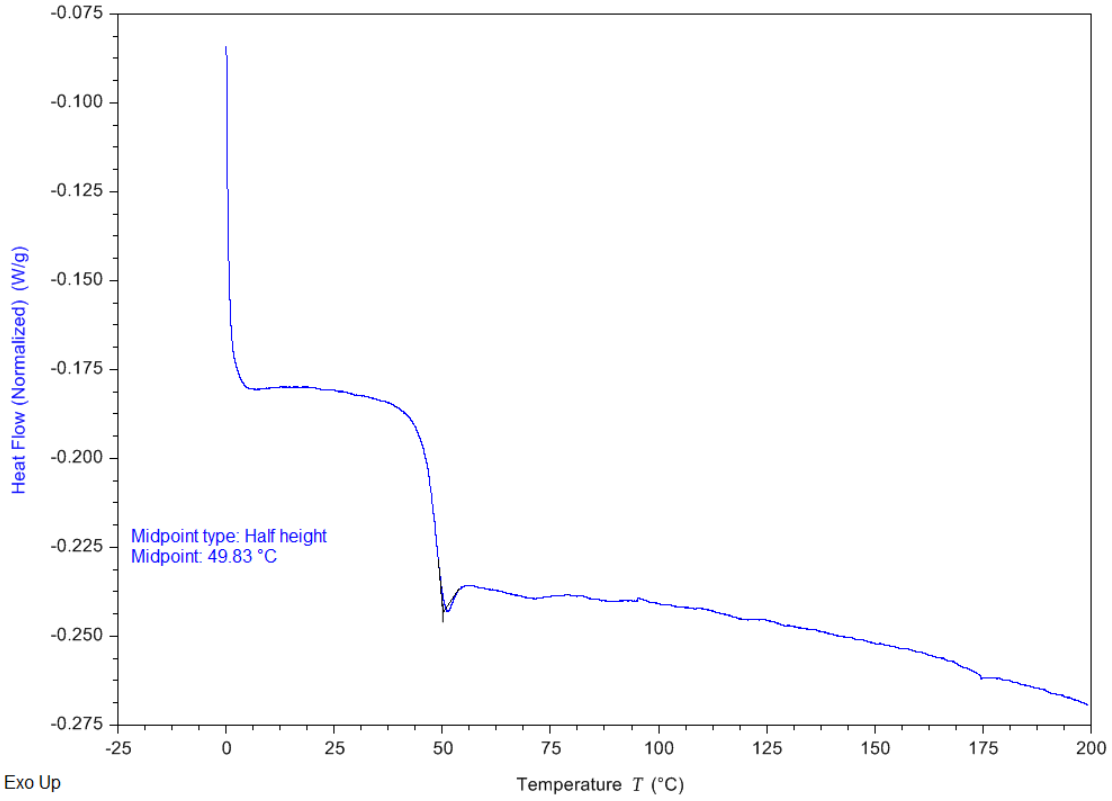

Figure S92. Representative and isolated DSC 2nd heat trace for p(NB-PLA) (M_n = 209,600 g/mol).

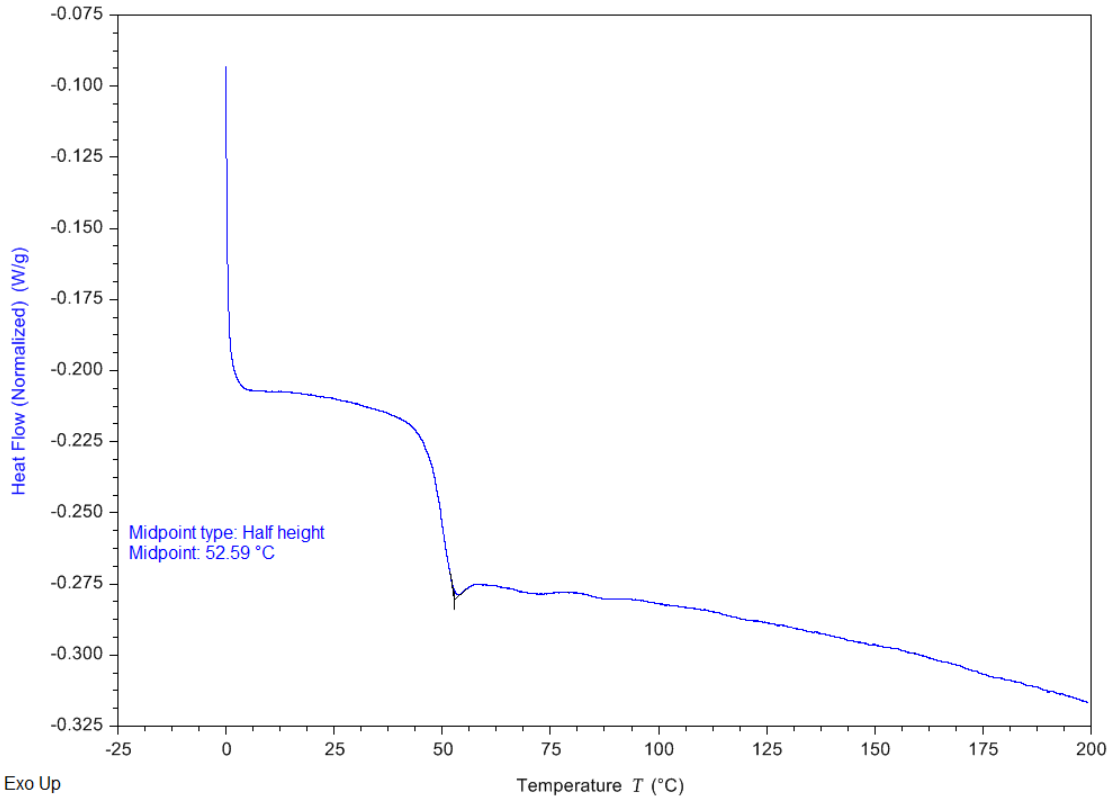

Figure S93. Representative and isolated DSC 2nd heat trace for p(NBI-PLA) (M_n = 254,500 g/mol).

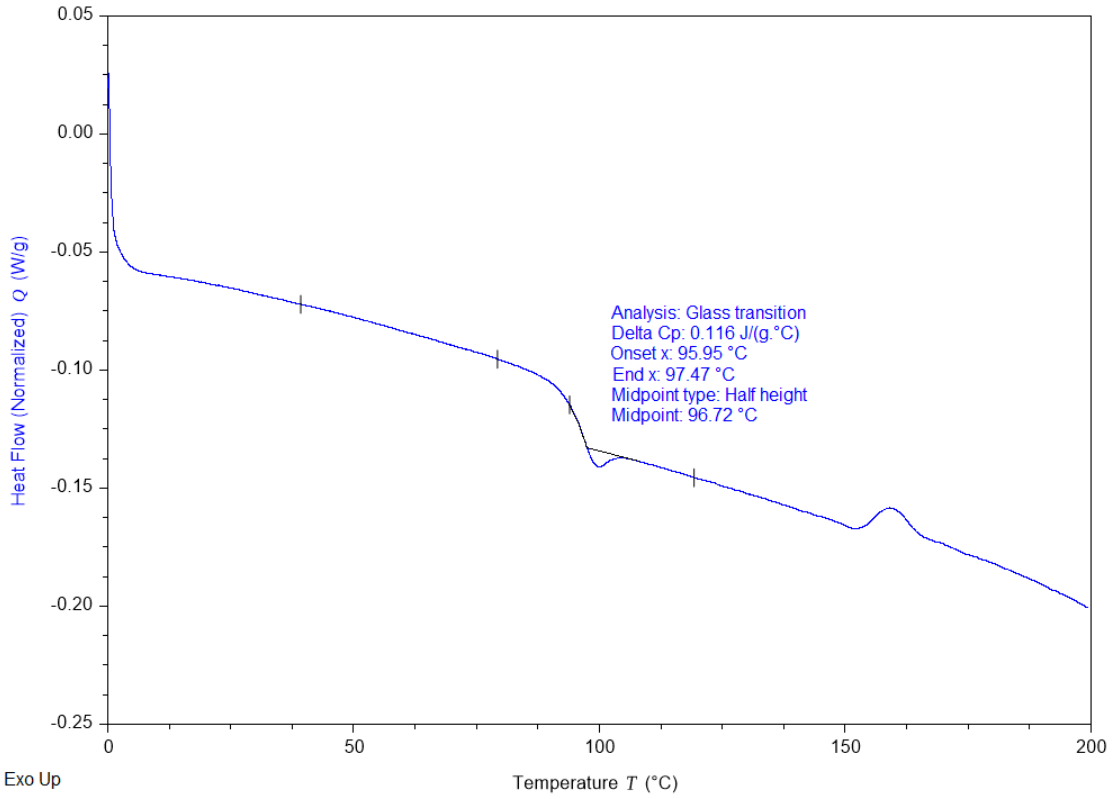

Figure S94. Representative and isolated DSC 2nd heat trace for p(NB-PS) (M_n = 1,242,000 g/mol) .

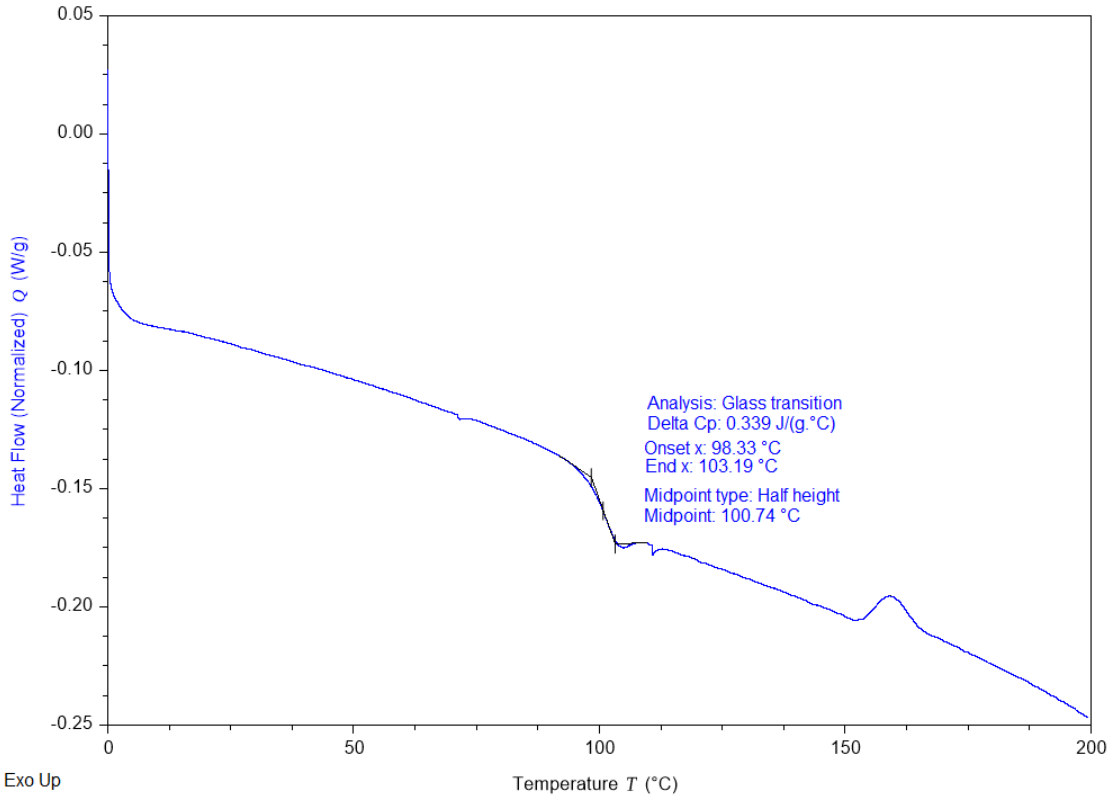

Figure S95. Representative and isolated DSC 2nd heat trace for p(NBI-PS) (M_n = 1,122,000 g/mol).

Rheological Properties:

Homopolymer MW Series Mastercurves:

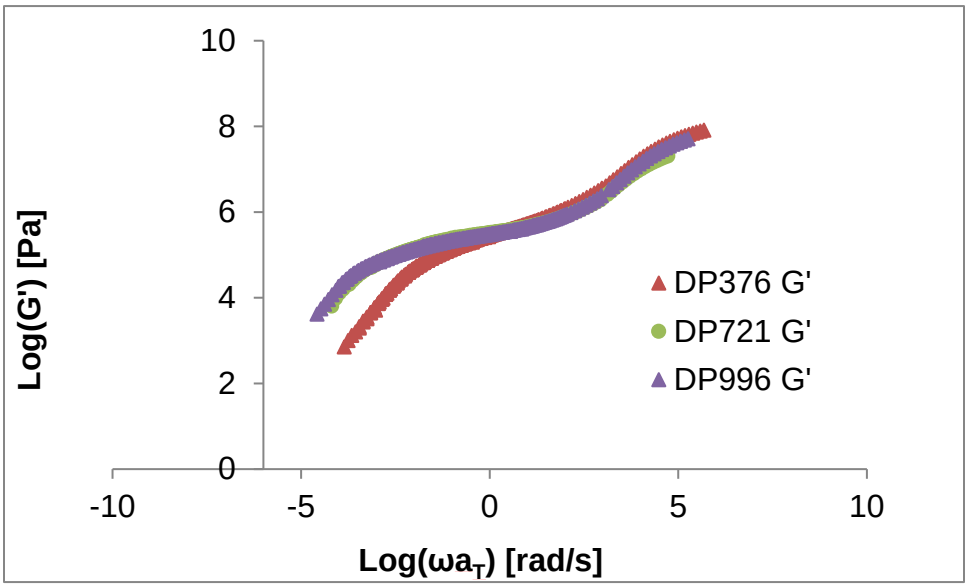

Figure S96. Storage modulus mastercurves for 3 of the p(NB-Hep) MW series at T_{ref} = T_g + 40 °C.

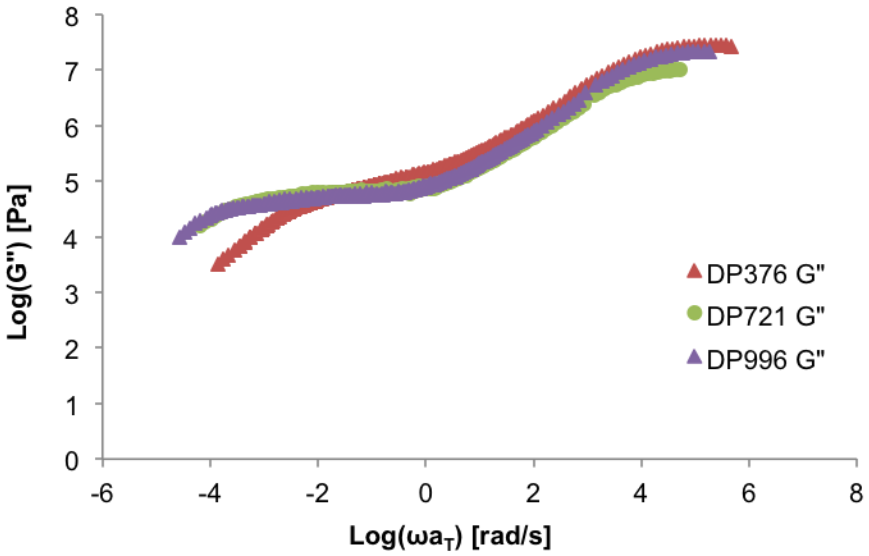

Figure S97. Loss modulus mastercurves for 3 of the p(NB-Hep) MW series at T_{ref} = T_g + 40 °C.

Table S16. The raw shift factors for each mastercurve produced for the p(NB-Hep) MW series.

	p(NB-Hep) DP 376		p(NB-Hep) DP 721		p(NB-Hep) DP 996	
Temperature (°C)	a_T	b_T	a_T	b_T	a_T	b_T
-35	4788.170	0.461	529.044	0.168	1824.610	0.316
-15	9.436	0.929	8.854	1.015	8.982	1.045
-5	1.000	1.000	1.000	1.000	1.000	1.000
5	0.176	1.068	0.189	0.931	0.176	0.969
15	0.035	1.172	0.050	0.947	-	-
25	0.009	1.177	0.007	0.898	0.012	0.906
30	0.006	1.189	-	-	-	-
35	0.003	1.219	0.002	0.941	-	-
45	0.001	1.278	0.001	1.084	0.001	0.849
65	-	-	-	-	0.000	0.938

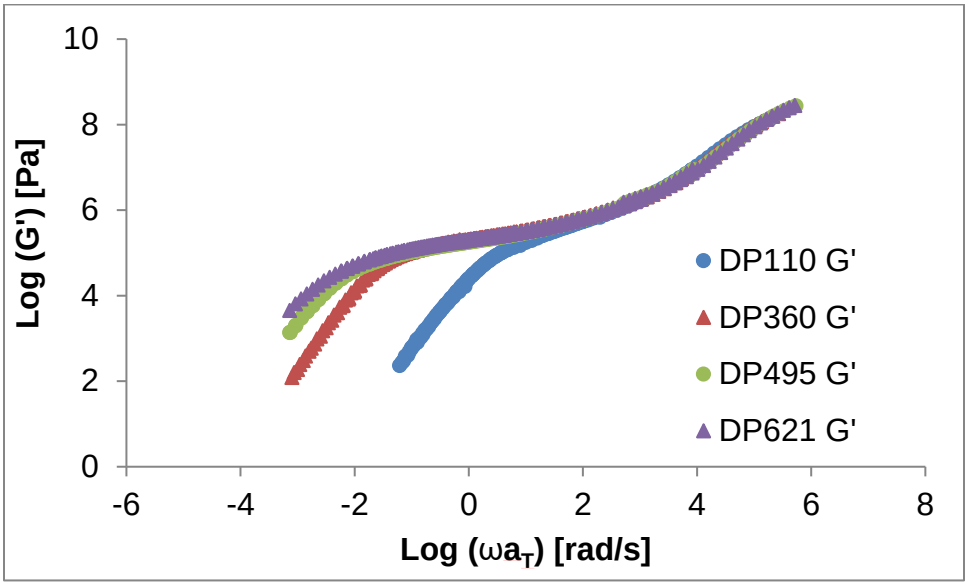

Figure S98. Storage modulus mastercurves for 4 of the p(NBI-Hep) MW series at T_{ref} = T_g + 40 °C.

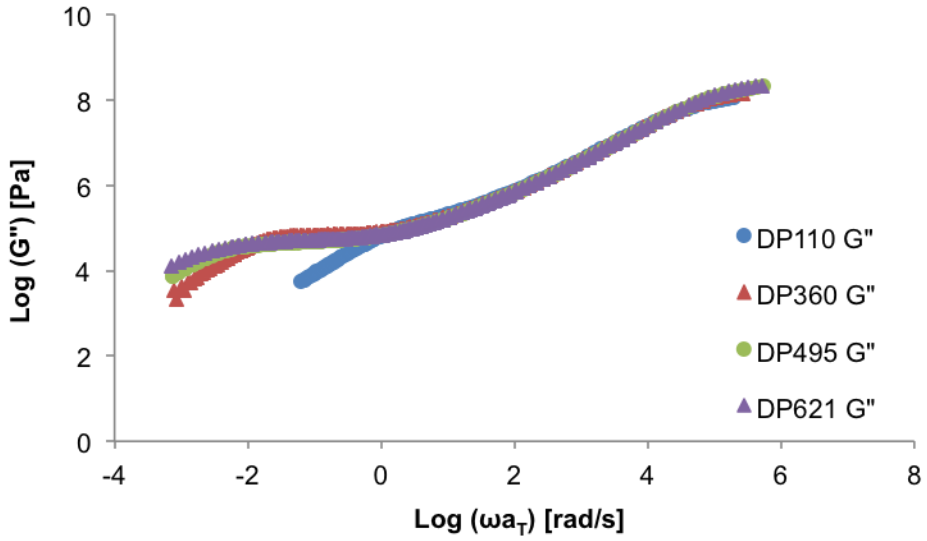

Figure S99. Loss modulus mastercurves for 4 of the p(NBI-Hep) MW series at T_{ref} = T_g + 40 °C.

Table S17. The raw shift factors for each mastercurve produced for the p(NBI-Hep) MW series.

	p(NBI-Hep) DP 110		**p(NBI-Hep) DP 360**		**p(NBI-Hep) DP 495**		**p(NBI-Hep) DP 621**	
Temperature (°C)	a_T	b_T	a_T	b_T	a_T	b_T	a_T	b_T
50	1996.270	1.778	2680.730	1.810	5417.370	2.784	5165.470	3.051
60	79.881	1.334	81.886	1.260	85.474	1.211	82.419	1.339
70	5.744	0.986	6.826	1.085	6.929	1.038	6.680	1.185
80	1.000	1.000	1.000	1.000	1.000	1.000	1.000	1.000
90	0.229	0.953	0.218	0.981	0.213	0.948	0.211	0.989
100	0.062	0.917	0.061	0.976	0.059	0.956	0.059	0.917
120	0.009	0.880	0.008	0.943	0.007	0.905	0.007	0.818

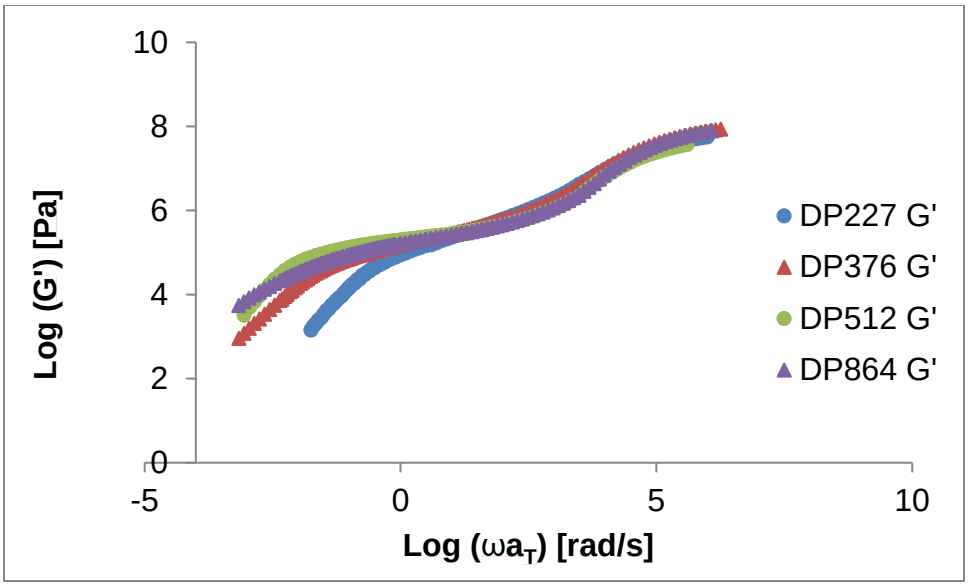

Figure S100. Storage modulus mastercurves for 4 of the p(NBI-Dec) MW series at T_{ref} = T_g + 40 °C.

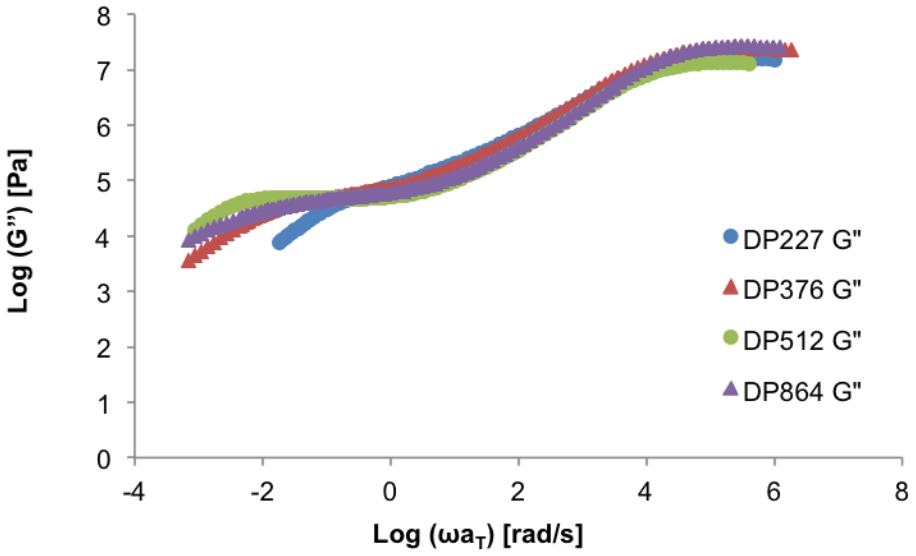

Figure S101. Loss modulus mastercurves for 4 of the p(NBI-Dec) MW series at T_{ref} = T_g + 40 °C.

Table S18. The raw shift factors for each mastercurve produced for the p(NBI-Dec) MW series.

	p(NBI-Dec) DP 227		p(NBI-Dec) DP 376		p(NBI-Dec) DP 512		p(NBI-Dec) DP 864	
Temperature (°C)	a_T	b_T	a_T	b_T	a_T	b_T	a_T	b_T
60	9952.080	0.414	18110.200	0.698	3992.450	0.330	12094.900	0.672
80	40.156	1.006	35.090	1.106	26.599	1.122	30.368	1.146
97	1.000	1.000	1.000	1.000	1.000	1.000	1.000	1.000
120	0.050	1.094	0.048	0.977	0.056	0.976	0.048	0.849
140	0.007	1.105	0.007	0.990	0.009	1.010	0.007	0.790

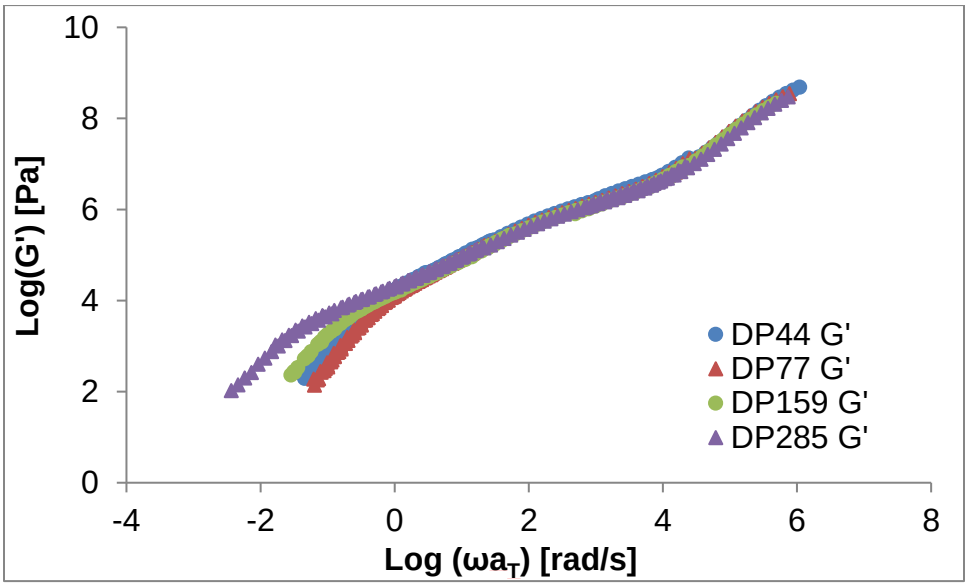

Figure S102. Storage modulus mastercurves for 4 of the p(NB-PLA) MW series at T_{ref} = T_g + 30 °C.

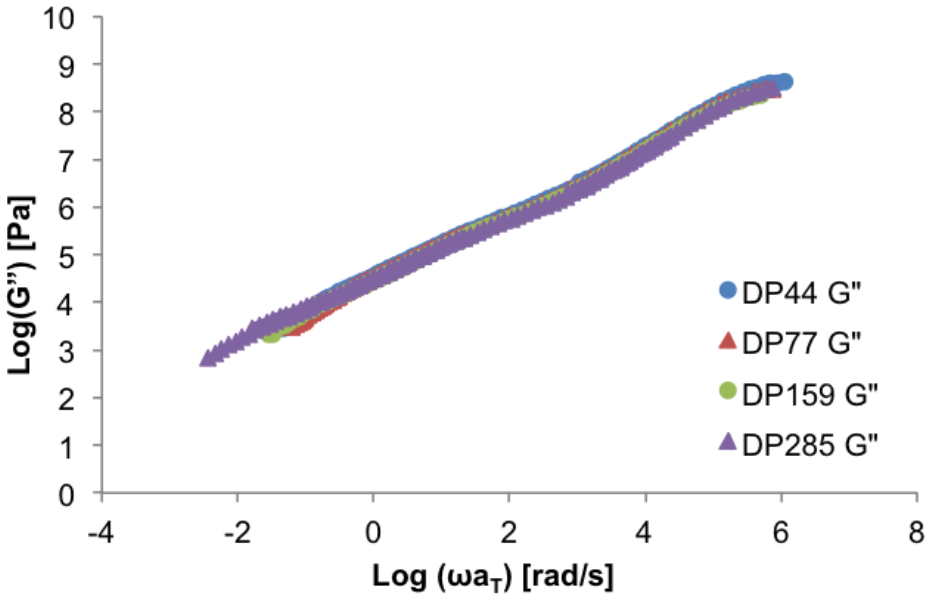

Figure S103. Loss modulus mastercurves for 4 of the p(NB-PLA) MW series at T_{ref} = T_g + 30 °C.

Table S19. The raw shift factors for each mastercurve produced for the p(NB-PLA) MW series.

	p(NB-PLA) DP 44		**p(NB-PLA) DP 77**		**p(NB-PLA) DP 159**		**p(NB-PLA) DP 285**	
Temperature (°C)	a_T	b_T	a_T	b_T	a_T	b_T	a_T	b_T
55	10979.900	1.940	7706.460	1.376	4933.350	1.155	7378.800	1.778
60	243.628	0.802	249.363	0.795	198.264	0.733	214.497	0.823
70	10.844	0.971	10.930	0.958	10.338	0.932	10.520	0.984
80	1.000	1.000	1.000	1.000	10.432	0.930	1.000	1.000
90	0.144	0.984	0.141	0.949	1.000	1.000	0.167	1.050
100	0.028	0.913	0.147	0.989	0.143	0.930	0.037	0.948

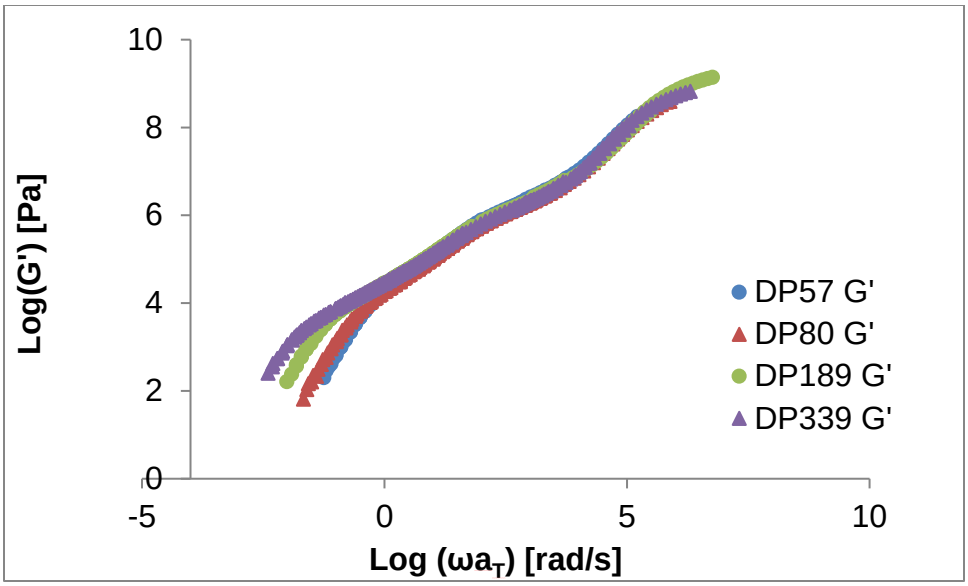

Figure S104. Storage modulus mastercurves for 4 of the p(NBI-PLA) MW series at T_{ref} = T_g + 30 °C.

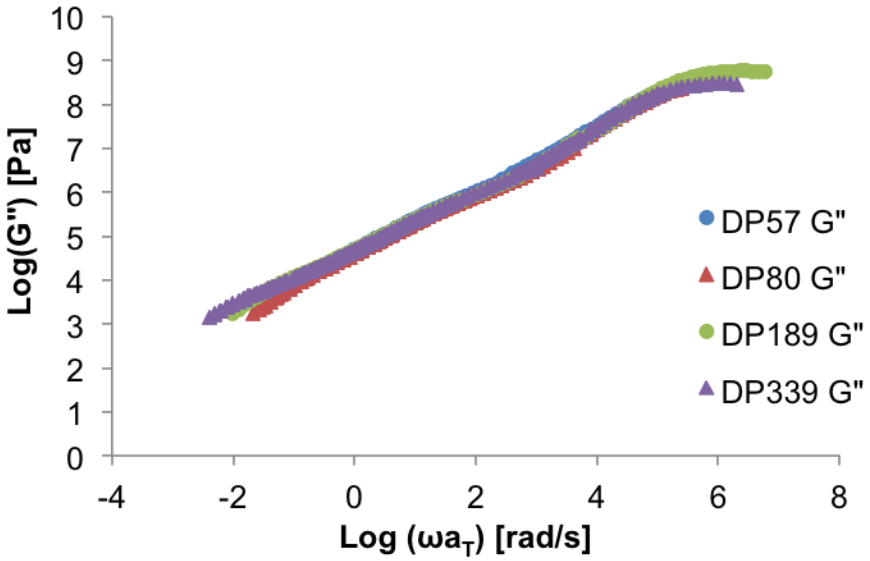

Figure S105. Loss modulus mastercurves for 4 of the p(NBI-PLA) MW series at T_{ref} = T_g + 30 °C.

Table S20. The raw shift factors for each mastercurve produced for the p(NBI-PLA) MW series.

	p(NBI-PLA) DP 57		p(NBI-PLA) DP 80		p(NBI-PLA) DP 189		p(NBI-PLA) DP 339	
Temperature (°C)	a_T	b_T	a_T	b_T	a_T	b_T	a_T	b_T
55	-	-	-	-	57909.700	3.162	20158.800	1.327
60	1650.110	1.715	1282.620	1.625	3054.880	2.943	1097.350	1.333
65	56.509	0.771	49.992	0.810	49.966	0.865	48.186	0.777
70	11.504	0.826	10.568	0.855	10.454	0.890	10.259	0.856
80	1.000	1.000	1.000	1.000	1.000	1.000	1.000	1.000
90	0.126	0.930	0.125	0.986	0.154	1.028	0.141	1.074
100	0.022	0.874	0.021	0.763	0.031	1.000	0.024	0.985
120	-	-	-	-	-	-	0.002	0.834

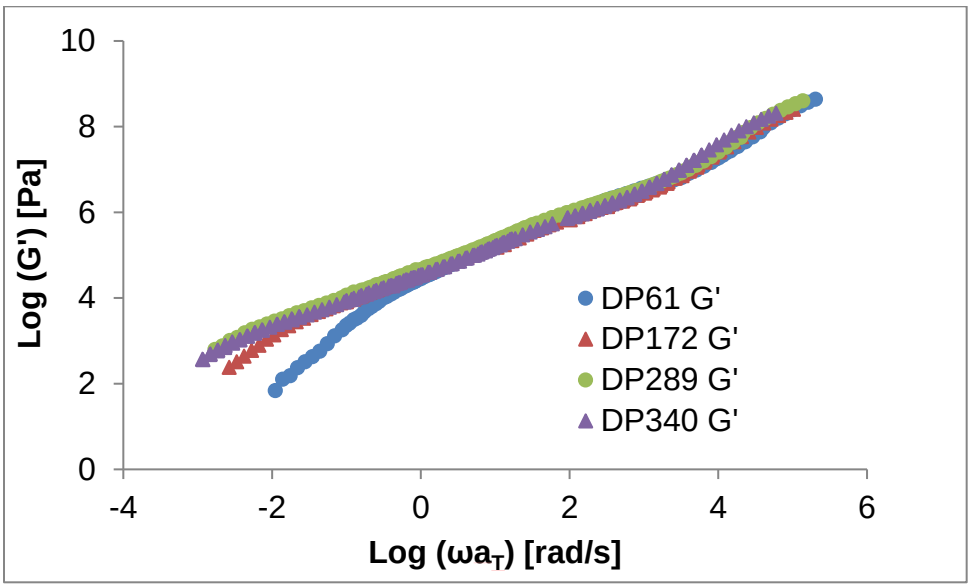

Figure S106. Storage modulus mastercurves for 4 of the p(NB-PS) MW series at $T_{ref} = T_g + 30$ °C.

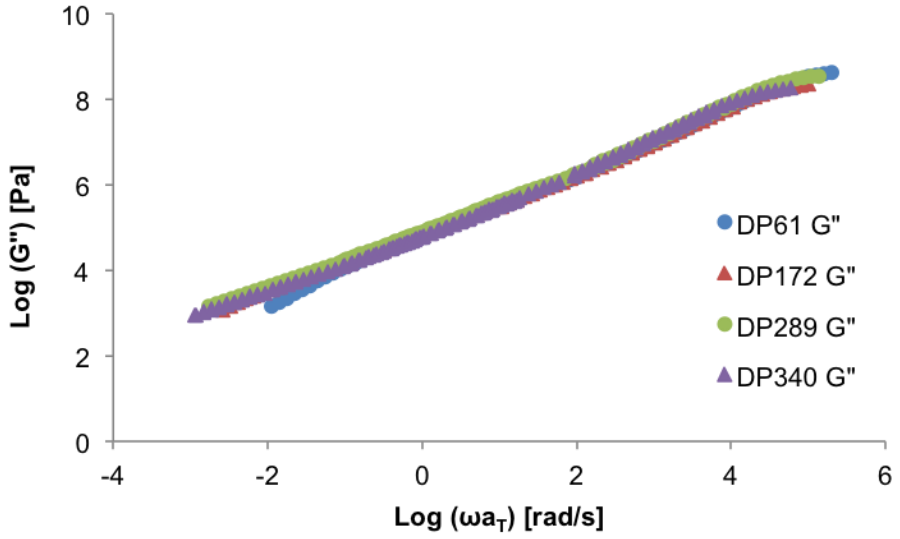

Figure S107. Storage modulus mastercurves for 4 of the p(NB-PS) MW series at $T_{ref} = T_g$ + 30 °C.

Table S21. The raw shift factors for each mastercurve produced for the p(NB-PS) MW series.

	p(NB-PS) DP 61		p(NB-PS) DP 172		p(NB-PS) DP 289		p(NB-PS) DP 340	
Temperature (°C)	a_T	b_T	a_T	b_T	a_T	b_T	a_T	b_T
105	2034.900	2.183	1026.100	1.520	1377.030	2.045	598.104	1.171
110	367.634	2.571	105.854	1.152	200.984	1.848	58.838	0.777
120	4.236	0.854	4.224	0.930	4.602	1.006	4.187	0.866
127	1.000	1.000	1.000	1.000	1.000	1.000	1.000	1.000
140	0.088	0.940	0.011	0.543	0.009	0.562	-	-
150	-	-	-	-	-	-	0.009	0.562
170	-	-	-	-	-	-	0.001	0.640

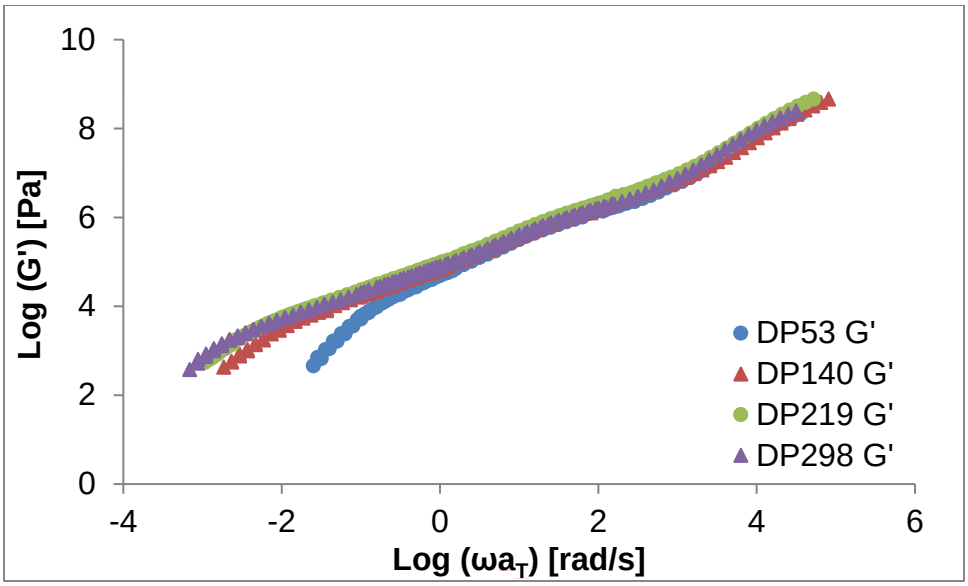

Figure S108. Storage modulus mastercurves for 4 of the p(NBI-PS) MW series at T_{ref} = T_g + 30 °C.

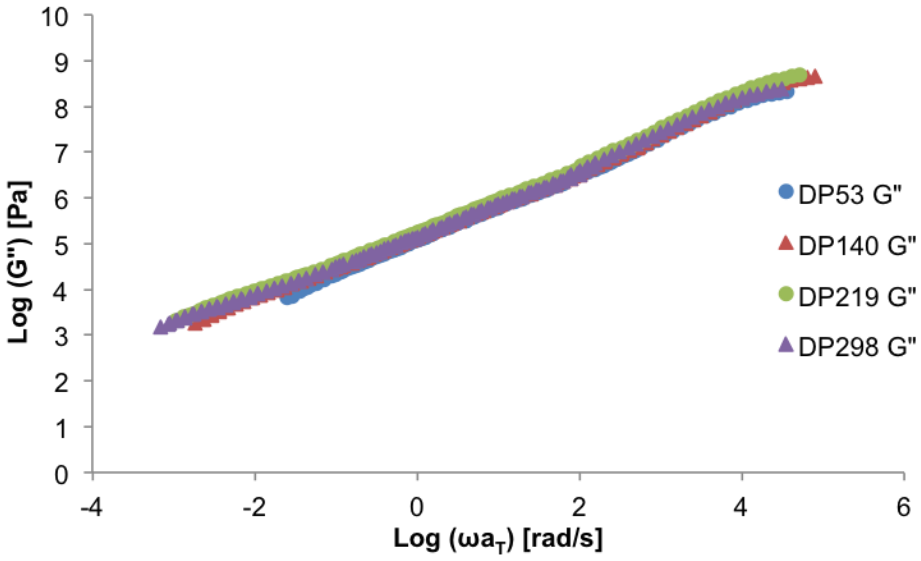

Figure S109. Loss modulus mastercurves for 4 of the p(NBI-PS) MW series at T_{ref} = T_g + 30 °C.

Table S22. The raw shift factors for each mastercurve produced for the p(NBI-PS) MW series.

	p(NBI-PS) DP 53		p(NBI-PS) DP 140		p(NBI-PS) DP 219		p(NBI-PS) DP 298	
Temperature (°C)	a_T	b_T	a_T	b_T	a_T	b_T	a_T	b_T
110	362.984	1.778	808.632	3.338	525.091	2.507	314.922	1.549
120	5.001	0.898	6.713	1.155	7.003	1.149	7.373	1.110
127	1.000	1.000	1.000	1.000	1.000	1.000	1.000	1.000
150	0.014	0.776	0.012	0.753	0.011	0.777	0.009	0.562
160	0.005	0.996	-	-	-	-	-	-
170	-	-	0.001	0.895	0.001	0.698	0.001	0.636

Homopolymer Van Gurp-Palmen Plots:

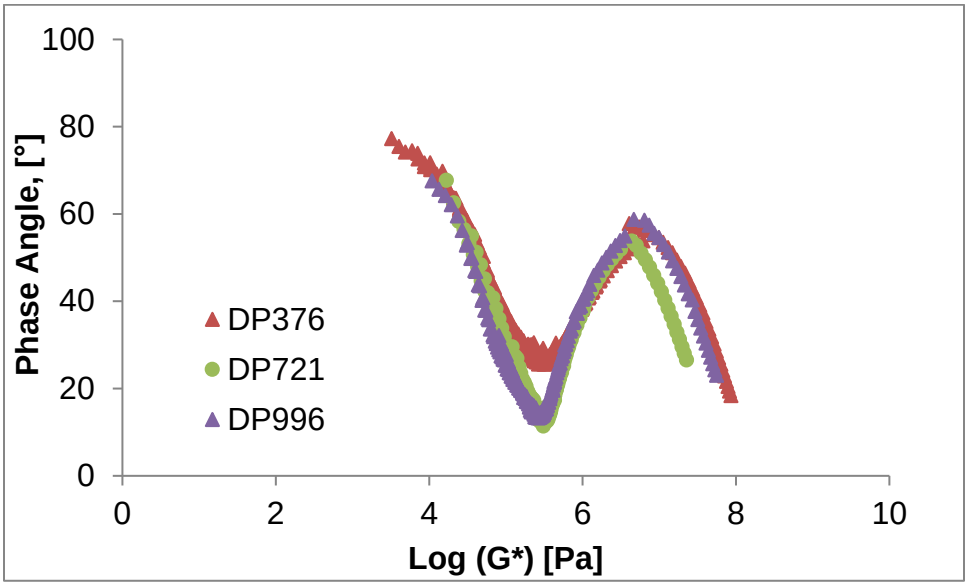

Figure S110. The Van Gurp-Palmen plots for 3 of the p(NB-Hep) MW series mastercurves at $T_{ref} = T_g + 40$ °C.

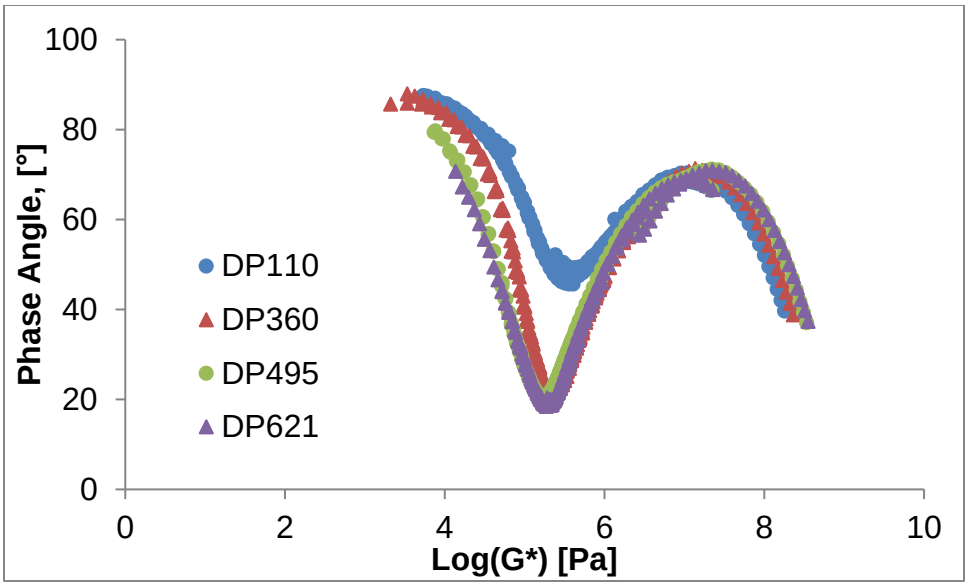

Figure S111. The Van Gurp-Palmen plots for 4 of the p(NBI-Hep) MW series mastercurves at $T_{ref} = T_g + 40$ °C.

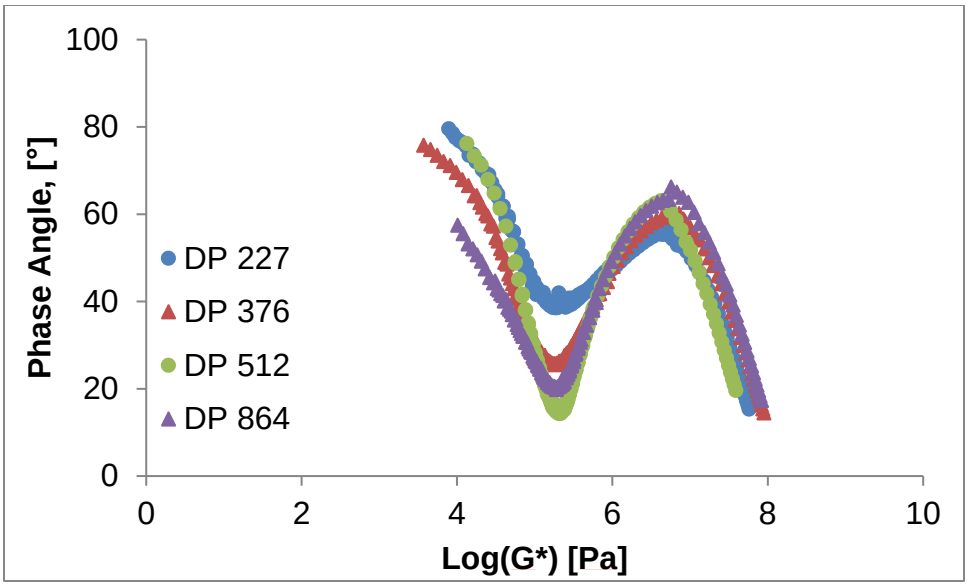

Figure S112. The Van Gurp-Palmen plots for 4 of the p(NBI-Dec) MW series mastercurves at $T_{ref} = T_g + 40$ °C.

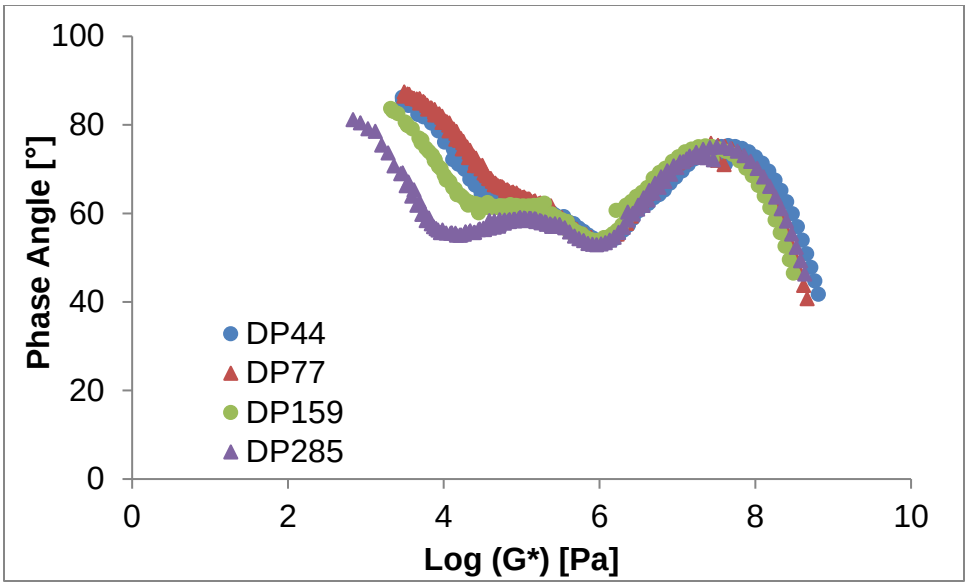

Figure S113. The Van Gurp-Palmen plots for 4 of the p(NB-PLA) MW series mastercurves at $T_{ref} = T_g + 30$ °C

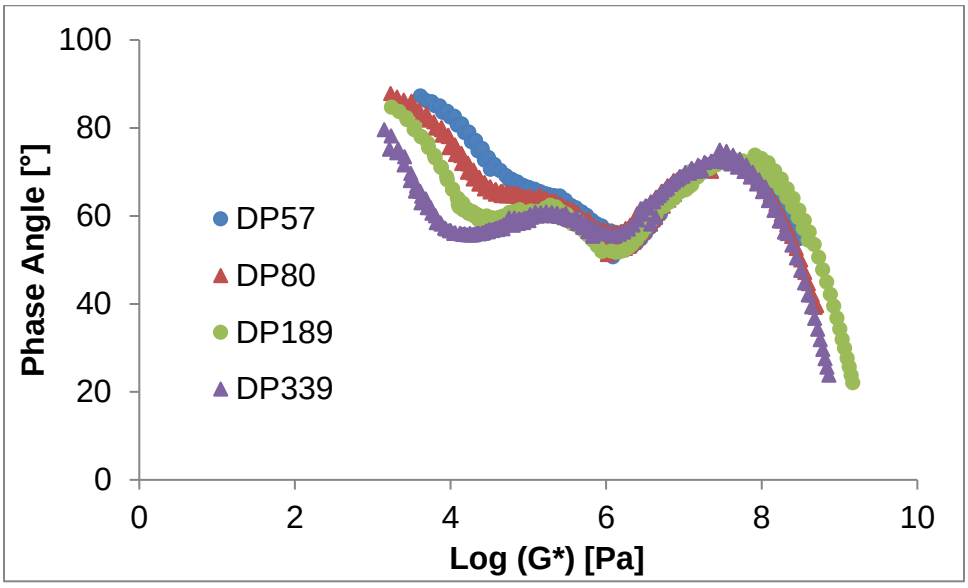

Figure S114. The Van Gurp-Palmen plots for 4 of the p(NBI-PLA) MW series mastercurves at $T_{ref} = T_g + 30$ °C

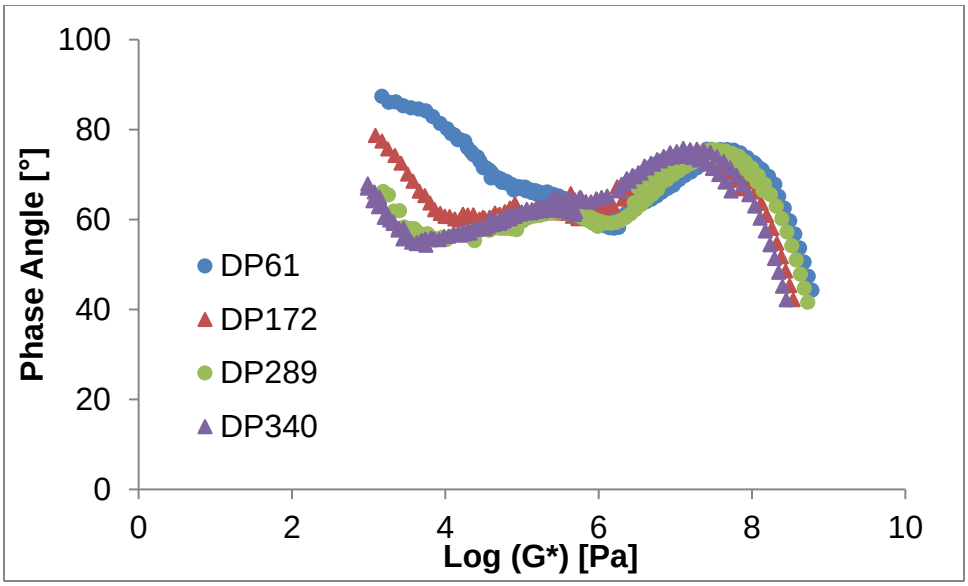

Figure S115. The Van Gurp-Palmen plots for 4 of the p(NB-PS) MW series mastercurves at $T_{ref} = T_g + 30$ °C.

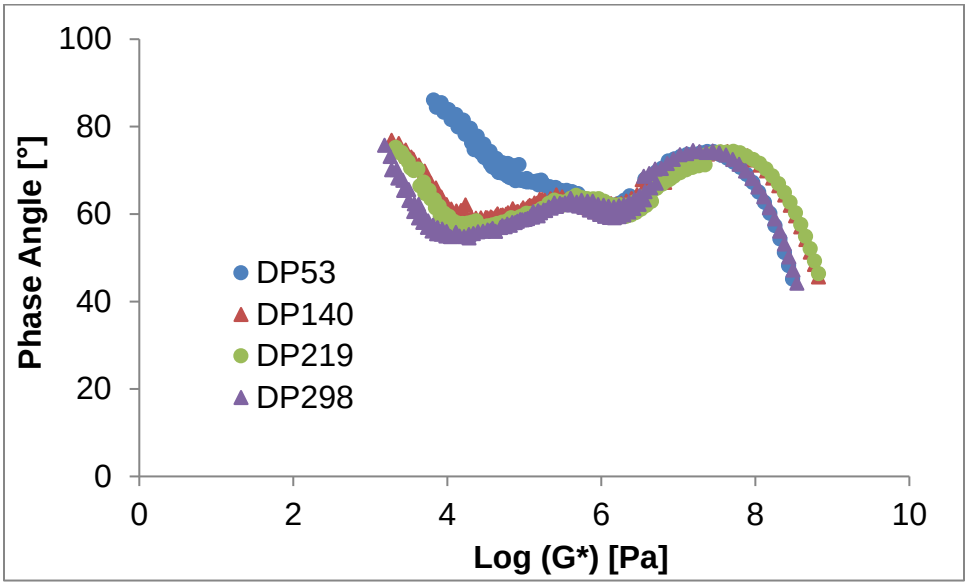

Figure S116. The Van Gurp-Palmen plots for 4 of the p(NBI-PS) MW series mastercurves at $T_{ref} = T_g + 30$ °C.

Linear Homopolymer Williams-Landel-Ferry (WLF) Shift Factor Relationship:

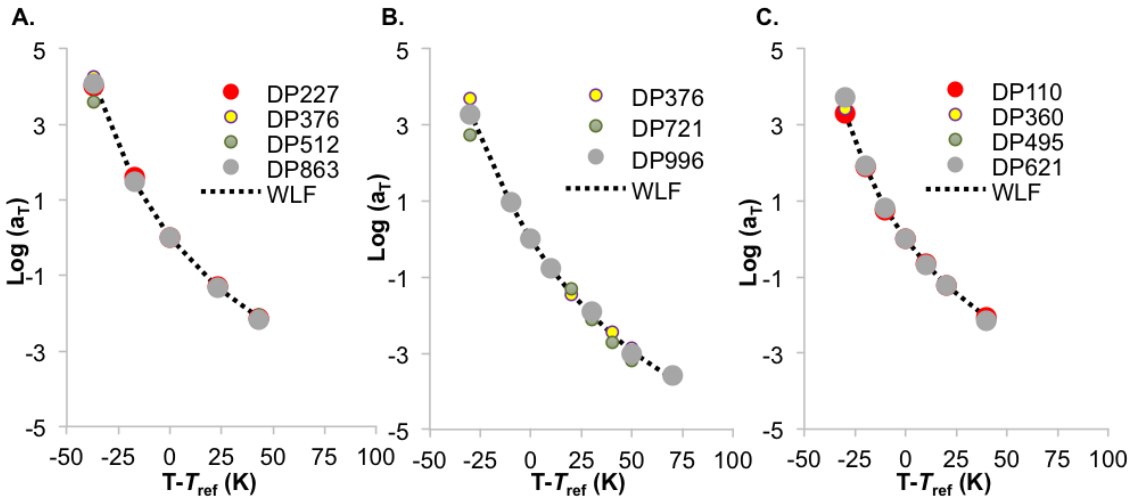

Figure S117. WLF graphs of all of the mastercurve shift factors from the time-temperature superposition for the p(NBI-Dec) MW series (A.), the p(NB-Hep) MW series (B.), and the p(NBI-Hep) MW series (C.).

Table S23. The calculated C-values for each of the linear polymer MW WLF analyses.

Calculated parameter	p(NBI-Dec)	p(NB-Hep)	p(NBI-Hep)
$C_{1,\ Ref}$	7.06	10.02	6.78
$C_{2,\ Ref}$	100.18	120.42	91.93
$C_{1,\ Tg}$	11.76	15.00	12.49
$C_{2,\ Tg}$	60.18	80.42	49.93

References:

1. J. A. Love, J. P. Morgan, T. M. Trnka, R. H. Grubbs *Angew. Chem., Int. Ed.* **2002**, *41*, 4035-4037.

2. S. C. Radzinski, J. C. Foster, R. C. Chapleski, D. Troya, J. B. Matson, *J. Am. Chem. Soc.* **2016**, 138, 6998-7004.

3. J. B. Matson, R. H. Grubbs, *J. Am. Chem. Soc.* **2008**, 130, 6731-6733.

4. B. M. Boyle, O. Heinz, G. M. Miyake, Y. Ding *Macromolecules*, **2019**, 52, 3426-3434.

5. R. Whitfield, A. Anastasaki, V. Nikolaou, G. R. Jones, N. G. Engelis, E. H. Discekici, C. Fleischmann, J. Willenbacher, C. J. Hawker, D. M. Haddleton, *J. Am. Chem. Soc.* **2017,** 139, 1003-1010.

6. S. C. Radzinski, J. C. Foster, S. J. Scannelli, J. R. Weaver, K. J. Arrington, J. B. Matson, *ACS Macro Lett.* **2017**, 6, 1175-1179.

7. B. R. Sveinbjornsson, R. A. Weitekamp, G. M. Miyake, Y. Xia, H. A. Atwater, R. H. Grubbs, *Proc. Natl. Acad. Sci. USA* **2012,** 109, 36, 14332-14336.